UNIVERSIDAD
NACIONAL
DE COLOMBIA
SEDE BOGOTÁ

Universität Stuttgart

Mechanobiological approach for skeletal muscle adaptation

Yesid Alexis Villota Narváez

Universidad Nacional de Colombia
Facultad de Ingeniería, Departamento de Ingeniería Mecánica
Bogotá, Colombia

University of Stuttgart
Faculty 2: Civil and Environmental Engineering
Stuttgart, Germany

2022

Mechanobiological approach for skeletal muscle adaptation

Yesid Alexis Villota Narváez

Thesis submitted in order to meet the requirements for the degree of:
Doctor en Ingeniería Mecánica y mecatrónica
Doctor in Engineering

Advisor: Ph.D. Diego Garzón Alvarado
Co-Advisor: Ph.D. Angélica Ramírez Martínez
Co-Advisor: Ph.D. Oliver Röhrle

Research field: Computational Modeling of Mechanobiological Systems

Research Group in Numerical Methods and Modeling (GNUM)
Universidad Nacional de Colombia
Facultad de Ingeniería, Departamento de Ingeniería Mecánica
Bogotá, Colombia

Research group in Continuum Biomechanics and Mechanobiology (CBM)
University of Stuttgart
Faculty 2: Civil and Environmental Engineering
Stuttgart, Germany

2022

Abstract

Skeletal muscle is the most adaptive tissue in the human body. Its adaptation includes changes in shape and size, changes at the organelle function and distribution inside muscle cells, and changes at the molecular scale. Macroscopic characteristics such as size and strength, are related to the cellular scale via protein content in myofibrils, which are the series arrangement of units that generate force (sarcomeres); at the organelle scale, adaptation occurs in the mytochondria content, as well as sarcoplasmic reticulum function; microscopic characteristics at the molecular scale are related to the type of protein molecules that myofibrils contain, the type of molecules include a variety of myosin heavy and light chains. This adaptation processes are the outcome of stimulus like diet, hormone levels, and physical activity. The last one will be particularly important for the aim of this thesis, which is the modeling of the evolution of the characteristics of muscle tissue under the effects of personalized training protocols, i.e. physical activity.

Abstract

Der Skelettmuskel ist das anpassungsfähigste Gewebe im menschlichen Körper. Zu seiner Anpassung gehören Veränderungen in Form und Größe, Veränderungen der Organellenfunktion und der Verteilung innerhalb der Muskelzellen sowie Veränderungen auf molekularer Ebene. Makroskopische Merkmale wie Größe und Stärke hängen mit der zellulären Skala über den Proteingehalt in den Myofibrillen zusammen, d.h. der Reihenanordnung von Einheiten, die Kraft erzeugen (Sarkomere); auf der Organellenskala erfolgt die Anpassung im Mytochondriengehalt sowie in der Funktion des sarkoplasmatischen Retikulums; mikroskopische Merkmale auf der molekularen Skala hängen mit der Art der Proteinmoleküle zusammen, die die Myofibrillen enthalten, wobei die Art der Moleküle eine Vielzahl von schweren und leichten Myosinketten umfasst. Diese Anpassungsprozesse sind das Ergebnis von Reizen wie Ernährung, Hormonspiegel und körperlicher Aktivität. Letzteres wird für das Ziel dieser Arbeit besonders wichtig sein, nämlich die Modellierung der Entwicklung der Eigenschaften des Muskelgewebes unter den Auswirkungen personalisierter Trainingsprotokolle, d.h. körperlicher Aktivität.

Abstract

Aproximación mecanobiológica para la adaptación de músculo esquelético

El músculo esquelético es el tejido más adaptable del cuerpo humano. Su adaptación incluye cambios en la forma y el tamaño, cambios en la función y distribución de los organelos dentro de las células musculares y cambios a escala molecular. Las características macroscópicas, como el tamaño y la fuerza, están relacionadas con la escala celular a través del contenido de proteínas en las miofibrillas, que son la disposición en serie de las unidades que generan la fuerza (sarcómeros); a escala de los organelos, la adaptación se produce en el contenido de las mitocondrias, así como en la función del retículo sarcoplásmico; las características microscópicas a escala molecular están relacionadas con el tipo de moléculas de proteínas que contienen las miofibrillas. El tipo de moléculas incluye una variedad de cadenas pesadas y ligeras de miosina. Los procesos de adaptación son el resultado de estímulos como la dieta, los niveles hormonales y la actividad física. Este último será especialmente importante para el objetivo de esta tesis, que es el modelamiento de la evolución de las características del tejido muscular bajo los efectos de protocolos de entrenamiento personalizados, es decir, la actividad física.

Contents

1 Introduction

Skeletal muscle plays a major role in physical and psychological health. According to World Health Organization, physical inactivity is the fourth leading risk factor for global mortality and a major factor in noncommunicable diseases, such as cardiovascular, cancers, and diabetes. Therefore, deep understanding of the relations between physical activity, exercise, and the biological responses at tissue level is important in order to improve therapies and recommendations.

Skeletal muscle is mostly recognized as the system that provides the ability to move; but it also supports posture; shield vital organs; and provides the main reservoir of protein, which contains the big amount of amino acids required in almost every biochemical process in animal systems. The importance of skeletal muscles is enhanced by its characteristic adaptability: short-intense activities produce adaptation to resistance, sustained-moderate activities produce adaptation to endurance, low-intensity activities or chronic rest produce a decrease in muscle size. Adaptation is, however the outcome of repeated loading conditions over an extended period. To better understand skeletal muscle adaptation, two research fields are clearly differentiated: biological and mechanical.

In the biological field, the adaptation of skeletal muscle at the organ scale is parallel to the adaptation at the cellular scale: muscle cells (also known as myofibers) that are adapted to resistance display many differences to myofibers adapted to endurance; these differences range from organelle function and number, to molecular differences in sarcomeres, which are the smallest force-production unit of myofibers. Here, the adaptation of skeletal muscle at the organ scale can be explained by its adaptation at the cellular scale; while the adaptation at the cellular scale is the outcome of many processes at the molecular scale known as signaling pathways.

In the mechanical field, research is focused on the mechanical properties of skeletal muscle tissue and its mathematical description. In contrast to any other material, the mechanical response of skeletal muscle is the superposition of a *passive* and an *active* response. First, the passive response is related to the classic material behavior of a material, but the detailed structure and local variability of muscle tissue give a particular complexity to its mathematical description. Second, the active response is related to the muscle's capacity to generate force; here, characteristics such as individual fiber force contribution, recruitment patterns, and speed of contraction, to name a few, increase even more the complexity of the mathematical description. Further, in the mechanical field, the passive and the active responses deal with the current state of the tissue; and, although the biochemical processes

of the activation of muscles fibers play an important role in the active part of the description, not much attention has been given to the biochemical processes related to the adaptation processes.

The biological and the mechanical fields are related in the description of skeletal muscle adaptation: the activation of the signaling pathways (biological field) inside muscles cannot be controlled voluntary, but the intensity of the stimulus that triggers those pathways can be controlled by physical activity (mechanical field). In this respect, computational models allow to stablish a bridge between the biological and the mechanical fields of the adaptation process. Thus, computational models help the understanding of the adaptation process in an integrated fashion.

In what follows, a brief description of skeletal muscles, concepts of the biochemical processes that will be important in the development of this thesis, aims of the thesis, and a short outline are presented.

The organization of skeletal muscle tissue, ranges from the organ scale (whole muscles) up to the molecular scale (protein content). The properties of skeletal muscle can be divided into two categories: Type I or slow, and type II or fast; however, this two categories are too simple to describe the complexity of the molecular structure of muscle fibers. To understand how the molecular structure of the muscle tissue affect the properties at the organ scale, a brief description of skeletal muscle function and structure is presented below.

1.1 Skeletal muscle

Skeletal muscle tissue is organized at different scales. The smallest muscle unit that generates force is the sarcomere, at the scale of 1 μm [64, 8, 58]. Series of sarcomeres conform the myofibril, which runs through the whole length of the muscle fiber, at the scale of 100 μm [42, 53, 138]. Muscle fibers, or myofibers, are constituted by the parallel arrangement of myofibrils [147, 94]. Sets of muscle fibers are packed into fascicles, at the tissue scale, 1 cm [80]. Finally, sets of fascicles are packed into whole muscles, at the organ scale, 10 cm [88, 95]. Skeletal muscle cells, fascicles, and whole muscles are bounded by connective tissue: whole muscles are covered by the epimysium, fascicles are surrounded by perimysium and muscle fibers are surrounded by endomysium [86].

1.1.1 Muscle fibers

A particular muscle is composed by a large number of fascicles. Each fascicle can have different fiber types known as slow twitch and fast twitch [35, 5, 19], but usually one type is dominant [7, 140]. Slow twitch fibers, also known as Type I fibers, are red and thin, they have

a high number of mitochondria, are highly capilarized, and have a strong ability to produce and maintain force [120, 78, 77], i.e., these fibers are resistant to fatigue. Fast twitch fibers, or Type II fibers, are white and large, are less resistant to fatigue, rely on oxidative metabolism (large number of mitochondria), contain a big amount of glycogen, but are poorly capilarized [120, 78, 77]. Type II fibers are divided into type IIA and type IIB fibers [159, 20]: type IIA fibers have a great glycogen content, a big number of mitochondria, and its fatigability is intermediate; type IIB fibers rely on the energy stored in glycogen, contain a smaller number of mitochondria, and are easily fatigable. The classification of fiber types into type I, IIA, and IIB is incomplete, refined histochemical techniques revealed the existence of many fiber subtypes [20, 7, 4, 156, 158, 123, 154]. The classification of fibers is also due to the expression of different protein isoforms, which are related to the rate of contraction of each fiber type [179, 66, 88, 140].

1.1.2 Sarcomere

In a myofibril, sarcomeres are bounded by dark bands called Z -lines, between 2 of those lines, there is a thinner line called M-line. Perpendicular to the M-line the thick filaments of myosin are attached, whereas the thin filaments of actin are attached perpendicular to Z-lines; actin and myosin filaments are known as myofilaments and range about 100 Å in length. These myofilaments are the constituents of the sliding filament theory of muscle contraction, according to which the two filaments momentarily bound one another to generate a shearing force. This interconnection is called a cross-bridge. Sarcomere length ranges from 1.5 μm when shortened, up to 4 μm when stretched, and have a resting length of 2.5 μm (where maximum force generation capacity occurs). [179, 138, 105, 57]

1.1.3 Myosin Heavy and Light Chains

The thick myosin filament attaches to the M-line of the sarcomere by a long rod comformed by many myosin tails, and a series of active heads that bend and bound to the thin actin filament. The myosin tails are composed of two long heavy chains, and each heavy chain has one head. The head is constituted by a lever domain, and a motor domain. The structure of the thick myosin filament is characterized by mainly two myosin chains: the myosin heavy chain (MHC) for the rod and motor domain, and the myosin light chain (MLC) for the lever domain [59, 101, 41, 40].

There is a variety of MHC as well as MLC isoforms [122, 177, 43, 13], but MHC is the basis to classify fibers as pure or hybrid: pure fibers express only one protein isoform (fibers type I, type IIA and type IIB express MHCI, MHCIIA, and MHCIIB isoforms respectively); and hybrid fibers express combinations of MHC in different proportions (for instance fibers type I/IIA, express simultaneously MHCI and MHCIIA) [124, 167, 177]

According to the classification of fiber types, some isoforms are more likely to be found in

one type than another, and also the myosin isoform content correlates to some contractile properties of the fiber types [125, 9, 6]. Due to the adaptive capacity of muscle tissue, and consequently of the individual fibers, the number of possible ratios [124, 167, 68] and combinations [158, 155] of MHC and MLC isoforms is great enough to even consider a continuum of contractile properties instead of characteristic ranges for the different fiber types [156, 4, 126].

1.2 Signaling pathways

A muscle under mechanical load activates sets of molecules interacting in signaling pathways, and these pathways control each aspect of muscle function and adaptation.

Many signals and processes occur simultaneously, but for the purpose of this thesis, two pathways are principal: the IGF1-AKT that relates to protein synthesis (muscle hypertrophy) and protein degradation (muscle atrophy); and the calmodulin-calcineurin-NFATc that switches the gene program of individual fibers to promote characteristics of one type or another. In this section a short overview of these pathways is presented.

1.2.1 IGF1-AKT

Among the signaling pathways for muscle adaptation, one of the most studied is the IGF1-AKT signaling pathway [90, 38, 36, 92, 141, 15], the key molecules of this pathway are: (1) the insulin like growth factor (IGF1), which is related to hypertrophy mediated by physical activity [172, 137]; (2) the serine/threonine kinase (AKT), which plays an important role in cell growth and proliferation, but is also related to atrophy process [152, 52]; (3) the mammalian target of rapamycin (mTOR), which is related to cell growth and protein synthesis [51, 70]; and (4) the forkhead box transcription factors (FOXO), which are found in a variety of processes including cell proliferation, apoptosis, metabolism, and stress resistance [15, 174]. Although the relationship between these biochemical species can be mediated by many other species, the most prominent relation starts with IGF1, which promotes AKT; AKT, in turn, promotes mTOR and inhibits FOXO; the promotion of mTOR activates protein synthesis; and finally, the promotion of FOXO inhibits mTOR and promotes atrophy.

1.2.2 Calmodulin-Calcineurin-NFATc

Features like the fiber type and protein-isoform content of the adaptation are controled by the Calcineurin-NFATc signaling pathway [33, 144], the key molecules of this pathway are: (1) calmodulin (CaM), a Ca^{2+} sensor that changes its conformation state to target molecules for different cellular processes [31, 87, 109]; (2) calcineurin (CaN), a Ca-CaM-dependent phosphatase involved in many signal transduction pathways, including the regulation of inmune response genes [113, 139, 72]; and (3) nuclear factor of activated T cells (NFATc), a

family of nuclear factors, expressed by many cells, involved in the gene transcription of the inmune response and cell differentiation [134, 117, 1].

Briefly, sustained levels of Ca^{2+} allow Ca^{2+} to bind and activate CaM, which then binds to CaN and produces the active CaM-CaN complex; CaM-CaN complex dephosphorylates cytosolic NFATc, and allows its translocation to the nucleus.

1.3 Aim of the thesis

The aim of this thesis is to model the connections between the mechanical input (physical activity or training), the time course of the associated signaling pathways, and the adaptation that results from the cumulative effect of the mechanical input. Specifically:

- To set the mathematical description of the mechanobiological process involved in skeletal muscle adaptation.

- To evaluate, computationally, the process of hypertrophy and sarcomerogenesis during periodical loading stimuli (training periods).

- To evaluate, computationally, the process of atrophy in the absence of mechanical stimuli.

1.4 Outline

The content of the next chapters is briefly commented below.

Chapter 2 details the mathematics of the continuum mechanical description of skeletal muscle as a hyperelastic materials, which includes passive and active responses, and tissue growth.

Chapter 3 presents the particular strain energy functions used in this thesis, and shows the results of the numerical implementation of the continuum mechanical model. This mechanical model is used later on to build the feedback between the biochemical models (originated in the signaling pathways) and both the growth and active responses of the muscle structure.

Chapter 4 presents the biochemical model for the IGF1-AKT signaling pathway, validation applied to atrophy, hypertrophy and detraining, and numerical examples. All the procedures and results of this chapter consider constant parameters.

Chapter 5 describes the computational model that integrates the mechanical model (chapter 2 and 3), and the biochemical model (chapter 4). A growth tensor and a feedback function are constructed to integrate the models, and the biochemical model is compared to the mechanobiological one.

Chapter 6 describes the compartment model for the Calcineurin-NFATc signaling pathway that is used to control the gene program of individual fibers to target type I or type II characteristics. The model is validated to continuous and pulsed stimulation.

Chapter 7 presents the logistic model for the transition of the MLC of fibers type II into MLC of fibers type I. The transition is controlled by the two possible states of the gene program (related to the model developed in chapter Chapter 6). The transition of MLC is validated to continuous stimulation, no-stimulation, and periodic stimulation.

Chapter 8 revisits the mechanobiological model and uses the transition of MLC of the previous chapter to update the specific force of individual fibers, and a homogenization of the specific force is used to calculate the evolution of the maximum isometric tension of the mechanical active behavior. The model is validated to maximum voluntary contraction (MVC) and MVC per cross sectional area.

Finally, the main outcomes and future work are discussed in Chapter 9.

2 Mechanical description of skeletal muscle response

Skeletal muscles generate force when they contract voluntarily. During contraction, the sarcomere units shorten, and the muscle as a whole shortens as well, this process is called **active response**. The active response provides the ability to generate movement by considering the connection between muscles to bones. This connection is possible by an arrangement of connective tissue, which is the main contributor to the material force-stretch response known as **passive response**. During muscle contraction, a superposition of the active and passive responses occurs, whereas in a relaxed state, only the passive response takes place. In addition, biological tissues present the ability to grow, skeletal muscle in particular is characterized by a great adaptability modulated by loading conditions; the mechanical description of this feature is known as **tissue growth**.

The highly organized pattern of muscle fibers explains the transversely isotropic mechanical behavior of skeletal muscle tissue [168, 114, 171]. Therefore, a hyperelastic transversely isotropic model is suitable for the description of muscle mechanical response [76].

This chapter presents the description of the mechanical passive, active, and growth responses of skeletal muscle tissue. The fundamental concepts of motion, deformation gradient and the Cauchy-Green strain tensor [16, 76] are presented in section 2.1; a general description of transversely isotropic hyperelastic materials [16, 76] is presented in section 2.2; the special treatment of compressible materials [76, 175] (with the aim of describing the passive response of muscle tissue as a nearly incompressible material) is presented in section 2.3; the active response treatment [103, 74, 67] is introduced in section 2.4; and finally, the growth description [55, 61, 62] is presented in section 2.5.

This chapter is only a compilation of the continuum mechanics of muscle tissue description, readers with a clear understanding of the foundations of the field can go directly to chapter 3.

2.1 Motion and Deformation Gradient

A continuum body in its initial or reference configuration Ω_0 is composed by material points $\mathbf{X}$. As the continuum body moves or evolves, it changes to configuration Ω at time t (current configuration), and a material point $\mathbf{X}$ moves or evolves to position $\mathbf{x}$; the description of this

evolution is given by the motion $\boldsymbol{\varphi}$ such that:

$$\mathbf{x} = \boldsymbol{\varphi}(\mathbf{X}, t) \tag{2-1}$$

The motion of a segment of a curve $d\mathbf{X}$ in the reference configuration to a segment $d\mathbf{x}$ in the current configuration is described by the quantity $\mathbf{F}$, given by:

$$\mathbf{F} = \frac{\partial \boldsymbol{\varphi}}{\partial \mathbf{X}} = \frac{\partial \mathbf{x}}{\partial \mathbf{X}} \tag{2-2}$$

defined as the deformation gradient, which contains the fundamental description of the deformation of the continuum body. Another fundamental quantity is the Jacobian or volume ratio:

$$J = \det \mathbf{F} = \frac{dv}{dV} \tag{2-3}$$

A convenient quantity that also describes deformation is the Right Cauchy-Green strain tensor:

$$\mathbf{C} = \mathbf{F}^T \mathbf{F}, \tag{2-4}$$

which by construction is symmetric, positive definite, and therefore its eigen-values are positive.

2.2 Hyperelastic model for skeletal muscle: Passive Response

A hyperelastic material is a particular kind of material that can be described by a strain energy function (SEF) $\mathcal{W}$, which is a function of material points $\mathbf{X}$ and the deformation state $\mathbf{F}$ or $\mathbf{C}$. Given a SEF $\mathcal{W}(\mathbf{X}, \mathbf{C})$, the Second Piola-Kirchhoff (SPK) stress $\mathbf{S}$ is:

$$\mathbf{S} = 2 \frac{\partial \mathcal{W}}{\partial \mathbf{C}} \tag{2-5}$$

and the Elasticity tensor $\mathbb{C}$:

$$\mathbb{C} = 2 \frac{\partial \mathbf{S}}{\partial \mathbf{C}} \tag{2-6}$$

The organized pattern of skeletal muscle tissue suggests a transversely isotropic material, where the direction of the fibers (myofibers) is defined by the unit field vector $\mathbf{a}° = \mathbf{a}(\mathbf{X})$. When tissue deforms, the fiber direction deforms to $\mathbf{a}(\varphi(\mathbf{X}))$, the length of the fibers change, and the measure of the stretch λ can be calculated as:

$$\lambda \mathbf{a} = \mathbf{F} \mathbf{a}° \tag{2-7}$$

From the left side of the last relation:

$$(\lambda \mathbf{a}) \cdot (\lambda \mathbf{a}) = \lambda^2 \mathbf{a} \cdot \mathbf{a} = \lambda^2, \tag{2-8}$$

and the from the right side:

$$(\mathbf{F}\mathbf{a}°)(\mathbf{F}\mathbf{a}°) = (\mathbf{F}\mathbf{a}°)^T (\mathbf{F}\mathbf{a}°) = \mathbf{a}° \cdot \mathbf{F}^T \mathbf{F} \mathbf{a}° = \mathbf{a}° \cdot \mathbf{C} \mathbf{a}°, \tag{2-9}$$

And finally, from 2-8 and 2-9

$$\lambda^2 = \mathbf{a}° \cdot \mathbf{C} \mathbf{a}°. \tag{2-10}$$

This last relation states that to calculate the stretch λ of a fiber, only the undeformed direction $\mathbf{a}°$ and the deformation gradient (or the Cauchy-Green tensor) are required.
The dependence of the SEF on the fiber direction $\mathbf{a}°$ is explicit in transversely isotropic materials:

$$\mathscr{W} = \mathscr{W}(\mathbf{X}, \mathbf{C}, \mathbf{a}°). \tag{2-11}$$

The SEF is independent on the frame of reference; therefore, $\mathscr{W}$ is simplified by the use of its invariants:

$$I_1 = \operatorname{tr} \mathbf{C} \tag{2-12a}$$
$$I_2 = \frac{1}{2} \left[(\operatorname{tr} \mathbf{C})^2 - \operatorname{tr} \mathbf{C}^2 \right] \tag{2-12b}$$
$$I_3 = \det \mathbf{C} = J^2. \tag{2-12c}$$

By extension, to include the fiber direction $\mathbf{a}°$, two extra *pseudo-invariants* are introduced:

$$I_4 = \mathbf{a}° \cdot \mathbf{C} \mathbf{a}° \tag{2-13a}$$
$$I_5 = \mathbf{a}° \cdot \mathbf{C}^2 \mathbf{a}°. \tag{2-13b}$$

The introduction of the set of invariants of $\mathbf{C}$ and pseudo-invariants of $\mathbf{a}°$ allows an explicit form of the SEF with scalar arguments:

$$\mathscr{W} = \mathscr{W}(I_1, I_2, I_3, I_4, I_5) \tag{2-14}$$

2.2.1 Second Piola Kirchhooff stress

By using equation 2-14 and the chain rule, equation 2-5 is now:

$$\mathbf{S} = 2 \sum_{\alpha=1}^{5} \frac{\partial \mathscr{W}}{\partial I_\alpha} \frac{\partial I_\alpha}{\partial \mathbf{C}} = 2 \sum_{\alpha=1}^{5} \mathscr{W}_\alpha \frac{\partial I_\alpha}{\partial \mathbf{C}}, \tag{2-15}$$

where $\mathscr{W}_a = \frac{\partial \mathscr{W}}{\partial I_a}$.

Once an explicit SEF is given, according to relation 2-15, only the derivatives of the invariants contribute to the tensor structure of **S**. Fortunately, those derivatives can be calculated in closed forms:

$$\frac{\partial I_1}{\partial \mathbf{C}} = \mathbb{1} \tag{2-16a}$$

$$\frac{\partial I_2}{\partial \mathbf{C}} = I_1 \,\mathbb{1} - \mathbf{C} \tag{2-16b}$$

$$\frac{\partial I_3}{\partial \mathbf{C}} = I_3 \,\mathbf{C}^{-1} \tag{2-16c}$$

$$\frac{\partial I_4}{\partial \mathbf{C}} = \mathbf{a}^\circ \otimes \mathbf{a}^\circ \tag{2-16d}$$

$$\frac{\partial I_5}{\partial \mathbf{C}} = \mathbf{a}^\circ \otimes \mathbf{C}\,\mathbf{a}^\circ + \mathbf{a}^\circ \cdot \mathbf{C} \otimes \mathbf{a}^\circ, \tag{2-16e}$$

where $\mathbb{1}$ is the 2-nd order identity tensor.

By replacing the derivatives of the invariants in equation 2-15, and organizing, the general expression of the second Piola-Kirchhoff stress tensor for a transversely isotropic material is:

$$\mathbf{S} = 2\left[\left(\mathscr{W}_1 + I_1\,\mathscr{W}_2\right)\mathbb{1} - \mathscr{W}_2\,\mathbf{C} + I_3\,\mathscr{W}_3\,\mathbf{C}^{-1} + \mathscr{W}_4\,\mathbf{a}^\circ \otimes \mathbf{a}^\circ + \mathscr{W}_5\left(\mathbf{a}^\circ \otimes \mathbf{C}\,\mathbf{a}^\circ + \mathbf{a}^\circ \cdot \mathbf{C} \otimes \mathbf{a}^\circ\right)\right] \tag{2-17}$$

2.2.2 Elasticity tensor

By replacing 2-15 in 2-6:

$$\mathbb{C} = 4\frac{\partial}{\partial \mathbf{C}}\left(\sum_{a=1}^{5}\mathscr{W}_a \frac{\partial I_a}{\partial \mathbf{C}}\right) = 4\sum_{a=1}^{5}\left(\frac{\partial I_a}{\partial \mathbf{C}} \otimes \frac{\partial \mathscr{W}_a}{\partial \mathbf{C}} + \mathscr{W}_a\frac{\partial^2 I_a}{\partial \mathbf{C}\,\partial \mathbf{C}}\right). \tag{2-18}$$

Further developing $\frac{\partial \mathscr{W}_a}{\partial \mathbf{C}}$,

$$\mathbb{C} = 4\sum_{a=1}^{5}\left(\frac{\partial I_a}{\partial \mathbf{C}} \otimes \left(\sum_{b=1}^{5}\frac{\partial \mathscr{W}_a}{\partial I_b}\frac{\partial I_b}{\partial \mathbf{C}}\right) + \mathscr{W}_a\frac{\partial^2 I_a}{\partial \mathbf{C}\,\partial \mathbf{C}}\right)$$

using $\mathscr{W}_{ba} = \frac{\partial \mathscr{W}_a}{\partial I_b}$ and organizing:

$$\mathbb{C} = 4\sum_{a=1}^{5}\left(\sum_{b=1}^{5}\left(\mathscr{W}_{ba}\frac{\partial I_a}{\partial \mathbf{C}} \otimes \frac{\partial I_b}{\partial \mathbf{C}}\right) + \mathscr{W}_a\frac{\partial}{\partial \mathbf{C}}\left(\frac{\partial I_a}{\partial \mathbf{C}}\right)\right) \tag{2-19}$$

The last relation requires the second derivatives of the invariants of **C**:

$$\frac{\partial}{\partial \mathbf{C}}\left(\frac{\partial I_1}{\partial \mathbf{C}}\right) = \mathbb{0} \tag{2-20a}$$

$$\frac{\partial}{\partial \mathbf{C}}\left(\frac{\partial I_2}{\partial \mathbf{C}}\right) = \mathbb{1} \otimes \mathbb{1} - \mathbb{I} \tag{2-20b}$$

$$\frac{\partial}{\partial \mathbf{C}}\left(\frac{\partial I_3}{\partial \mathbf{C}}\right) = I_3\,\mathbf{C}^{-1} \otimes \mathbf{C}^{-1} + I_3\,\frac{\partial \mathbf{C}^{-1}}{\partial \mathbf{C}} \tag{2-20c}$$

$$\frac{\partial}{\partial \mathbf{C}}\left(\frac{\partial I_4}{\partial \mathbf{C}}\right) = \mathbb{0} \tag{2-20d}$$

$$\frac{\partial}{\partial \mathbf{C}}\left(\frac{\partial I_5}{\partial \mathbf{C}}\right) = \frac{\partial^2 I_5}{\partial \mathbf{C}\,\partial \mathbf{C}}, \tag{2-20e}$$

where $\mathbb{0}$ is the 4-th order zero tensor, and $\mathbb{I}$ is the 4-th order identity tensor.

By substituting 2-20 into equation 2-19, the general explicit form of the elasticity tensor is obtained.

$$
\begin{aligned}
\mathbb{C} = 4 \quad & \big[\left(\mathscr{W}_{11} + 2\,\mathscr{W}_{12}\,I_1 + \mathscr{W}_{22}\,I_1^2 + \mathscr{W}_2 \right) \mathbb{1} \otimes \mathbb{1} \\
& - \left(\mathscr{W}_{12} + \mathscr{W}_{22}\,I_1 \right) \left(\mathbf{C} \otimes \mathbb{1} + \mathbb{1} \otimes \mathbf{C} \right) \\
& + \mathscr{W}_{22}\,\mathbf{C} \otimes \mathbf{C} \\
& - \mathscr{W}_2\,\mathbb{I} \\
& + \left(\mathscr{W}_{13}\,I_3 + \mathscr{W}_{23}\,I_1\,I_3 \right) \left(\mathbf{C}^{-1} \otimes \mathbb{1} + \mathbb{1} \otimes \mathbf{C}^{-1} \right) \\
& - \mathscr{W}_{23}\,I_3 \left(\mathbf{C}^{-1} \otimes \mathbf{C} + \mathbf{C} \otimes \mathbf{C}^{-1} \right) \\
& + \left(\mathscr{W}_3\,I_3 + \mathscr{W}_{33}\,I_3^2 \right) \mathbf{C}^{-1} \otimes \mathbf{C}^{-1} \\
& + \mathscr{W}_{34}\,I_3 \left(\mathbf{C}^{-1} \otimes \mathbf{a}^\circ \otimes \mathbf{a}^\circ + \mathbf{a}^\circ \otimes \mathbf{a}^\circ \otimes \mathbf{C}^{-1} \right) \\
& + \mathscr{W}_{35}\,I_3 \left(\mathbf{C}^{-1} \otimes \frac{\partial I_5}{\partial \mathbf{C}} + \frac{\partial I_5}{\partial \mathbf{C}} \otimes \mathbf{C}^{-1} \right) \\
& + \left(\mathscr{W}_{14} + \mathscr{W}_{24}\,I_1 \right) \left(\mathbb{1} \otimes \mathbf{a}^\circ \otimes \mathbf{a}^\circ + \mathbf{a}^\circ \otimes \mathbf{a}^\circ \otimes \mathbb{1} \right) \\
& + \left(\mathscr{W}_{15} + \mathscr{W}_{25}\,I_1 \right) \left(\mathbb{1} \otimes \frac{\partial I_5}{\partial \mathbf{C}} + \frac{\partial I_5}{\partial \mathbf{C}} \otimes \mathbb{1} \right) \\
& - \mathscr{W}_{24} \left(\mathbf{C} \otimes \mathbf{a}^\circ \otimes \mathbf{a}^\circ + \mathbf{a}^\circ \otimes \mathbf{a}^\circ \otimes \mathbf{C} \right) \\
& - \mathscr{W}_{25} \left(\mathbf{C} \otimes \frac{\partial I_5}{\partial \mathbf{C}} + \frac{\partial I_5}{\partial \mathbf{C}} \otimes \mathbf{C} \right) \\
& + \mathscr{W}_{44}\,\mathbf{a}^\circ \otimes \mathbf{a}^\circ \otimes \mathbf{a}^\circ \otimes \mathbf{a}^\circ \\
& + \mathscr{W}_{45} \left(\mathbf{a}^\circ \otimes \mathbf{a}^\circ \otimes \frac{\partial I_5}{\partial \mathbf{C}} + \frac{\partial I_5}{\partial \mathbf{C}} \otimes \mathbf{a}^\circ \otimes \mathbf{a}^\circ \right) \\
& + \mathscr{W}_{55}\,\frac{\partial I_5}{\partial \mathbf{C}} \otimes \frac{\partial I_5}{\partial \mathbf{C}} \\
& + \mathscr{W}_3\,I_3\,\frac{\partial \mathbf{C}^{-1}}{\partial \mathbf{C}} \\
& + \mathscr{W}_5\,\frac{\partial^2 I_5}{\partial \mathbf{C}\,\partial \mathbf{C}} \, \big]
\end{aligned}
\tag{2-21}
$$

2.3 Compressible Hyperelastic model for skeletal muscle: Passive Response

Some materials behave differently in bulk compared to shear, in these cases it is convenient to split the deformation locally into a volumetric part (also known as dilational) and isochoric

part (also known as deviatoric). A common procedure to split the deformation gradient is the multiplicative decomposition:

$$\mathbf{F} = \mathbf{F}_{\mathrm{vol}}\,\overline{\mathbf{F}} \tag{2-22}$$

where $\mathbf{F}_{\mathrm{vol}}$ is the volumetric part of the deformation gradient $\mathbf{F}$, defined as:

$$\mathbf{F}_{\mathrm{vol}} = J^{1/3}\,\mathbb{1}. \tag{2-23}$$

From $\mathbf{F}_{\mathrm{vol}}$, the definition of the modified deformation gradient $\overline{\mathbf{F}}$ is given:

$$\overline{\mathbf{F}} = J^{-1/3}\,\mathbf{F}. \tag{2-24}$$

Using the modified deformation gradient in the Cauchy-Green tensor $\mathbf{C}$:

$$\mathbf{C} = \mathbf{F}^T\,\mathbf{F} = \left(J^{1/3}\,\overline{\mathbf{F}}^T\right)\left(J^{1/3}\,\overline{\mathbf{F}}\right) = J^{2/3}\,\overline{\mathbf{F}}^T\,\overline{\mathbf{F}} = J^{2/3}\,\overline{\mathbf{C}}. \tag{2-25}$$

From the last relation, the modified Cauchy-Green tensor is defined as:

$$\overline{\mathbf{C}} = J^{-2/3}\,\mathbf{C}, \tag{2-26}$$

and the modified invariants as:

$$\overline{I}_1 = \mathrm{tr}\,\overline{\mathbf{C}} = J^{-2/3}\,I_1 \tag{2-27a}$$

$$\overline{I}_2 = \frac{1}{2}\left[\left(\mathrm{tr}\,\overline{\mathbf{C}}\right)^2 - \mathrm{tr}\,\overline{\mathbf{C}}^2\right] = J^{-4/3}\,I_2 \tag{2-27b}$$

$$\overline{I}_3 = \det\overline{\mathbf{C}} = J^{-2}\,I_3 \tag{2-27c}$$

$$\overline{I}_4 = \mathbf{a}°\cdot\overline{\mathbf{C}}\,\mathbf{a}° = J^{-2/3}\,I_4 \tag{2-27d}$$

$$\overline{I}_5 = \mathbf{a}°\cdot\overline{\mathbf{C}}^2\,\mathbf{a}° = J^{-4/3}\,I_5. \tag{2-27e}$$

The split of the deformation is also considered in a decoupled form of the SEF: The volumetric part of the deformation captures the contribution of the volume fraction J (which defines I_3 according to 2-12c), and is obtained from the volumetric part of the SEF $\mathcal{W}_{\mathrm{vol}}(J)$; the isochoric part of the deformation captures the contribution of all invariants of $\overline{\mathbf{C}}$ except $\overline{I}_3$ and is obtained from the isochoric part of the SEF $\mathcal{W}_{\mathrm{iso}}\left(\overline{I}_1,\overline{I}_2,\overline{I}_4,\overline{I}_5\right)$. The decoupled SEF is:

$$\mathcal{W}\left(I_1,I_2,I_3,I_4,I_5\right) = \mathcal{W}_{\mathrm{vol}}\left(J\right) + \mathcal{W}_{\mathrm{iso}}\left(\overline{I}_1,\overline{I}_2,\overline{I}_4,\overline{I}_5\right) \tag{2-28}$$

The use of the decoupled SEF produce some consequences on the SPK stress tensor and elasticity tensor, but the definitions given in equations 2-5 and 2-6 remain unchanged. The consequences are presented below.

2.3.1 Decoupled Second Piola Kirchhoff stress

The use of the decoupled SEF leads to a decoupled $\mathbf{S}$:

$$\mathbf{S} = 2\,\frac{\partial \mathscr{W}}{\partial \mathbf{C}} = 2\,\frac{\partial \mathscr{W}_{\mathrm{vol}}\left(J\right)}{\partial \mathbf{C}} + 2\,\frac{\partial \mathscr{W}_{\mathrm{iso}}\left(\overline{I}_1, \overline{I}_2, \overline{I}_4, \overline{I}_5\right)}{\partial \mathbf{C}} \tag{2-29}$$

$$\mathbf{S} = \mathbf{S}_{\mathrm{vol}} + \mathbf{S}_{\mathrm{iso}} \tag{2-30}$$

2.3.1.1 Volumetric part of $\mathbf{S}$

By the chain rule,

$$\mathbf{S}_{\mathrm{vol}} = 2\,\frac{\partial \mathscr{W}_{\mathrm{vol}}\left(J\right)}{\partial \mathbf{C}} = 2\,\frac{\partial \mathscr{W}_{\mathrm{vol}}\left(J\right)}{\partial J}\,\frac{\partial J}{\partial \mathbf{C}} \tag{2-31}$$

The derivative of J is obtained from equation 2-12c, and making use of the derivative of I_3 given in equation 2-16c:

$$\frac{\partial J}{\partial \mathbf{C}} = \frac{\partial J}{\partial I_3}\,\frac{\partial I_3}{\partial \mathbf{C}} = \frac{\partial I_3^{1/2}}{\partial I_3}\,I_3\,\mathbf{C}^{-1} = \frac{1}{2}\,I_3^{1/2}\,\mathbf{C}^{-1} = \frac{1}{2}\,J\,\mathbf{C}^{-1} \tag{2-32}$$

Calling $p = \partial \mathscr{W}_{\mathrm{vol}}\left(J\right)/\partial J$, the volumetric part of SPK is:

$$\mathbf{S}_{\mathrm{vol}} = J\,p\,\mathbf{C}^{-1} \tag{2-33}$$

2.3.1.2 Isochoric part of $\mathbf{S}$

By the chain rule,

$$\mathbf{S}_{\mathrm{iso}} = 2\,\frac{\partial \mathscr{W}_{\mathrm{iso}}\left(\overline{I}_1, \overline{I}_2, \overline{I}_4, \overline{I}_5\right)}{\partial \mathbf{C}} = 2\,\frac{\partial \mathscr{W}_{\mathrm{iso}}\left(\overline{I}_1, \overline{I}_2, \overline{I}_4, \overline{I}_5\right)}{\partial \overline{\mathbf{C}}} : \frac{\partial \overline{\mathbf{C}}}{\partial \mathbf{C}} \tag{2-34}$$

First, the fourth rank tensor $\partial \overline{\mathbf{C}}/\partial \mathbf{C}$ is developed:

$$\begin{aligned}
\frac{\partial \overline{\mathbf{C}}}{\partial \mathbf{C}} = \ & \frac{\partial J^{-2/3}\mathbf{C}}{\partial \mathbf{C}} = \mathbf{C} \otimes \frac{\partial J^{-2/3}}{\partial \mathbf{C}} + J^{-2/3}\,\frac{\partial \mathbf{C}}{\partial \mathbf{C}} \\
= \ & \mathbf{C} \otimes \frac{\partial J^{-2/3}}{\partial J}\,\frac{\partial J}{\partial \mathbf{C}} + J^{-2/3}\,\mathbb{I} \\
= \ & \mathbf{C} \otimes \left(-\frac{2}{3}\,J^{-5/3}\right)\left(\frac{J}{2}\,\mathbf{C}^{-1}\right) + J^{-2/3}\,\mathbb{I} \\
= \ & J^{-2/3}\left(\mathbb{I} - \frac{1}{3}\,\mathbf{C} \otimes \mathbf{C}^{-1}\right) \\
= \ & J^{-2/3}\,\mathbb{P}^{T},
\end{aligned} \tag{2-35}$$

where the projector $\mathbb{P}$ has been defined as:

$$\mathbb{P}^T = \mathbb{I} - \frac{1}{3}\,\mathbf{C} \otimes \mathbf{C}^{-1}, \qquad \mathbb{P} = \mathbb{I} - \frac{1}{3}\,\mathbf{C}^{-1} \otimes \mathbf{C}. \tag{2-36}$$

Equation 2-34 can also be written as

$$\mathbf{S}_{\text{iso}} = 2\,\frac{\partial\,\mathscr{W}_{\text{iso}}\left(\overline{I}_1,\overline{I}_2,\overline{I}_4,\overline{I}_5\right)}{\partial\overline{\mathbf{C}}} : \frac{\partial\overline{\mathbf{C}}}{\partial\mathbf{C}} = 2\left(\frac{\partial\overline{\mathbf{C}}}{\partial\mathbf{C}}\right)^T : \frac{\partial\,\mathscr{W}_{\text{iso}}\left(\overline{I}_1,\overline{I}_2,\overline{I}_4,\overline{I}_5\right)}{\partial\overline{\mathbf{C}}}, \tag{2-37}$$

and with the use of result 2-35, $\mathbf{S}_{\text{iso}}$ is finally obtained:

$$\mathbf{S}_{\text{iso}} = J^{-2/3}\,\mathbb{P} : \overline{\mathbf{S}}, \qquad \overline{\mathbf{S}} = 2\,\frac{\partial\,\mathscr{W}_{\text{iso}}\left(\overline{I}_1,\overline{I}_2,\overline{I}_4,\overline{I}_5\right)}{\partial\overline{\mathbf{C}}} \tag{2-38}$$

$\overline{\mathbf{S}}$ is mathematically equal to the expression in 2-17 evaluated in $\overline{I}_i$, except for the term $\overline{I}_3\,\mathscr{W}_3\,\overline{\mathbf{C}}^{-1}$, which vanishes because $\mathscr{W}_{\text{iso}}$ does not depend on $\overline{I}_3$. Actually, the term $\overline{I}_3\,\mathscr{W}_3\,\overline{\mathbf{C}}^{-1}$ is $\mathbf{S}_{\text{vol}}$ given in equation 2-33.

2.3.2 Decoupled elasticity tensor

The use of the decoupled SEF leads to a decoupled elasticity tensor $\mathbb{C}$:

$$\mathbb{C} = 2\,\frac{\partial\mathbf{S}}{\partial\mathbf{C}} = 2\,\frac{\partial\mathbf{S}_{\text{vol}}}{\partial\mathbf{C}} + 2\,\frac{\partial\mathbf{S}_{\text{iso}}}{\partial\mathbf{C}} \tag{2-39}$$

$$\mathbb{C} = \mathbb{C}_{\text{vol}} + \mathbb{C}_{\text{iso}} \tag{2-40}$$

2.3.2.1 Volumetric part of $\mathbb{C}$

Using 2-33,

$$\begin{aligned}\mathbb{C}_{\text{vol}} = \quad & 2\,\frac{\partial\mathbf{S}_{\text{vol}}}{\partial\mathbf{C}} = 2\,\frac{\partial\,J\,p\,\mathbf{C}^{-1}}{\partial\mathbf{C}} = 2\,\mathbf{C}^{-1} \otimes \frac{\partial\,J\,p}{\partial\mathbf{C}} + 2\,J\,p\,\frac{\partial\,\mathbf{C}^{-1}}{\partial\mathbf{C}} \\ & = 2\,\mathbf{C}^{-1} \otimes \left(J\,\frac{\partial p}{\partial\mathbf{C}} + p\,\frac{\partial J}{\partial\mathbf{C}}\right) - 2\,J\,p\,\mathbf{C}^{-1} \odot \mathbf{C}^{-1},\end{aligned} \tag{2-41}$$

where the fourth rank tensor $\mathbf{C}^{-1} \odot \mathbf{C}^{-1}$ has been defined as:

$$\frac{\partial\,\mathbf{C}^{-1}}{\partial\mathbf{C}} = -\mathbf{C}^{-1} \odot \mathbf{C}^{-1} \tag{2-42}$$

In equation 2-41, the term $\partial p/\partial\mathbf{C}$, by the chain rule, is simply $(\partial p/\partial J)(\partial J/\partial\mathbf{C})$. Using $\partial J/\partial\mathbf{C}$ from equation 2-32 and organizing, equation 2-41 becomes:

$$\mathbb{C}_{\text{vol}} = J\tilde{p}\,\mathbf{C}^{-1} \otimes \mathbf{C}^{-1} - 2\,J\,p\,\mathbf{C}^{-1} \odot \mathbf{C}^{-1} \tag{2-43}$$

where $\tilde{p}$ was defined as:

$$\tilde{p} = J \frac{\partial p}{\partial J} + p. \tag{2-44}$$

To see the index form of $\partial \mathbf{C}^{-1}/\partial \mathbf{C}$, first consider the derivative of the 2-nd order identity tensor:

$$\left(\frac{\partial \mathbb{1}}{\partial \mathbf{C}} \right)_{ijkl} = 0$$

$$\left(\frac{\partial \left(\mathbf{C}\,\mathbf{C}^{-1} \right)}{\partial \mathbf{C}} \right)_{ijkl} = \frac{\partial \left(C_{im}\, C_{mj}^{-1} \right)}{\partial C_{kl}} = 0 \tag{2-45}$$

$$\frac{\partial\, C_{im}}{\partial C_{kl}}\, C_{mj}^{-1} + C_{im} \frac{\partial\, C_{mj}^{-1}}{\partial C_{kl}} = 0$$

The second term of the left hand side includes $\partial \mathbf{C}^{-1}/\partial \mathbf{C}$,

$$C_{im} \frac{\partial\, C_{mj}^{-1}}{\partial C_{kl}} = -\frac{\partial\, C_{im}}{\partial C_{kl}}\, C_{mj}^{-1}$$

$$C_{ni}^{-1}\, C_{im} \frac{\partial\, C_{mj}^{-1}}{\partial C_{kl}} = -C_{ni}^{-1} \frac{\partial\, C_{im}}{\partial C_{kl}}\, C_{mj}^{-1} \tag{2-46}$$

$$\delta_{nm} \frac{\partial\, C_{mj}^{-1}}{\partial C_{kl}} = -C_{ni}^{-1} \frac{1}{2} \left(\delta_{ik}\, \delta_{ml} + \delta_{il}\, \delta_{mk} \right) C_{mj}^{-1}$$

$$\frac{\partial\, C_{nj}^{-1}}{\partial C_{kl}} = -\frac{1}{2} \left(C_{nk}^{-1}\, C_{lj}^{-1} + C_{nl}^{-1}\, C_{kj}^{-1} \right)$$

Changing index n for i, and using the symmetry of $\mathbf{C}$

$$\left(\frac{\partial\, \mathbf{C}^{-1}}{\partial \mathbf{C}} \right)_{ijkl} = -\frac{1}{2} \left(C_{ik}^{-1}\, C_{jl}^{-1} + C_{il}^{-1}\, C_{jk}^{-1} \right) = \left(-\mathbf{C}^{-1} \odot \mathbf{C}^{-1} \right)_{ijkl} \tag{2-47}$$

2.3.2.2 Isochoric part of $\mathbb{C}$

Using $\mathbf{S}_{\text{iso}}$ defined in 2-38:

$$\mathbb{C}_{\text{iso}} = 2 \frac{\partial\, \mathbf{S}_{\text{iso}}}{\partial \mathbf{C}} = 2 \frac{\partial\, J^{-2/3}\, \mathbb{P} : \overline{\mathbf{S}}}{\partial \mathbf{C}} = 2 \left(\mathbb{P} : \overline{\mathbf{S}} \right) \otimes \frac{\partial\, J^{-2/3}}{\partial \mathbf{C}} + 2\, J^{-2/3} \frac{\partial\, \mathbb{P} : \overline{\mathbf{S}}}{\partial \mathbf{C}} \tag{2-48}$$

In this equation, the term $\partial\, J^{-2/3}/\partial \mathbf{C}$, by the chain rule, is $(\partial\, J^{-2/3}/\partial J)(\partial\, J/\partial \mathbf{C})$. Using $\partial\, J/\partial \mathbf{C}$ from equation 2-32, $\mathbb{P}$ from equation 2-36, and organizing:

$$\mathbb{C}_{\text{iso}} = -\frac{2}{3}\, J^{-2/3} \left(\mathbb{P} : \overline{\mathbf{S}} \right) \otimes \mathbf{C}^{-1} + 2\, J^{-2/3} \frac{\partial}{\partial \mathbf{C}} \left(\overline{\mathbf{S}} - \frac{1}{3} \left(\mathbf{C}^{-1} \otimes \mathbf{C} \right) : \overline{\mathbf{S}} \right) \tag{2-49}$$

$\mathbf{S}_{\text{iso}}$ can be recognized in the first term. To address the second term, first notice that:

$$\mathbf{C}^{-1} \otimes \mathbf{C} = \left(J^{-2/3}\, \overline{\mathbf{C}}^{-1} \right) \otimes \left(J^{2/3}\, \overline{\mathbf{C}} \right) = \overline{\mathbf{C}}^{-1} \otimes \overline{\mathbf{C}} \tag{2-50}$$

and then,

$$\left(\overline{\mathbf{C}}^{-1} \otimes \overline{\mathbf{C}} \right) : \overline{\mathbf{S}} = \left(\overline{\mathbf{C}} : \overline{\mathbf{S}} \right) \overline{\mathbf{C}}^{-1} = \left(\overline{\mathbf{S}} : \overline{\mathbf{C}} \right) \overline{\mathbf{C}}^{-1}. \tag{2-51}$$

Now, using the chain rule and replacing the result of equation 2-51 into 2-49:

$$\mathbb{C}_{\text{iso}} = -\frac{2}{3}\, \mathbf{S}_{\text{iso}} \otimes \mathbf{C}^{-1} + 2\, J^{-2/3}\, \frac{\partial}{\partial \overline{\mathbf{C}}} \left(\overline{\mathbf{S}} - \frac{1}{3}\, \left(\overline{\mathbf{S}} : \overline{\mathbf{C}} \right) \overline{\mathbf{C}}^{-1} \right) : \frac{\partial \overline{\mathbf{C}}}{\partial \mathbf{C}}. \tag{2-52}$$

In this equation, replacing $\partial \overline{\mathbf{C}}/\partial \mathbf{C}$ from equation 2-35, and expanding the second term:

$$\mathbb{C}_{\text{iso}} = -\frac{2}{3}\, \mathbf{S}_{\text{iso}} \otimes \mathbf{C}^{-1} + 2\, J^{-4/3}\, \frac{\partial \overline{\mathbf{S}}}{\partial \overline{\mathbf{C}}} : \mathbb{P}^{T} - \frac{2}{3}\, J^{-4/3}\, \frac{\partial \left(\overline{\mathbf{S}} : \overline{\mathbf{C}} \right) \overline{\mathbf{C}}^{-1}}{\partial \overline{\mathbf{C}}} : \mathbb{P}^{T} \tag{2-53}$$

Remark that $2\, \partial \overline{\mathbf{S}}/\partial \overline{\mathbf{C}}$ is mathematically equal to 2-21 evaluated in $\overline{I}_i$ except for all terms involving $\overline{I}_3$, and derivatives of $\mathscr{W}_{\text{iso}}$ with respect to $\overline{I}_3$ vanish because $\mathscr{W}_{\text{iso}}$ does not depend on $\overline{I}_3$. Here $\overline{\mathbb{C}}$ is introduced:

$$\overline{\mathbb{C}} = 2\, J^{-4/3}\, \frac{\partial \overline{\mathbf{S}}}{\partial \overline{\mathbf{C}}}. \tag{2-54}$$

And now, the last term of 2-53 without $\mathbb{P}^{T}$ is developed:

$$2\, J^{-4/3}\, \frac{\partial \left(\overline{\mathbf{S}} : \overline{\mathbf{C}} \right) \overline{\mathbf{C}}^{-1}}{\partial \overline{\mathbf{C}}} = 2\, J^{-4/3}\, \overline{\mathbf{C}}^{-1} \otimes \frac{\partial \left(\overline{\mathbf{S}} : \overline{\mathbf{C}} \right)}{\partial \overline{\mathbf{C}}} + 2\, J^{-4/3}\, \left(\overline{\mathbf{S}} : \overline{\mathbf{C}} \right) \frac{\partial \overline{\mathbf{C}}^{-1}}{\partial \overline{\mathbf{C}}}. \tag{2-55}$$

The first term of 2-55 is:

$$\begin{aligned} 2\, J^{-4/3}\, \overline{\mathbf{C}}^{-1} \otimes \frac{\partial \left(\overline{\mathbf{S}} : \overline{\mathbf{C}} \right)}{\partial \overline{\mathbf{C}}} \quad &= \overline{\mathbf{C}}^{-1} \otimes \left(\overline{\mathbf{C}} : 2\, J^{-4/3}\, \frac{\partial \overline{\mathbf{S}}}{\partial \overline{\mathbf{C}}} + 2\, J^{-4/3}\, \overline{\mathbf{S}} : \frac{\partial \overline{\mathbf{C}}}{\partial \overline{\mathbf{C}}} \right) \\ &= \overline{\mathbf{C}}^{-1} \otimes \left(\overline{\mathbf{C}} : \overline{\mathbb{C}} + 2\, J^{-4/3}\, \overline{\mathbf{S}} \right) \end{aligned} \tag{2-56}$$

where definition 2-54 and $\overline{\mathbf{S}} : \mathbb{I} = \overline{\mathbf{S}}$ were replaced. Finally, using $\overline{\mathbf{C}}^{-1} \otimes \overline{\mathbf{C}}$ from 2-50, and $\overline{\mathbf{C}}^{-1} = J^{2/3}\, \mathbf{C}^{-1}$ from equation 2-26, the result is:

$$2\, J^{-4/3}\, \overline{\mathbf{C}}^{-1} \otimes \frac{\partial \left(\overline{\mathbf{S}} : \overline{\mathbf{C}} \right)}{\partial \overline{\mathbf{C}}} = \mathbf{C}^{-1} \otimes \mathbf{C} : \overline{\mathbb{C}} + 2\, J^{-2/3}\, \mathbf{C}^{-1} \otimes \overline{\mathbf{S}}. \tag{2-57}$$

The second term of 2-55 is:

$$2\, J^{-4/3}\, \left(\overline{\mathbf{S}} : \overline{\mathbf{C}} \right) \frac{\partial \overline{\mathbf{C}}^{-1}}{\partial \overline{\mathbf{C}}} = 2\, J^{-4/3}\, \left(\overline{\mathbf{S}} : J^{-2/3}\, \mathbf{C} \right) \left(-\overline{\mathbf{C}}^{-1} \odot \overline{\mathbf{C}}^{-1} \right) \tag{2-58}$$

where $\partial \overline{\mathbf{C}}^{-1}/\partial \overline{\mathbf{C}}$ from equation 2-42 was replaced. Noticing that $\overline{\mathbf{C}}^{-1} \odot \overline{\mathbf{C}}^{-1} = J^{2/3}\,\mathbf{C}^{-1} \odot J^{2/3}\,\mathbf{C}^{-1}$:

$$2\,J^{-4/3}\left(\overline{\mathbf{S}}:\overline{\mathbf{C}}\right)\frac{\partial \overline{\mathbf{C}}^{-1}}{\partial \overline{\mathbf{C}}} = 2\,J^{-2/3}\left(\overline{\mathbf{S}}:\mathbf{C}\right)\left(-\mathbf{C}^{-1}\odot\mathbf{C}^{-1}\right) \tag{2-59}$$

Replacing 2-57 and 2-59 in 2-55:

$$2\,J^{-4/3}\frac{\partial \left(\overline{\mathbf{S}}:\overline{\mathbf{C}}\right)\overline{\mathbf{C}}^{-1}}{\partial \overline{\mathbf{C}}} = \mathbf{C}^{-1}\otimes\mathbf{C}:\overline{\mathbb{C}} + 2\,J^{-2/3}\,\mathbf{C}^{-1}\otimes\overline{\mathbf{S}} + 2\,J^{-2/3}\left(\overline{\mathbf{S}}:\mathbf{C}\right)\left(-\mathbf{C}^{-1}\odot\mathbf{C}^{-1}\right). \tag{2-60}$$

Replacing the last equation and equation 2-54 in 2-53:

$$\begin{aligned}
\mathbb{C}_{\text{iso}} = \quad & -\frac{2}{3}\mathbf{S}_{\text{iso}}\otimes\mathbf{C}^{-1} + \overline{\mathbb{C}}:\mathbb{P}^{T} \\
& -\frac{1}{3}\left[\mathbf{C}^{-1}\otimes\mathbf{C}:\overline{\mathbb{C}} + 2\,J^{-2/3}\,\mathbf{C}^{-1}\otimes\overline{\mathbf{S}} - 2\,J^{-2/3}\left(\overline{\mathbf{S}}:\mathbf{C}\right)\left(\mathbf{C}^{-1}\odot\mathbf{C}^{-1}\right)\right]:\mathbb{P}^{T}
\end{aligned} \tag{2-61}$$

Distributing $\mathbb{P}^{T}$ in the second line:

$$\begin{aligned}
\mathbb{C}_{\text{iso}} = \quad & -\frac{2}{3}\mathbf{S}_{\text{iso}}\otimes\mathbf{C}^{-1} + \overline{\mathbb{C}}:\mathbb{P}^{T} - \frac{1}{3}\mathbf{C}^{-1}\otimes\mathbf{C}:\overline{\mathbb{C}}:\mathbb{P}^{T} - \frac{2}{3}\,J^{-2/3}\,\mathbf{C}^{-1}\otimes\overline{\mathbf{S}}:\mathbb{P}^{T} \\
& -\frac{2}{3}\,J^{-2/3}\left(\overline{\mathbf{S}}:\mathbf{C}\right)\left(-\mathbf{C}^{-1}\odot\mathbf{C}^{-1}\right):\mathbb{P}^{T}
\end{aligned} \tag{2-62}$$

In the second and third term of the last equation, $\overline{\mathbb{C}}:\mathbb{P}^{T}$ can be factorized, after that, $\mathbb{P}$ can be recognized. The fourth term of the last equation ($J^{-2/3}\,\mathbf{C}^{-1}\otimes\overline{\mathbf{S}}:\mathbb{P}^{T}$) is simply $\mathbf{C}^{-1}\otimes\mathbf{S}_{\text{iso}}$ (see equation 2-38). Developing these observations and organizing:

$$\mathbb{C}_{\text{iso}} = \quad \mathbb{P}:\overline{\mathbb{C}}:\mathbb{P}^{T} - \frac{2}{3}\left(\mathbf{S}_{\text{iso}}\otimes\mathbf{C}^{-1} + \mathbf{C}^{-1}\otimes\mathbf{S}_{\text{iso}}\right) - \frac{2}{3}\,J^{-2/3}\left(\overline{\mathbf{S}}:\mathbf{C}\right)\left(-\mathbf{C}^{-1}\odot\mathbf{C}^{-1}\right):\mathbb{P}^{T} \tag{2-63}$$

The term $\left(-\mathbf{C}^{-1}\odot\mathbf{C}^{-1}\right):\mathbb{P}^{T}$, using 2-42 and 2-36, is developed as:

$$\left(-\mathbf{C}^{-1}\odot\mathbf{C}^{-1}\right):\mathbb{P}^{T} = \frac{\partial\mathbf{C}^{-1}}{\partial\mathbf{C}}:\left(\mathbb{I} - \frac{1}{3}\mathbf{C}\otimes\mathbf{C}^{-1}\right) = \frac{\partial\mathbf{C}^{-1}}{\partial\mathbf{C}}:\mathbb{I} - \frac{1}{3}\frac{\partial\mathbf{C}^{-1}}{\partial\mathbf{C}}:\mathbf{C}\otimes\mathbf{C}^{-1} \tag{2-64}$$

Now, using the index notation of $\partial\mathbf{C}^{-1}/\partial\mathbf{C}$ given in 2-47, the final term on the right hand side of equation 2-64 in index notation is:

$$\begin{aligned}
\left(\frac{\partial\mathbf{C}^{-1}}{\partial\mathbf{C}}\right)_{ijkl}\left(\mathbf{C}\otimes\mathbf{C}^{-1}\right)_{klmn} \quad & = -\frac{1}{2}\left(C_{ik}^{-1}C_{jl}^{-1} + C_{il}^{-1}C_{jk}^{-1}\right)C_{kl}\,C_{mn}^{-1} \\
& = -\frac{1}{2}\left(C_{ik}^{-1}C_{kl}\,C_{jl}^{-1}C_{mn}^{-1} + C_{il}^{-1}C_{jk}^{-1}C_{kl}\,C_{mn}^{-1}\right) \\
& = -\frac{1}{2}\left(\delta_{il}\,C_{jl}^{-1}C_{mn}^{-1} + C_{il}^{-1}\delta_{jl}\,C_{mn}^{-1}\right) \\
& = -\frac{1}{2}\left(C_{ji}^{-1}C_{mn}^{-1} + C_{ij}^{-1}C_{mn}^{-1}\right) \\
& = -\frac{1}{2}\left(C_{ij}^{-1}C_{mn}^{-1} + C_{ij}^{-1}C_{mn}^{-1}\right) \\
& = \left(-\mathbf{C}^{-1}\otimes\mathbf{C}^{-1}\right)_{ijmn}.
\end{aligned} \tag{2-65}$$

with this result for the last term of 2-64, and 2-42 for the first, equation 2-64 becomes:

$$\left(-\mathbf{C}^{-1} \odot \mathbf{C}^{-1}\right) : \mathbb{P}^{T} = -\mathbf{C}^{-1} \odot \mathbf{C}^{-1} + \frac{1}{3}\mathbf{C}^{-1} \otimes \mathbf{C}^{-1} \tag{2-66}$$

This last result, was required in equation 2-63; in that equation, to have a complete expression for $\mathbb{C}_{\text{iso}}$ independent of $\mathbb{P}$, developing $\mathbb{P} : \overline{\mathbb{C}} : \mathbb{P}^{T}$ is necessary:

$$\begin{aligned}
\mathbb{P} : \overline{\mathbb{C}} : \mathbb{P}^{T} &= \left(\mathbb{I} - \frac{1}{3}\mathbf{C}^{-1} \otimes \mathbf{C}\right) : \overline{\mathbb{C}} : \left(\mathbb{I} - \frac{1}{3}\mathbf{C} \otimes \mathbf{C}^{-1}\right) \\
&= \mathbb{I} : \overline{\mathbb{C}} : \mathbb{I} - \frac{1}{3}\mathbf{C}^{-1} \otimes \mathbf{C} : \overline{\mathbb{C}} : \mathbb{I} - \frac{1}{3}\mathbb{I} : \overline{\mathbb{C}} : \mathbf{C} \otimes \mathbf{C}^{-1} + \frac{1}{9}\mathbf{C}^{-1} \otimes \mathbf{C} : \overline{\mathbb{C}} : \mathbf{C} \otimes \mathbf{C}^{-1},
\end{aligned} \tag{2-67}$$

Notice that, from the definition of $\mathbb{C}$ (equation 2-6), and the definition of $\mathbf{S}$ (equation 2-5), $\mathbb{C}_{ijkl} = \frac{\partial}{\partial C_{kl}}\frac{\partial \mathcal{W}}{\partial C_{ij}} = \frac{\partial}{\partial C_{ij}}\frac{\partial \mathcal{W}}{\partial C_{kl}}$; therefore $\mathbb{C} = \mathbb{C}^{T}$, which is also valid for $\overline{\mathbb{C}}$, then:

$$\mathbf{C} : \overline{\mathbb{C}} = \overline{\mathbb{C}}^{T} : \mathbf{C} = \overline{\mathbb{C}} : \mathbf{C}. \tag{2-68}$$

Using the previous result in 2-67, and factorizing:

$$\mathbb{P} : \overline{\mathbb{C}} : \mathbb{P}^{T} = \overline{\mathbb{C}} - \frac{1}{3}\left(\mathbf{C}^{-1} \otimes \left(\overline{\mathbb{C}} : \mathbf{C}\right) + \left(\overline{\mathbb{C}} : \mathbf{C}\right) \otimes \mathbf{C}^{-1}\right) + \frac{1}{9}\left(\mathbf{C} : \overline{\mathbb{C}} : \mathbf{C}\right)\mathbf{C}^{-1} \otimes \mathbf{C}^{-1} \tag{2-69}$$

Finally, using 2-66 and 2-69 in equation 2-63, the final expression for $\mathbb{C}_{\text{iso}}$ is:

$$\begin{aligned}
\mathbb{C}_{\text{iso}} = \quad &\overline{\mathbb{C}} - \frac{1}{3}\left(\mathbf{C}^{-1} \otimes \left(\overline{\mathbb{C}} : \mathbf{C}\right) + \left(\overline{\mathbb{C}} : \mathbf{C}\right) \otimes \mathbf{C}^{-1}\right) + \frac{1}{9}\left(\mathbf{C} : \overline{\mathbb{C}} : \mathbf{C}\right)\mathbf{C}^{-1} \otimes \mathbf{C}^{-1} \\
&+ \frac{2}{3}J^{-2/3}\left(\overline{\mathbf{S}} : \mathbf{C}\right)\left(\mathbf{C}^{-1} \odot \mathbf{C}^{-1} - \frac{1}{3}\mathbf{C}^{-1} \otimes \mathbf{C}^{-1}\right) \\
&- \frac{2}{3}\left(\mathbf{S}_{\text{iso}} \otimes \mathbf{C}^{-1} + \mathbf{C}^{-1} \otimes \mathbf{S}_{\text{iso}}\right),
\end{aligned} \tag{2-70}$$

where $\overline{\mathbf{S}}$ and $\mathbf{S}_{\text{iso}}$ were defined in equation 2-38, and $\overline{\mathbb{C}}$ was defined in equation 2-54.

2.4 Hyperelastic model for skeletal muscle: Active Response

The aim of this section is to build the SPK stress $(\mathbf{S}_{\text{a}})$ and elasticity tensor $(\mathbb{C}_{a})$ contributions due to the active behavior of muscle tissue. First, based on a split decomposition of the modified deformation gradient, some definitions are presented; after that, a SEF for the active behavior is introduced; and finally the $\mathbf{S}_{\text{a}}$ and $\mathbb{C}_{a}$ are developed.

The active response will be considered in a decomposition of the modified deformation gradient $\overline{\mathbf{F}}$ into an elastic part $\overline{\mathbf{F}}_{e}$, and an active part $\overline{\mathbf{F}}_{a}$ that represents the deformation due

to sarcomere contraction and, therefore, depends only on the fiber directions ($\overline{\mathbf{F}}_a$ will be addressed in the next chapter):

$$\overline{\mathbf{F}} = \overline{\mathbf{F}}_e \overline{\mathbf{F}}_a. \tag{2-71}$$

from this relation,

$$\overline{\mathbf{F}}_e = \overline{\mathbf{F}}\, \overline{\mathbf{F}}_a^{-1}, \qquad \overline{\mathbf{F}}_e^{T} = \overline{\mathbf{F}}_a^{-T} \overline{\mathbf{F}}^{T} \tag{2-72}$$

Following the definition of the Cauchy-Green tensor:

$$\overline{\mathbf{C}}_e = \overline{\mathbf{F}}_e^{T}\, \overline{\mathbf{F}}_e, \tag{2-73}$$

replacing 2-72,

$$\overline{\mathbf{C}}_e = \overline{\mathbf{F}}_a^{-T}\, \overline{\mathbf{F}}^{T}\, \overline{\mathbf{F}}\, \overline{\mathbf{F}}_a^{-1} = \overline{\mathbf{F}}_a^{-T}\, \overline{\mathbf{C}}\, \overline{\mathbf{F}}_a^{-1} = J^{-2/3}\, \overline{\mathbf{F}}_a^{-T}\, \mathbf{C}\, \overline{\mathbf{F}}_a^{-1} \tag{2-74}$$

where the definition of $\overline{\mathbf{C}}$ (eq. 2-26) has been used, by analogy to that definition:

$$\overline{\mathbf{C}}_e = J^{-2/3}\, \mathbf{C}_e \tag{2-75}$$

using this definition in equation 2-74:

$$\mathbf{C}_e = \overline{\mathbf{F}}_a^{-T}\, \mathbf{C}\, \overline{\mathbf{F}}_a^{-1} \tag{2-76}$$

The isochoric part of the decoupled energy presented in 2-28 is now decoupled as a passive and an active contribution

$$\mathcal{W}_{\mathrm{iso}}\left(\overline{I}_1, \overline{I}_2, \overline{I}_4, \overline{I}_5, \overline{J}_4, \overline{J}_5\right) = \mathcal{W}_{\mathrm{p}}\left(\overline{I}_1, \overline{I}_2, \overline{I}_4, \overline{I}_5\right) + \mathcal{W}_{\mathrm{a}}\left(\overline{J}_4, \overline{J}_5\right) \tag{2-77}$$

where two new pseudo-invariants have been introduced:

$$\overline{J}_4 = \mathbf{a}^{\circ} \cdot \overline{\mathbf{C}}_e\, \mathbf{a}^{\circ} \tag{2-78a}$$

$$\overline{J}_5 = \mathbf{a}^{\circ} \cdot \overline{\mathbf{C}}_e^{2}\, \mathbf{a}^{\circ} \tag{2-78b}$$

Pseudo-invariants $\overline{J}_4$ and $\overline{J}_5$ are analogous to $\overline{I}_4$ and $\overline{I}_5$ except for the use of $\overline{\mathbf{C}}_e$ in the first ones, and the use of $\overline{\mathbf{C}}$ in the second ones. $\overline{I}_4$ and $\overline{I}_5$ are related to the passive stretch of the tissue and, therefore, the direction $\mathbf{a}^{\circ}$ is sometimes attributed to the direction of the collagen fibers. The collagen fibers, however, are wrapped around the myofibers and, because of that, the average effect of collagen will be assumed to be co-aligned with the effect of myofibers; in other words, there is no need to distinguish between the direction of myofibers and the direction of collagen. Following the derivatives of I_4, and I_5 (equations 2-16d, 2-16e, 2-20d and 2-20e) :

$$\frac{\partial \overline{J}_4}{\partial \overline{\mathbf{C}}_e} = \mathbf{a}^{\circ} \otimes \mathbf{a}^{\circ} \tag{2-79a}$$

$$\frac{\partial \overline{J}_5}{\partial \overline{\mathbf{C}}_e} = \mathbf{a}^\circ \otimes \overline{\mathbf{C}}_e \, \mathbf{a}^\circ + \mathbf{a}^\circ \cdot \overline{\mathbf{C}}_e \otimes \mathbf{a}^\circ \tag{2-79b}$$

$$\frac{\partial}{\partial \overline{\mathbf{C}}_e} \left(\frac{\partial \overline{J}_4}{\partial \overline{\mathbf{C}}_e} \right) = \mathbb{0} \tag{2-79c}$$

$$\frac{\partial}{\partial \overline{\mathbf{C}}_e} \left(\frac{\partial \overline{J}_5}{\partial \overline{\mathbf{C}}_e} \right) = \frac{\partial^2 \overline{J}_5}{\partial \overline{\mathbf{C}}_e \, \partial \overline{\mathbf{C}}_e} \tag{2-79d}$$

In analogy to the split decomposition of the SPK stress tensor (equation 2-29):

$$\mathbf{S}_{\mathrm{iso}} = 2 \frac{\partial \mathscr{W}_{\mathrm{iso}}}{\partial \mathbf{C}} = 2 \frac{\partial \mathscr{W}_{\mathrm{p}} \left(\overline{I}_1, \overline{I}_2, \overline{I}_4, \overline{I}_5 \right)}{\partial \mathbf{C}} + 2 \frac{\partial \mathscr{W}_{\mathrm{a}} \left(\overline{J}_4, \overline{J}_5 \right)}{\partial \mathbf{C}} \tag{2-80}$$

$$\mathbf{S}_{\mathrm{iso}} = \mathbf{S}_{\mathrm{p}} + \mathbf{S}_{\mathrm{a}} \tag{2-81}$$

$\mathbf{S}_{\mathrm{p}}$ is mathematically equal to $\mathbf{S}_{\mathrm{iso}}$ that was developed in the passive behavior (equation 2-38). $\mathbf{S}_{\mathrm{a}}$ will be addressed in the next section.

Similarly, in analogy to the split decomposition of the elasticity tensor (equation 2-39):

$$\mathbb{C}_{\mathrm{iso}} = 2 \frac{\partial \mathbf{S}_{\mathrm{iso}}}{\partial \mathbf{C}} = 2 \frac{\partial \mathbf{S}_{\mathrm{p}}}{\partial \mathbf{C}} + 2 \frac{\partial \mathbf{S}_{\mathrm{a}}}{\partial \mathbf{C}} \tag{2-82}$$

$$\mathbb{C}_{\mathrm{iso}} = \mathbb{C}_{\mathrm{p}} + \mathbb{C}_{\mathrm{a}} \tag{2-83}$$

Again, $\mathbb{C}_{\mathrm{p}}$ is mathematically equal to the $\mathbb{C}_{\mathrm{iso}}$ developed in the passive behavior (equation 2-70). $\mathbb{C}_{\mathrm{a}}$ will be addressed after developing $\mathbf{S}_{\mathrm{a}}$.

2.4.1 Active part of the Second Piola-Kirchhoff stress

By the chain rule:

$$\mathbf{S}_{\mathrm{a}} = 2 \frac{\partial \mathscr{W}_{\mathrm{a}} \left(\overline{J}_4, \overline{J}_5 \right)}{\partial \mathbf{C}} = 2 \frac{\partial \mathscr{W}_{\mathrm{a}}}{\partial \mathbf{C}_e} : \frac{\partial \mathbf{C}_e}{\partial \mathbf{C}}. \tag{2-84}$$

In index notation:

$$
\begin{aligned}
S_{a_{IJ}} &= 2 \frac{\partial \mathscr{W}_{\mathrm{a}}}{\partial C_{e_{MN}}} \frac{\partial C_{e_{MN}}}{\partial C_{IJ}} = 2 \frac{\partial \mathscr{W}_{\mathrm{a}}}{\partial C_{e_{MN}}} \frac{\partial \overline{F}_{a_{Mi}}^{-T} C_{ij} \overline{F}_{a_{jN}}^{-1}}{\partial C_{IJ}} \\
&= 2 \frac{\partial \mathscr{W}_{\mathrm{a}}}{\partial C_{e_{MN}}} \left[\overline{F}_{a_{Mi}}^{-T} \frac{\partial C_{ij}}{\partial C_{IJ}} \overline{F}_{a_{jN}}^{-1} \right] \\
&= 2 \frac{\partial \mathscr{W}_{\mathrm{a}}}{\partial C_{e_{MN}}} \left[\overline{F}_{a_{Mi}}^{-T} \frac{1}{2} \left(\delta_{iI} \delta_{jJ} + \delta_{iJ} \delta_{jI} \right) \overline{F}_{a_{jN}}^{-1} \right] \\
&= 2 \frac{\partial \mathscr{W}_{\mathrm{a}}}{\partial C_{e_{MN}}} \frac{1}{2} \left[\overline{F}_{a_{MI}}^{-T} \overline{F}_{a_{JN}}^{-1} + \overline{F}_{a_{MJ}}^{-T} \overline{F}_{a_{IN}}^{-1} \right]
\end{aligned} \tag{2-85}
$$

Expanding the brackets:

$$S_{a_{IJ}} = \overline{F}_{a_{MI}}^{-T} \frac{\partial \mathscr{W}_a}{\partial C_{e_{MN}}} \overline{F}_{a_{JN}}^{-1} + \overline{F}_{a_{MJ}}^{-T} \frac{\partial \mathscr{W}_a}{\partial C_{e_{MN}}} \overline{F}_{a_{IN}}^{-1} \tag{2-86}$$

In the first term of 2-86, changing the order of the indexes (Transposing) of $\overline{F}_{a_{MI}}^{-T}$ and $\overline{F}_{a_{JN}}^{-1}$, and changing the position of $\overline{F}_{a_{MJ}}^{-T}$ and $\overline{F}_{a_{IN}}^{-1}$ in the second term of 2-86 lead to:

$$S_{a_{IJ}} = \overline{F}_{a_{IM}}^{-1} \frac{\partial \mathscr{W}_a}{\partial C_{e_{MN}}} \overline{F}_{a_{NJ}}^{-T} + \overline{F}_{a_{IN}}^{-1} \frac{\partial \mathscr{W}_a}{\partial C_{e_{MN}}} \overline{F}_{a_{MJ}}^{-T} \tag{2-87}$$

Using the symmetry of $\mathbf{C}$, $C_{e_{MN}} = C_{e_{NM}}$:

$$\begin{aligned} S_{a_{IJ}} &= \overline{F}_{a_{IM}}^{-1} \frac{\partial \mathscr{W}_a}{\partial C_{e_{MN}}} \overline{F}_{a_{NJ}}^{-T} + \overline{F}_{a_{IN}}^{-1} \frac{\partial \mathscr{W}_a}{\partial C_{e_{NM}}} \overline{F}_{a_{MJ}}^{-T} \\ &= 2 \overline{F}_{a_{IM}}^{-1} \left(\frac{\partial \mathscr{W}_a}{\partial \mathbf{C}_e} \right)_{MN} \overline{F}_{a_{NJ}}^{-T} \\ &= \left(\overline{\mathbf{F}}_a^{-1} \left(2 \frac{\partial \mathscr{W}_a}{\partial \mathbf{C}_e} \right) \overline{\mathbf{F}}_a^{-T} \right)_{IJ} \end{aligned} \tag{2-88}$$

again, by the chain rule:

$$S_{a_{IJ}} = \left(\overline{\mathbf{F}}_a^{-1} \left(2 \frac{\partial \mathscr{W}_a}{\partial \overline{\mathbf{C}}_e} : \frac{\partial \overline{\mathbf{C}}_e}{\partial \mathbf{C}_e} \right) \overline{\mathbf{F}}_a^{-T} \right)_{IJ} \tag{2-89}$$

in analogy to 2-35,

$$\begin{aligned} \frac{\partial \overline{\mathbf{C}}_e}{\partial \mathbf{C}_e} &= J^{-2/3} \left(\mathbb{I} - \frac{1}{3} \mathbf{C}_e \otimes \mathbf{C}_e^{-1} \right) \\ &= J^{-2/3} \mathbb{P}_e^T, \end{aligned} \tag{2-90}$$

where $\mathbb{P}_e$ is defined as:

$$\mathbb{P}_e^T = \mathbb{I} - \frac{1}{3} \mathbf{C}_e \otimes \mathbf{C}_e^{-1} \qquad \mathbb{P}_e = \mathbb{I} - \frac{1}{3} \mathbf{C}_e^{-1} \otimes \mathbf{C}_e \tag{2-91}$$

Finally, with result 2-90, and the property $\mathbf{A} : \mathbb{B} = \mathbb{B}^T : \mathbf{A}$.

$$\mathbf{S}_a = J^{-2/3} \overline{\mathbf{F}}_a^{-1} \left(\mathbb{P}_e : \tilde{\mathbf{S}}_a \right) \overline{\mathbf{F}}_a^{-T}, \qquad \tilde{\mathbf{S}}_a = 2 \frac{\partial \mathscr{W}_a}{\partial \overline{\mathbf{C}}_e} \tag{2-92}$$

$\tilde{\mathbf{S}}_a$ is mathematically equal to $\mathbf{S}$ defined in 2-17; here, as $\mathscr{W}_a$ only depends on $\overline{J}_4$ and $\overline{J}_5$, then using 2-79a and 2-79b, $\tilde{\mathbf{S}}_a$ is simply:

$$\tilde{\mathbf{S}}_a = \mathscr{W}_{a_4} \mathbf{a}° \otimes \mathbf{a}° + \mathscr{W}_{a_5} \left(\mathbf{a}° \otimes \overline{\mathbf{C}}_e \mathbf{a}° + \mathbf{a}° \cdot \overline{\mathbf{C}}_e \otimes \mathbf{a}° \right) \tag{2-93}$$

where $\mathscr{W}_{a_i} = \partial \mathscr{W}_a / \partial \overline{J}_i$.

2.4.2 Active part of the elasticity tensor

By the chain rule:

$$\mathbb{C}_a = 2\,\frac{\partial \mathbf{S}_a}{\partial \mathbf{C}} = 2\,\frac{\partial \mathbf{S}_a}{\partial \mathbf{C}_e} : \frac{\partial \mathbf{C}_e}{\partial \mathbf{C}} \tag{2-94}$$

In index notation:

$$\mathbb{C}_{a_{ijkl}} = 2\,\frac{\partial S_{a_{ij}}}{\partial C_{e_{mn}}}\,\frac{\partial C_{e_{mn}}}{\partial C_{kl}} \tag{2-95}$$

$S_{a_{ij}}$ and the derivative $\partial C_{e_{mn}}/\partial C_{kl}$ follow 2-85. With that, the right hand side of 2-95 is:

$$\begin{aligned}
&2\,\frac{\partial}{\partial C_{e_{mn}}}\left(2\,\frac{\partial \mathscr{W}_{\mathrm{a}}}{\partial C_{e_{MN}}}\frac{1}{2}\left[\overline{F}_{a_{Mi}}^{-T}\,\overline{F}_{a_{jN}}^{-1} + \overline{F}_{a_{Mj}}^{-T}\,\overline{F}_{a_{iN}}^{-1}\right]\right)\frac{1}{2}\left[\overline{F}_{a_{mk}}^{-T}\,\overline{F}_{a_{ln}}^{-1} + \overline{F}_{a_{ml}}^{-T}\,\overline{F}_{a_{kn}}^{-1}\right] \\
&=\frac{1}{2}\left[\overline{F}_{a_{iM}}^{-1}\,\overline{F}_{a_{jN}}^{-1} + \overline{F}_{a_{jM}}^{-1}\,\overline{F}_{a_{iN}}^{-1}\right]2\,\frac{\partial}{\partial C_{e_{mn}}}\left(2\,\frac{\partial \mathscr{W}_{\mathrm{a}}}{\partial C_{e_{MN}}}\right)\frac{1}{2}\left[\overline{F}_{a_{mk}}^{-T}\,\overline{F}_{a_{nl}}^{-T} + \overline{F}_{a_{ml}}^{-T}\,\overline{F}_{a_{nk}}^{-T}\right]
\end{aligned} \tag{2-96}$$

where the notation $\overline{F}_{a_{ij}}^{-1} = \overline{F}_{a_{ji}}^{-T}$, has been used conveniently. The brackets on the left and right follow the index notation of $\partial\,\overline{\mathbf{F}}_a^{-1}/\partial\overline{\mathbf{F}}_a$ (compare to equation 2-47):

$$\mathbb{C}_{a_{ijkl}} = \left(\frac{\partial\,\overline{\mathbf{F}}_a^{-1}}{\partial\overline{\mathbf{F}}_a}\right)_{ijMN}2\,\frac{\partial}{\partial C_{e_{mn}}}\left(2\,\frac{\partial \mathscr{W}_{\mathrm{a}}}{\partial C_{e_{MN}}}\right)\left(\frac{\partial\,\overline{\mathbf{F}}_a^{-T}}{\partial\overline{\mathbf{F}}_a}\right)_{mnkl} \tag{2-97}$$

The term $2\,\partial \mathscr{W}_{\mathrm{a}}/\partial C_{e_{MN}} = 2\left(\partial \mathscr{W}_{\mathrm{a}}/\partial\overline{\mathbf{C}}_e : \partial\,\overline{\mathbf{C}}_e/\partial\mathbf{C}_e\right)_{MN}$ can be replaced by $\left(J^{-2/3}\,\mathbb{P}_e : \tilde{\mathbf{S}}_a\right)_{MN}$ (see equations 2-89 to 2-92):

$$\begin{aligned}
\mathbb{C}_{a_{ijkl}} &= \left(\frac{\partial\,\overline{\mathbf{F}}_a^{-1}}{\partial\overline{\mathbf{F}}_a}\right)_{ijMN}2\,\frac{\partial}{\partial C_{e_{mn}}}\left(2\,\frac{\partial \mathscr{W}_{\mathrm{a}}}{\partial\overline{\mathbf{C}}_e}:\frac{\partial\overline{\mathbf{C}}_e}{\partial\mathbf{C}_e}\right)_{MN}\left(\frac{\partial\,\overline{\mathbf{F}}_a^{-T}}{\partial\overline{\mathbf{F}}_a}\right)_{mnkl} \\
&= \left(\frac{\partial\,\overline{\mathbf{F}}_a^{-1}}{\partial\overline{\mathbf{F}}_a}\right)_{ijMN}2\,\frac{\partial\left(J^{-2/3}\,\mathbb{P}_e : \tilde{\mathbf{S}}_a\right)_{MN}}{\partial C_{e_{mn}}}\left(\frac{\partial\,\overline{\mathbf{F}}_a^{-T}}{\partial\overline{\mathbf{F}}_a}\right)_{mnkl}.
\end{aligned} \tag{2-98}$$

Finally, using the $\odot$ product defined in 2-42 :

$$\mathbb{C}_a = \overline{\mathbf{F}}_a^{-1}\odot\overline{\mathbf{F}}_a^{-1} : \left[2\,\frac{\partial\left(J^{-2/3}\,\mathbb{P}_e : \tilde{\mathbf{S}}_a\right)}{\partial\mathbf{C}_e}\right] : \overline{\mathbf{F}}_a^{-T}\odot\overline{\mathbf{F}}_a^{-T}. \tag{2-99}$$

The term in brackets is mathematically equal to $\mathbb{C}_{\mathrm{iso}}$ presented in equation 2-48 and 2-70. The analogy consists on replacing $\overline{\mathbf{S}}$ by $\tilde{\mathbf{S}}_a$ (equations 2-92 and 2-93), and $\mathbf{S}_{\mathrm{iso}}$ by $J^{-2/3}\,\mathbb{P}_e : \tilde{\mathbf{S}}_a$. Equation 2-70 also requires an intermediate tensor $\overline{\mathbb{C}}$ that should be replaced by:

$$\tilde{\mathbb{C}} = 2\,J^{-4/3}\,\frac{\partial\tilde{\mathbf{S}}}{\partial\overline{\mathbf{C}}_e}. \tag{2-100}$$

$2\,\partial\tilde{\mathbf{S}}/\partial\overline{\mathbf{C}}_e$ is mathematically equal to $\mathbb{C}$ defined in 2-21; here, as $\mathscr{W}_a$ only depends on $\overline{J}_4$ and $\overline{J}_5$, then using 2-79a and 2-79b, $\tilde{\mathbb{C}}$ is simply:

$$
\begin{aligned}
\tilde{\mathbb{C}} = 2\,J^{-4/3}\Big[\quad & \mathscr{W}_{a_{44}}\ \mathbf{a}^\circ \otimes \mathbf{a}^\circ \otimes \mathbf{a}^\circ \otimes \mathbf{a}^\circ \\
& + \mathscr{W}_{a_{45}} \left(\mathbf{a}^\circ \otimes \mathbf{a}^\circ \otimes \frac{\partial\overline{J}_5}{\partial\overline{\mathbf{C}}_e} + \frac{\partial\overline{J}_5}{\partial\overline{\mathbf{C}}_e} \otimes \mathbf{a}^\circ \otimes \mathbf{a}^\circ \right) \\
& + \mathscr{W}_{a_{55}} \frac{\partial\overline{J}_5}{\partial\overline{\mathbf{C}}_e} \otimes \frac{\partial\overline{J}_5}{\partial\overline{\mathbf{C}}_e} \\
& + \mathscr{W}_{a_5} \frac{\partial^2\overline{J}_5}{\partial\overline{\mathbf{C}}_e\,\partial\overline{\mathbf{C}}_e} \quad \Big]
\end{aligned}
\tag{2-101}
$$

2.5 Hyperelastic model for skeletal muscle: Tissue growth

One key feature of muscle adaptation is tissue growth (increase or decrease in muscle size). Previous work has addressed the mechanics of growth by the incorporation of a growth tensor. In any case, soft tissue growth can be the outcome of mechanical or non-mechanical stimulation. Skeletal muscle, hypertrophy in particular, can be considered as a non-mechanically driven growth process because the increase in muscle size occurs in a much larger time scale relative to the time of mechanical stress or stretch of skeletal muscle tissue during exercise training. The aim of this section is to build the SPK stress tensor $\mathbf{S}$ and the elasticity tensor $\mathbb{C}$ that include the additional deformation due to growth.

First consider the deformation of a growing structure through the following split decomposition:

$$
\mathbf{F} = \hat{\mathbf{F}}\,\mathbf{F}_g \tag{2-102}
$$

where $\hat{\mathbf{F}}$ is the deformation of the structure that include volumetric and isochoric deformations (related to the material properties of the structure), and $\mathbf{F}_g$ is the growth tensor. The Cauchy-Green tensor for this deformation gradient is:

$$
\begin{aligned}
\mathbf{C} &= \left(\hat{\mathbf{F}}\,\mathbf{F}_g\right)^T \left(\hat{\mathbf{F}}\,\mathbf{F}_g\right) = \mathbf{F}_g^T\,\hat{\mathbf{F}}^T\,\hat{\mathbf{F}}\,\mathbf{F}_g \\
\mathbf{C} &= \mathbf{F}_g^T\,\hat{\mathbf{C}}\,\mathbf{F}_g
\end{aligned}
\tag{2-103}
$$

where $\hat{\mathbf{C}}$ is the Cauchy-Green tensor related to the regular material behavior of the tissue. From the previous equation:

$$
\hat{\mathbf{C}} = \mathbf{F}_g^{-T}\,\mathbf{C}\,\mathbf{F}_g^{-1} \tag{2-104}
$$

Compare the structure of $\hat{\mathbf{C}}$ with the structure of $\mathbf{C}_e$ of equation 2-76, this similarity will be helpful to develop $\mathbf{S}$ and $\mathbb{C}$.

Now, it will be assumed that the properties of the material are not affected by growth and, therefore, the material SEF $\mathscr{W}$ is not affected by growth:

$$\mathscr{W} = \mathscr{W}\left(\hat{I}_1, \hat{I}_2, \hat{I}_3, \hat{I}_4, \hat{I}_5\right) \tag{2-105}$$

Compare this SEF to the SEF defined in equation 2-28: $\hat{I}_i$ are the invariants of $\hat{\mathbf{C}}$ in a growing material, just as I_i are the invariants of $\mathbf{C}$ in a regular material.

2.5.1 Second Piola Kirchhoff stress for growing tissue

The deformation caused by growth is not stress free:

$$\mathbf{S} = 2\frac{\partial\mathscr{W}}{\partial\mathbf{C}} = 2\frac{\partial\mathscr{W}}{\partial\hat{\mathbf{C}}} : \frac{\partial\hat{\mathbf{C}}}{\partial\mathbf{C}} \tag{2-106}$$

Compare this equation to the right hand side of 2-84; since the mathematical structure of both equations is the same, according to equation 2-88, $\mathbf{S}$ is easily found to be:

$$\mathbf{S} = \mathbf{F}_g^{-1}\left(2\frac{\partial\mathscr{W}}{\partial\hat{\mathbf{C}}}\right)\mathbf{F}_g^{-T} \tag{2-107}$$

Considering that during growth only the passive behavior of muscle tissue is relevant, the term $2\,\partial\mathscr{W}/\partial\hat{\mathbf{C}}$ is the SPK described in section 2.3.1 and defined by equations 2-30, 2-33, and 2-38.

2.5.2 Elasticity tensor for growing tissue

By the chain rule:

$$\mathbb{C} = 2\frac{\partial\mathbf{S}}{\partial\mathbf{C}} = 2\frac{\partial\mathbf{S}}{\partial\hat{\mathbf{C}}} : \frac{\partial\hat{\mathbf{C}}}{\partial\mathbf{C}} \tag{2-108}$$

Compare this equation to the right hand side of 2-94; again, the mathematical structures are the same, according to equations 2-97 and 2-99, $\mathbb{C}$ is:

$$\mathbb{C} = \mathbf{F}_g^{-1} \odot \mathbf{F}_g^{-1} : \left(2\,\frac{\partial\mathbf{S}}{\partial\hat{\mathbf{C}}}\right) : \mathbf{F}_g^{-T} \odot \mathbf{F}_g^{-T}. \tag{2-109}$$

As mentioned before, considering only the passive behavior of muscle tissue, the term $2\,\partial\mathbf{S}/\partial\hat{\mathbf{C}}$ is the elasticity tensor described in section 2.3.2 and defined by equations 2-40, 2-43, and 2-70.

2.6 Conclusion

All the content detailed in this chapter is available in general continuum mechanics and specialized literature of muscle mechanical behavior, but full derivations are normally omitted making the understanding of the field particularly difficult for beginners. Recall that two main characteristics of skeletal muscle are the active response and the ability to grow; the active response is addressed by an active contribution to the SEF, whereas growth requires a growth tensor that is in principle arbitrary. The next chapter focuses on the definition and implementation of the SEF of the passive and active responses, and the discussion of some forms of growth tensor.

Appendix

2.A Derivatives of the invariants of $\mathbf{C}$

2.A.0.1 Properties

These particular properties are necessary to develop the derivatives presented in this appendix section. Let $\mathbf{A}$ and $\mathbf{B}$ two 2-nd order tensors, and $\mathbb{1}$ the 2-nd order identity tensor:

- $\mathbf{A} : \mathbf{B} = A_{ij}\, B_{ij} = A_{ji}^T\, B_{ij} = \left(\mathbf{A}^T\, \mathbf{B}\right)_{jj} = \mathrm{tr}\left(\mathbf{A}^T\, \mathbf{B}\right)$

- $\mathrm{tr}\,\mathbf{A} = \mathbb{1} : \mathbf{A}$, in index notation: $\mathbb{1} : \mathbf{A} = \delta_{ij} A_{ij} = A_{ii} = \mathrm{tr}\,\mathbf{A}$.

For a symmetric tensor $\mathbf{A}$ $(A_{ij} = A_{ji})$:

- $\left(\dfrac{\partial \mathbf{A}}{\partial \mathbf{A}}\right)_{ijkl} = \dfrac{\partial A_{ij}}{\partial A_{kl}} = \dfrac{1}{2}\left(\delta_{ik}\,\delta_{jl} + \delta_{il}\,\delta_{jk}\right)$

2.A.1 First derivatives of the invariants and pseudo-invariants of $\mathbf{C}$

2.A.1.1 First derivative of I_1

$$\left(\frac{\partial I_1}{\partial \mathbf{C}}\right)_{kl} = \left(\frac{\partial\, \mathrm{tr}\,\mathbf{C}}{\partial \mathbf{C}}\right)_{kl} = \frac{\partial C_{ii}}{\partial C_{kl}} = \frac{1}{2}\left(\delta_{ik}\,\delta_{il} + \delta_{il}\,\delta_{ik}\right) = \delta_{ik}\,\delta_{il} = \delta_{kl} = \left(\mathbb{1}\right)_{kl} \tag{2-110}$$

2.A.1.2 First derivative of I_2

$$\begin{aligned}
\frac{\partial I_2}{\partial \mathbf{C}} &= \frac{\partial}{\partial \mathbf{C}}\left[\frac{1}{2}\left(\left(\mathrm{tr}\,\mathbf{C}\right)^2 - \mathrm{tr}\,\mathbf{C^2}\right)\right] = \frac{\partial}{\partial \mathbf{C}}\left[\frac{1}{2}\left(\mathrm{tr}\,\mathbf{C}\right)^2\right] - \frac{\partial}{\partial \mathbf{C}}\left[\frac{1}{2}\,\mathrm{tr}\,\mathbf{C^2}\right] \\
&= \frac{1}{2}\,2\,\mathrm{tr}\,\mathbf{C}\,\frac{\partial\,\mathrm{tr}\,\mathbf{C}}{\partial \mathbf{C}} - \frac{1}{2}\frac{\partial\,\mathbb{1} : \mathbf{C^2}}{\partial \mathbf{C}}.
\end{aligned} \tag{2-111}$$

The first term in last equation is the first derivative of I_1 multiplied by I_1 $(I_1\,\mathbb{1})$. The second term, in index notation:

$$\begin{aligned}
\left(\frac{\partial\,\mathbb{1} : \mathbf{C^2}}{\partial \mathbf{C}}\right)_{kl} &= \frac{\partial\,\delta_{ij}\, C_{im}\, C_{mj}}{\partial C_{kl}} = \frac{\partial\, C_{im}\, C_{mi}}{\partial C_{kl}} = \frac{\partial C_{im}}{\partial C_{kl}}\, C_{mi} + C_{im}\,\frac{\partial C_{mi}}{\partial C_{kl}} \\
&= \frac{1}{2}\left(\delta_{ik}\,\delta_{ml} + \delta_{il}\,\delta_{mk}\right) C_{mi} + \frac{1}{2} C_{im}\left(\delta_{mk}\,\delta_{il} + \delta_{ml}\,\delta_{ik}\right) \\
&= \frac{1}{2}\left(C_{lk} + C_{kl}\right) + \frac{1}{2}\left(C_{lk} + C_{kl}\right) = C_{lk} + C_{kl} = \left(\mathbf{C} + \mathbf{C}^T\right)_{kl} \\
&= \left(2\,\mathbf{C}\right)_{kl}
\end{aligned} \tag{2-112}$$

where the symmetry of C was used. Finally:

$$\frac{\partial I_2}{\partial \mathbf{C}} = I_1 \, \mathbb{1} - \mathbf{C} \tag{2-113}$$

2.A.1.3 First derivative of I_3

The following derivation is based on differential increments of a scalar function with tensor arguments [76].

Consider a scalar function Φ of a tensor $\mathbf{A}$; the value of Φ at an increased value of $\mathbf{A}$ is:

$$\Phi \left(\mathbf{A} + d\mathbf{A} \right) = \Phi \left(\mathbf{A} \right) + d\Phi + O(d\mathbf{A}) \tag{2-114}$$

The differential of Φ is defined as:

$$d\Phi = \frac{\partial \Phi \left(\mathbf{A} \right)}{\partial \mathbf{A}} : d\mathbf{A} = \mathrm{tr} \left(\left(\frac{\partial \Phi \left(\mathbf{A} \right)}{\partial \mathbf{A}} \right)^T d\mathbf{A} \right), \tag{2-115}$$

where the right relation is a consequence of the double contraction property.
Consider $\Phi \left(\mathbf{A} \right) = \det \mathbf{A}$, and calculate the value of the determinant at an increased value of $\mathbf{A}$, before using relation 2-114, the argument of the determinant is expanded as:

$$\det \left(\mathbf{A} + d\mathbf{A} \right) = \det \left(\mathbf{A} \left(\mathbb{1} + \mathbf{A}^{-1} d\mathbf{A} \right) \right) = \det \mathbf{A} \, \det \left(\mathbb{1} + \mathbf{A}^{-1} d\mathbf{A} \right), \tag{2-116}$$

where the determinant of a product was used.
Now, recall the characteristic equation of a tensor $\mathbf{B}$:

$$\det \left(\mathbf{B} - \lambda_B \mathbb{1} \right) = -\lambda_B^3 + I_{B1} \, \lambda_B^2 - I_{B2} \lambda_B + I_{B3} \tag{2-117}$$

with λ_B the eigen-values, and I_{Bi} the invariants of $\mathbf{B}$. Replacing λ_B by -1, and $\mathbf{B}$ by $\mathbf{A}^{-1} d\mathbf{A}$ in last equation leads to:

$$\det \left(\mathbf{A}^{-1} d\mathbf{A} + \mathbb{1} \right) = 1 + I_1' + I_2' + I_3' = 1 + \mathrm{tr} \left(\mathbf{A}^{-1} d\mathbf{A} \right) + O \left(d\mathbf{A} \right) \tag{2-118}$$

where I_i' are the invariants of $\mathbf{A}^{-1} d\mathbf{A}$.
Now, replacing 2-115 in 2-114, and substituting $\Phi \left(\mathbf{A} \right)$ by $\det \mathbf{A}$

$$\det \left(\mathbf{A} + d\mathbf{A} \right) = \det \left(\mathbf{A} \right) + \mathrm{tr} \left(\left(\frac{\partial \det \left(\mathbf{A} \right)}{\partial \mathbf{A}} \right)^T d\mathbf{A} \right) + O(d\mathbf{A}) \tag{2-119}$$

from this equation, $d \left(\det \mathbf{A} \right)$ can be identified:

$$d \left(\det \mathbf{A} \right) = \det \left(\mathbf{A} + d\mathbf{A} \right) - \det \left(\mathbf{A} \right) = \mathrm{tr} \left(\left(\frac{\partial \det \left(\mathbf{A} \right)}{\partial \mathbf{A}} \right)^T d\mathbf{A} \right) + O(d\mathbf{A}), \tag{2-120}$$

using the double contraction property:

$$d\left(\det \mathbf{A}\right) = \left(\frac{\partial \det\left(\mathbf{A}\right)}{\partial \mathbf{A}}\right) : d\mathbf{A} + O(d\mathbf{A}) \tag{2-121}$$

and replacing the last relation of 2-118 into 2-116:

$$\det\left(\mathbf{A} + d\mathbf{A}\right) = \det \mathbf{A} \left(1 + \operatorname{tr}\left(\mathbf{A}^{-1} d\mathbf{A}\right) + O\left(d\mathbf{A}\right)\right), \tag{2-122}$$

from this equation, $d\left(\det \mathbf{A}\right)$ is identified again:

$$d\left(\det \mathbf{A}\right) = \det\left(\mathbf{A} + d\mathbf{A}\right) - \det \mathbf{A} = \det \mathbf{A} \left(\operatorname{tr}\left(\mathbf{A}^{-1} d\mathbf{A}\right) + O\left(d\mathbf{A}\right)\right), \tag{2-123}$$

using the double contraction property:

$$d\left(\det \mathbf{A}\right) = \det \mathbf{A}\, \mathbf{A}^{-T} : d\mathbf{A} + O\left(d\mathbf{A}\right), \tag{2-124}$$

By comparison of equations 2-121 and 2-124,

$$\frac{\partial \det\left(\mathbf{A}\right)}{\partial \mathbf{A}} = \det \mathbf{A}\, \mathbf{A}^{-T} \tag{2-125}$$

Coming back to tensor $\mathbf{C}$, and by the use its symmetry:

$$\frac{\partial \det\left(\mathbf{C}\right)}{\partial \mathbf{C}} = \frac{\partial I_3}{\partial \mathbf{C}} = I_3\, \mathbf{C}^{-1} \tag{2-126}$$

2.A.1.4 First derivative of I_4

$$\begin{aligned}
\left(\frac{\partial I_4}{\partial \mathbf{C}}\right)_{kl} &= \frac{\partial\, a_i^\circ\, C_{ij}\, a_j^\circ}{\partial C_{kl}} = a_i^\circ \frac{\partial C_{ij}}{\partial C_{kl}} a_j^\circ = a_i^\circ \frac{1}{2}\left(\delta_{ik}\,\delta_{jl} + \delta_{il}\,\delta_{jk}\right) a_j^\circ = \frac{1}{2}\left(a_k^\circ\, a_l^\circ + a_l^\circ\, a_k^\circ\right) \\
&= \frac{1}{2}\left(a_k^\circ\, a_l^\circ + a_k^\circ\, a_l^\circ\right) = a_k^\circ\, a_l^\circ = \left(\mathbf{a}^\circ \otimes \mathbf{a}^\circ\right)_{kl}
\end{aligned} \tag{2-127}$$

2.A.1.5 First derivative of I_5

$$\begin{aligned}
\left(\frac{\partial I_5}{\partial \mathbf{C}}\right)_{kl} &= \frac{\partial\, a_i^\circ\, C_{ij}\, C_{jm}\, a_m^\circ}{\partial C_{kl}} = a_i^\circ \frac{\partial C_{ij}}{\partial C_{kl}} C_{jm}\, a_m^\circ + a_i^\circ\, C_{ij} \frac{\partial C_{jm}}{\partial C_{kl}} a_m^\circ \\
&= a_i^\circ \frac{1}{2}\left(\delta_{ik}\,\delta_{jl} + \delta_{il}\,\delta_{jk}\right) C_{jm}\, a_m^\circ + a_i^\circ\, C_{ij} \frac{1}{2}\left(\delta_{jk}\,\delta_{ml} + \delta_{jl}\,\delta_{mk}\right) a_m^\circ \\
&= \frac{1}{2}\left(a_k^\circ\, C_{lm}\, a_m^\circ + a_l^\circ\, C_{km}\, a_m^\circ + a_i^\circ\, C_{ik}\, a_l^\circ + a_i^\circ\, C_{il}\, a_k^\circ\right) \\
&= \frac{1}{2}\left(a_k^\circ\, C_{lm}\, a_m^\circ + a_m^\circ\, C_{mk}^T\, a_l^\circ + a_i^\circ\, C_{ik}\, a_l^\circ + a_k^\circ\, C_{li}^T\, a_i^\circ\right) \\
&= \frac{1}{2}\left(a_k^\circ\,\left(\mathbf{C}\,\mathbf{a}^\circ\right)_l + \left(a^\circ\,\mathbf{C}\right)_k\, \mathbf{a}_l^\circ + \left(\mathbf{a}^\circ\,\mathbf{C}\right)_k\, a_l^\circ + a_k^\circ\,\left(\mathbf{C}\,\mathbf{a}^\circ\right)_l\right) \\
&= \left(\mathbf{a}^\circ \otimes \mathbf{C}\,\mathbf{a}^\circ + \mathbf{a}^\circ\,\mathbf{C} \otimes \mathbf{a}^\circ\right)_{kl}
\end{aligned} \tag{2-128}$$

where the symmetry of $\mathbf{C}$ has been used.

2.A.2 Second derivatives of the invariants and pseudo-invariants of $\mathbf{C}$

2.A.2.1 Second derivative of I_1

$$\frac{\partial}{\partial \mathbf{C}} \left(\frac{\partial I_1}{\partial \mathbf{C}} \right) = \frac{\partial \mathbb{1}}{\partial \mathbf{C}} = \mathbb{0} \tag{2-129}$$

2.A.2.2 Second derivative of I_2

$$\frac{\partial}{\partial \mathbf{C}} \left(\frac{\partial I_2}{\partial \mathbf{C}} \right) = \frac{\partial}{\partial \mathbf{C}} \left(I_1 \mathbb{1} - \mathbf{C} \right) \tag{2-130}$$

in index notation

$$
\begin{aligned}
\left(\frac{\partial}{\partial \mathbf{C}} \left(I_1 \mathbb{1} - \mathbf{C} \right) \right)_{ijkl} &= \frac{\partial}{\partial C_{kl}} \left(I_1 \mathbb{1} - \mathbf{C} \right)_{ij} = \frac{\partial}{\partial C_{kl}} \left(I_1 \delta_{ij} - C_{ij} \right) = \delta_{ij} \frac{\partial I_1}{\partial C_{kl}} - \frac{\partial C_{ij}}{\partial C_{kl}} \\
&= \delta_{ij} \delta_{kl} - \left(\mathbb{I} \right)_{ijkl} \\
&= \left(\mathbb{1} \otimes \mathbb{1} - \mathbb{I} \right)_{ijkl}
\end{aligned}
\tag{2-131}
$$

2.A.2.3 Second derivative of I_3

$$\frac{\partial}{\partial \mathbf{C}} \left(\frac{\partial I_3}{\partial \mathbf{C}} \right) = \frac{\partial}{\partial \mathbf{C}} \left(I_3 \mathbf{C}^{-1} \right) \tag{2-132}$$

in index notation

$$
\begin{aligned}
\left(\frac{\partial}{\partial \mathbf{C}} \left(I_3 \mathbf{C}^{-1} \right) \right)_{ijkl} &= \frac{\partial}{\partial C_{kl}} \left(I_3 \mathbf{C}^{-1} \right)_{ij} = C_{ij}^{-1} \frac{\partial I_3}{\partial C_{kl}} + I_3 \frac{\partial C_{ij}^{-1}}{\partial C_{kl}} \\
&= C_{ij}^{-1} I_3 C_{kl}^{-1} + I_3 \frac{\partial C_{ij}^{-1}}{\partial C_{kl}} \\
&= \left(I_3 \mathbf{C}^{-1} \otimes \mathbf{C}^{-1} + I_3 \frac{\partial \mathbf{C}^{-1}}{\partial \mathbf{C}} \right)_{ijkl}
\end{aligned}
\tag{2-133}
$$

2.A.2.4 Second derivative of I_4

$$\frac{\partial}{\partial \mathbf{C}} \left(\frac{\partial I_4}{\partial \mathbf{C}} \right) = \left(\frac{\partial \, \mathbf{a}^\circ \otimes \mathbf{a}^\circ}{\partial \mathbf{C}} \right) = \mathbb{0} \tag{2-134}$$

2.A.2.5 Second derivative of I_5

In general, pseudo-invariant I_5 is not used due to its strong relation to I_4; here, the derivative of I_5 is presented for completeness:

$$\frac{\partial}{\partial \mathbf{C}} \left(\frac{\partial I_5}{\partial \mathbf{C}} \right) = \frac{\partial}{\partial \mathbf{C}} \left(\mathbf{a}^\circ \otimes \mathbf{C}\, \mathbf{a}^\circ + \mathbf{a}^\circ\, \mathbf{C} \otimes \mathbf{a}^\circ \right) \tag{2-135}$$

In index notation:

$$
\begin{aligned}
\left(\frac{\partial}{\partial \mathbf{C}} \left(\frac{\partial I_5}{\partial \mathbf{C}} \right) \right)_{ijkl} \quad
&= \frac{\partial}{\partial C_{kl}} \left(a_i^\circ\, C_{jm}\, a_m^\circ + a_m^\circ\, C_{mi}\, a_j^\circ \right) \\
&= a_i^\circ\, \frac{\partial C_{jm}}{\partial C_{kl}}\, a_m^\circ + a_m^\circ\, \frac{\partial C_{mi}}{\partial C_{kl}}\, a_j^\circ \\
&= \frac{1}{2}\, a_i^\circ\, \left(\delta_{jk}\delta_{ml} + \delta_{jl}\delta_{mk} \right)\, a_m^\circ + \frac{1}{2}\, a_m^\circ\, \left(\delta_{mk}\delta_{il} + \delta_{ml}\delta_{ik} \right)\, a_j^\circ \\
&= \frac{1}{2}\, \left(a_i^\circ\, \delta_{jk}\, a_l^\circ + a_i^\circ\, \delta_{jl}\, a_k^\circ \right) + \frac{1}{2}\, \left(a_k^\circ\, \delta_{il}\, a_j^\circ + a_l^\circ\, \delta_{ik}\, a_j^\circ \right) \\
&= \frac{1}{2}\, \left(a_i^\circ\, \delta_{jk}\, a_l^\circ + a_i^\circ\, \delta_{jl}\, a_k^\circ + a_j^\circ\, \delta_{il}\, a_k^\circ + a_j^\circ\, \delta_{ik}\, a_l^\circ \right)
\end{aligned}
\tag{2-136}
$$

3 Specialization of the hyperelastic model

The previous chapter described completely the mathematics of the continuum mechanics of the hyperelastic model for skeletal muscle. Recall that skeletal muscle response is the superposition of a passive and an active behavior (figure 3.0.1), and also that muscle is characterized by its adaptability in size, i.e. growth.
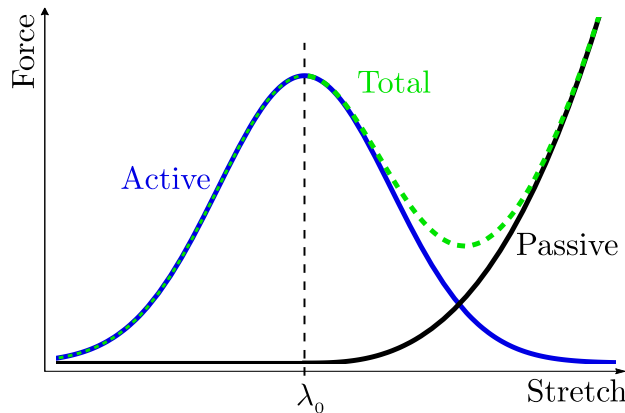
Figure 3.0.1: Force-Stretch relation for a sarcomere. λ_o is the optimal sarcomere stretch that produces the maximum sarcomere force. From λ_o, decreasing or increasing stretch will produce a drop in the generated force. At the organ scale, the characteristic bell shape of the active response holds.

This chapter is divided into 4 sections: the specialization of the SEF for the passive behavior is presented in section 3.1; the deformation gradient and SEF of the active behavior are presented in section 3.2; growth tensors and growth multipliers are discussed in section 3.3; and finally, parameters, FEM structure and simulations of the passive and active response are presented in section 3.4.

Following the notation presented in chapter 2, $\mathbf{a}°$ represents the direction of muscle fibers, and also the average direction of collagen fibers.

3.1 Muscle tissue Passive response

The model for the passive behavior presented in section 2.3 requires the expression of a SEF. In this work, the SEF for the passive response is based on a Neo-Hookean model, and considers strong correlation between $\overline{I}_4 = \mathbf{a}° \cdot \mathbf{C}\, \mathbf{a}°$ and $\overline{I}_5 = \mathbf{a}° \cdot \mathbf{C}^2\, \mathbf{a}°$; these two characteristics allow the passive contribution of the SEF to be a function of only $\overline{I}_1$ and $\overline{I}_4$ [24]. According to the split decomposition (equation 2-28), the proposed SEF for the passive behavior is:

$$\Psi = \overbrace{\Psi_{\text{vol}}\left(J\right)}^{\text{Volumetric}} + \overbrace{\Psi_p\left(\overline{I}_1, \overline{I}_4\right)}^{\text{Passive}} \tag{3-1}$$

Following Martins et al. [103], the volumetric contribution is given by:

$$\Psi_{\text{vol}}\left(J\right) = \frac{1}{D}\left(J - 1\right)^2, \tag{3-2}$$

where J is the determinant of the deformation gradient, and D is a property of the material that controls the bulk modulus (large values of $1/D$ can lead to volumetric locking, small values lead to compression or expansion; values around 100 times the shear modulus are recommended [12, 30]).

Following [24], the passive contribution is:

$$\Psi_p\left(\overline{I}_1, \overline{I}_4\right) = \; c_1\left(\overline{I}_1 - 3\right) + \Psi_f\left(\overline{I}_4\right) \tag{3-3}$$

with

$$\Psi_f\left(\overline{I}_4\right) = \begin{cases} 0 & \text{if} \quad \overline{I}_4 < \overline{I}_{40} \\ \frac{c_3}{c_4}\left[\exp\left(c_4\left(\overline{I}_4 - \overline{I}_{40}\right)\right) - c_4\left(\overline{I}_4 - \overline{I}_{40}\right) - 1\right] & \text{if} \quad \overline{I}_4 > \overline{I}_{40}, \end{cases} \tag{3-4}$$

in the last two equations: $\overline{I}_1$ is the first invariant of the modified Cauchy-Green tensor; $\overline{I}_4$ characterizes the stretch of the collagen fibers that depends on the modified Cauchy-Green tensor and the direction of the collagen fibers; $\overline{I}_{40}$ accounts for the fact that collagen fibers in the unloaded state are usually crimped and get uncurled under tensile loads [14]; c_1 and c_3 are stress like parameters; and c_4 is a dimensionless parameter.

3.2 Muscle tissue Active response

The active response of skeletal muscle requires the treatment of the active part of the deformation gradient, and the active contribution to the SEF, the following two sections address these features.

3.2.1 Active deformation gradient

The active part of the deformation gradient depends only on the fiber direction $\mathbf{a}°$ (as it was briefly mentioned in chapter 2), but two extra vectors are required to describe space. Whatever two vectors perpendicular to $\mathbf{a}°$ are good enough, because in a transversely isotropic material, the properties of the tissue in the plane transverse to the fibers are assumed to be homogeneous. With the use of a vectors basis $\{\boldsymbol{e}_1, \boldsymbol{e}_2, \boldsymbol{e}_3\}$, and its dual basis $\{\boldsymbol{E}^1, \boldsymbol{E}^2, \boldsymbol{E}^3\}$, $\overline{\mathbf{F}}_a$ is given by:

$$\overline{\mathbf{F}}_a = \lambda_1 \, \boldsymbol{e}_1 \otimes \boldsymbol{E}^1 + \lambda_2 \, \boldsymbol{e}_2 \otimes \boldsymbol{E}^2 + \lambda_3 \, \boldsymbol{e}_3 \otimes \boldsymbol{E}^3, \tag{3-5}$$

where $\boldsymbol{e}_1 = \mathbf{a}°$, $\boldsymbol{e}_2$ and $\boldsymbol{e}_3$ are perpendicular to $\boldsymbol{e}_1$, and λ_i are the active stretches in the respective direction $\boldsymbol{e}_i$. Notice that when the muscle is not active, $\lambda_i = 1$, therefore:

$$\boldsymbol{e}_1 \otimes \boldsymbol{E}^1 + \boldsymbol{e}_2 \otimes \boldsymbol{E}^2 + \boldsymbol{e}_3 \otimes \boldsymbol{E}^3 = \mathbb{1}, \tag{3-6}$$

then,

$$\boldsymbol{e}_2 \otimes \boldsymbol{E}^2 + \boldsymbol{e}_3 \otimes \boldsymbol{E}^3 = \mathbb{1} - \boldsymbol{e}_1 \otimes \boldsymbol{E}^1. \tag{3-7}$$

Now, calling $\lambda_a = \lambda_1$, the active stretch along the fiber direction; noticing that $\lambda_2 = \lambda_3$, because the material is assumed homogeneous in the plane transverse to the fibers; and calling $\lambda_t = \lambda_2 = \lambda_3$, for an incompressible material:

$$\det \overline{\mathbf{F}}_a = \lambda_1 \, \lambda_2 \, \lambda_3 = \lambda_a \, \lambda_t^2 = 1 \tag{3-8}$$

and then:

$$\lambda_t = \lambda_a^{-1/2} \tag{3-9}$$

Using this last observation and equation 3-7, the active deformation gradient tensor is:

$$\overline{\mathbf{F}}_a = \lambda_a \, \boldsymbol{e}_1 \otimes \boldsymbol{E}^1 + \lambda_a^{-1/2} \left(\mathbb{1} - \boldsymbol{e}_1 \otimes \boldsymbol{E}^1 \right), \tag{3-10}$$

The last equation shows that the dynamics of $\overline{\mathbf{F}}_a$ depends only on the active stretch λ_a, because the direction of fibers $\mathbf{a}°$ are fixed in the reference configuration. In this work it is assumed that muscle tissue can be found at any given active stretch during active response, and also that this response occurs in a quasi-static process (inertial forces will be ignored). The quasi-static assumption also means that $\dot{\lambda}_a$ will be ignored.

3.2.2 Active strain energy function

The total SEF is a superposition of a passive and an active contribution. The passive contribution depends only on fixed parameters of the tissue, but the active contribution needs to include additional characteristics of skeletal muscle function. Although pseudo

invariants $\overline{J}_4$ and $\overline{J}_5$ were introduced section 2.4, a short comment on their relation to pseudo invariants $\overline{I}_4$ and $\overline{I}_5$ is necessary.

Pseudo-invariants $\overline{I}_4$ and $\overline{I}_5$ are close in mathematical formulation to $\overline{J}_4$ and $\overline{J}_5$ (equations 2-27d, 2-27e, 2-78a, and 2-78b), but the concepts that they represent are different. The total deformation $\overline{\mathbf{F}}$ is a composition of an elastic deformation $\overline{\mathbf{F}}_e$ and an active deformation $\overline{\mathbf{F}}_a$ ($\overline{\mathbf{F}} = \overline{\mathbf{F}}_e\overline{\mathbf{F}}_a$); during muscle active response, the total deformation affects $\overline{I}_4$, but only the elastic deformation affects $\overline{J}_4$; in contrast, the behavior of muscle without active deformation requires that $\overline{\mathbf{F}}_a = \mathbb{1}$ (equation 3-6), which leads to $\overline{\mathbf{F}}_e = \overline{\mathbf{F}}$; thus, in this case, $\overline{J}_4 = \overline{I}_4$ and $\overline{J}_5 = \overline{I}_5$. This implies that the active contribution of the SEF cannot be a function of $\overline{J}_4$ and $\overline{J}_5$ only, but it requires additional parameters that are described below.

Following Grasa et al. [67] and other references [74, 132], the active contribution is a function of: (i) the elastic stretch of muscle fibers $\overline{J}_4$; (ii) the active stretch of muscle fibers λ_a that resembles the sliding of actin and myosin filaments; (iii) the rate of change of the active stretch $\dot{\lambda}_a$; and (iv) an activation parameter β that accounts for the number of motor neurons recruited. Similar to the passive response, $\overline{J}_5$ is not considered due to its correlation to $\overline{J}_4$. The active contribution of the SEF is:

$$\Psi_a\left(\overline{J}_4, \lambda_a, \dot{\lambda}_a, \beta\right) = \sigma_o\, f_1\left(\lambda_a\right) f_2\left(\dot{\lambda}_a\right) f_3\left(\overline{J}_4\right) \beta\left(t\right), \tag{3-11}$$

where σ_o is the maximum isometric tension; function f_1 is the active force-stretch relation (fig. 3.0.1); function f_2 is the force-velocity relation (the maximum force generated depends on how fast a muscle contracts); function f_3 is the energy related to cross bridges; and function β controls the force generated by the muscle at time t (full activation produces maximum force, zero activation produces a force equal to zero).

Following Grasa et. al [67], the functions in equation 3-11 are defined as follows:

$$\begin{aligned} f_1\left(\lambda_a\right) &= \exp\left[-\frac{1}{2}\left(\frac{\lambda_a - \lambda_o}{1-\alpha}\right)^2\right] \\ f_2\left(\dot{\lambda}_a\right) &= 1 \\ f_3\left(\overline{J}_4\right) &= \frac{2}{3}\left(2\,\overline{J}_4^{-3/2} - \frac{3}{2}\,\overline{J}_4 - \frac{1}{2}\right) \end{aligned} \tag{3-12}$$

$\beta\left(t\right)$: proportional to the number of motor neurons activated per simulation step.

In function f_1, λ_o is the sarcomere stretch that produces maximum force, and α controls the dispersion of force around λ_o. In function f_2, the force-velocity relation is considered irrelevant, because the time course of muscle adaptation process is much longer than the activation time course, and also because of the quasi-static assumption. Function f_3 ensures that there is no active energy contribution when muscle tissue is in a relaxed state: $f_3(\overline{J}_4 = 1) = 0$. Function $\beta(t)$ ensures that, if tissue is stretched without active deformation (which is $\overline{J}_4 = \overline{I}_4$), there is no active contribution, this means that during passive response, the

active contribution to the SEF does not vanish because of the value of $\overline{J}_4$ but because of the activation parameter β.

The mechanical model allows the description of the deformations of muscle tissue. When a change in size due to muscle hypertrophy or atrophy is considered, it will affect the deformation gradient via the growth tensor that is described in the next section.

3.3 Muscle tissue Growth

Section 2.5 presented the tissue growth model. Some similarities between the growth model and the active response can be noticed when comparing $\mathbf{C}_e$ (equation 2-76) to $\hat{\mathbf{C}}$ (equation 2-104), and $\mathbf{S}_a$ (equation 2-92) to $\mathbf{S}$ (equation 2-107). A similarity between the specialization of the active deformation gradient (section 3.2.1) and the growth tensor is explored in the next section; a brief review of growth multiplier formulations is also presented.

3.3.1 Growth tensor

The construction of the growth tensor $\mathbf{F}_g$ follows the construction of the active deformation gradient: one of the three vectors required to describe space is the fiber direction $\mathbf{a}°$, but the other two vectors are not as arbitrary as in the case of the active deformation gradient because growth is anisotropic in general. Again, with the use of vectors basis $\{\boldsymbol{e}_1, \boldsymbol{e}_2, \boldsymbol{e}_3\}$, and $\{\boldsymbol{E}^1, \boldsymbol{E}^2, \boldsymbol{E}^3\}$, a general formulation of $\mathbf{F}_g$ is:

$$\mathbf{F}_g = \vartheta_1\, \boldsymbol{e}_1 \otimes \boldsymbol{E}^1 + \vartheta_2\, \boldsymbol{e}_2 \otimes \boldsymbol{E}^2 + \vartheta_3\, \boldsymbol{e}_3 \otimes \boldsymbol{E}^3, \tag{3-13}$$

where, assuming an orthotropic basis $\{\boldsymbol{e}_1, \boldsymbol{e}_2, \boldsymbol{e}_3\}$, ϑ_i are the *growth multipliers* that define how tissue grows along each direction $\boldsymbol{e}_i$. One of the main issues of the mechanics of growth is the modeling of the growth multipliers; the complexity of the growth phenomenon includes: anysotropy, microstructure, inhomogeneities, cell proliferation, or extracellular matrix changes [55]. Nontheless, as mentioned in section 2.5, two big characteristics of growth can be distinguised: mechanically or non-mechanically driven processes. On muscle tissue, most of the literature has focused on the mechanically driven description [181, 61, 62, 3, 146]. The model for muscle adaptation presented in this work assumes that muscle adapts in length or cross-sectional area (CSA), then, just as with the active deformation gradient, whatever $\boldsymbol{e}_2$ and $\boldsymbol{e}_3$ perpendicular to $\boldsymbol{e}_1$ are good enough, in that case:

$$\mathbf{F}_g = \vartheta_L\, \boldsymbol{e}_1 \otimes \boldsymbol{E}^1 + \vartheta_A\, \left(\mathbb{1} - \boldsymbol{e}_1 \otimes \boldsymbol{E}^1\right) \tag{3-14}$$

ϑ_L accounts for the increase in length of myofibrils by the addition of sarcomeres in series, whereas ϑ_A accounts for the increase in CSA of myofibers by the addition of myofibrils in parallel.

3.3.1.1 Growth multiplier examples

The increase in muscle length was studied by Zöllner et al. [181]. The growth tensor presented by Zöllner is obtained from 3-14 by considering $\vartheta_A = 1$. (no increase in CSA):

$$\mathbf{F}_g = \vartheta_L \, \boldsymbol{e}_1 \otimes \boldsymbol{E}^1 + 1. \left(\mathbb{1} - \boldsymbol{e}_1 \otimes \boldsymbol{E}^1\right) = \mathbb{1} + (\vartheta_L - 1) \, \boldsymbol{e}_1 \otimes \boldsymbol{E}^1 \qquad (3\text{-}15)$$

where ϑ_L is modelled by an evolution equation:

$$\dot{\vartheta}_L = \kappa(\vartheta_L) \, \phi(\lambda_e), \qquad (3\text{-}16)$$

where $\kappa(\vartheta_L)$ is a growth law that targets a maximum length $\vartheta_{\max}$, and $\phi(\lambda_e)$ is the strain stimulation that must be sustained in time to allow the evolution of the sarcomere number.

$$\kappa(\vartheta_L) = \frac{1}{\tau}\left[\frac{\vartheta_{\max} - \vartheta}{\vartheta_{\max} - 1}\right]^{\gamma}, \qquad \phi(\lambda_e) = \begin{cases} 0 & \text{if} \quad \lambda_e < \lambda^{\text{crit}} \\ 1 & \text{if} \quad \lambda_e > \lambda^{\text{crit}}. \end{cases} \qquad (3\text{-}17)$$

The characteristic time τ, and the shape parameter γ control the speed of growth; and growth is activated only if the strain stimulation λ_e exceeds a critical value λ^{crit}.

The previous example of growth tensor and multiplier describes sarcomere addition (myofibril lengthening). A similar growth tensor (adjusting growth directions) describes cardiac muscle conditions such as cardiac wall thickening, and cardiac dilation; in contrast to one privileged direction of growth, athlete's heart considers volumetric growth. In athlete's heart $\vartheta_1 = \vartheta_2 = \vartheta_3$, and therefore:

$$\mathbf{F}_g = \vartheta_g \mathbb{1} \qquad (3\text{-}18)$$

In each heart condition, function ϕ is triggered by deformation $\mathbf{F}_e$ (elastic part of the deformation gradient), or stress $\mathbf{C}_e \mathbf{S}_e$, but functions $\dot{\vartheta}$ and $\kappa(\vartheta)$ keep the same shape as in equations 3-16 and 3-17 [55].

Implementation of the examples presented in this section are not relevant for the rest of the thesis and will not be presented (see [55] for a detailed description). Although tissue growth and remodeling is a popular theme in the continuum mechanics community, in the particular case of skeletal muscle, only the example of sarcomere addition presented in this section addresses skeletal muscle adaptation. The model of muscle tissue growth developed in this thesis, and its implementation will be presented in chapter 5.

3.4 Implementation

The FEM simulations performed in this work use idealized muscle structures as shown in figure 3.4.1. The tensile test structure was built from a cylindrical shape of 20 cm long (l_0),

and 2.34 cm diameter (d_0), figure 3.4.1-a; the structure for the active response was a variation of the tensile-test structure with a belly 6.5 cm diameter half height (d_b), figure 3.4.1-b. The geometries were discretized into structured meshes of 832 8-noded brick elements with a total of 1107 nodes. Boundary conditions for the tensile test are: nodes at the bottom surface were kept fixed for displacement; nodes at the top surface were displaced in axial direction and restrained in transverse direction. Boundary conditions for the active response are: nodes at top and bottom surfaces were kept fixed for displacement (an isometric contraction was produced by a variation of the activation parameter β from 0 to 1, and a variation of the active stretch λ_a between 0.3 and 1.6). Table 3.4.1 shows the set of parameters for the implementation of the mechanical model.
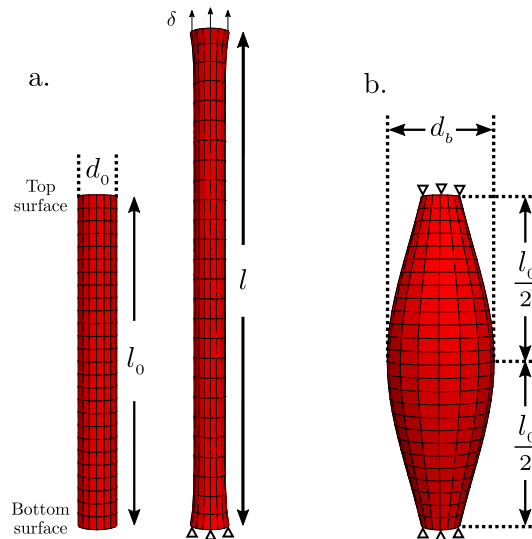
Figure 3.4.1: FEM Structure for tensile test (a), and active response (b).

Table 3.4.1: Parameters for the skeletal muscle mechanical model. Passive response parameters were obtained from [24], active response parameters were obtained from [132], σ_0 from [111].

Parameter	Value	Units	Response
$1/D$	10.0	MPa	Passive
c_1	0.008837	MPa	Passive
c_3	0.009877	MPa	Passive
c_4	2.237879	—	Passive
$\overline{I}_{40}$	1.254400	—	Passive
σ_0	0.1088	MPa	Active
λ_0	1.0000	—	Active
α	0.83616	—	Active

3.4.1 Simulation Passive response

A sketch of the simulation of a tensile test is presented in figure 3.4.1-a. Top surface was displaced, and reaction forces were calculated at each displacement step. First Piola-Kirchhoff stress (FPK) was calculated as the reaction force at the top surface divided by the reference CSA. Stretch λ was calculated as the distance between top and bottom surfaces at each step (l), divided by the initial length of the structure (l_0).
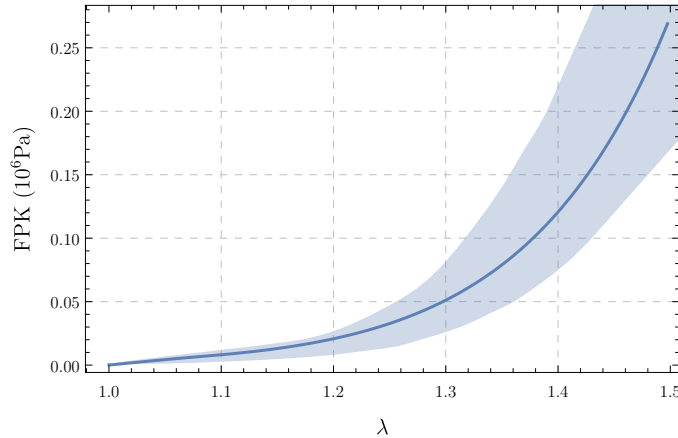
Figure 3.4.2: Passive behavior of skeletal muscle tissue. First Piola-Kirchhoff stress FPK - stretch relation for muscle structure under tensile test. Numerical simulation (continuous line) compared to experiments (blue shaded area that shows the deviations of the results by Calvo et al. [24]).

Although some variability of the passive response occurs with a mesh refinement (see appendix 3.A), the experimental deviations allow some variability of the passive parameters to recover the targeted behavior; thus, for the purposes of this work, the selected mesh (832 8-noded brick elements) with properties presented in table 3.4.1 produces a passive response in good agreement to experimental deviations, see figure 3.4.2.

3.4.2 Simulation Active response

To build the force-stretch relation of the active response, making use of the quasi-static assumption, the active deformation stretch was fixed at a value λ_a and then, the activation parameter β was increased gradually from 0 ($\Psi_a = 0$ and the tissue response is passive independent of λ_a) to 1 (Ψ_a is at the maximum value allowed by λ_a).

Figure 3.4.3 shows the active response of an ideal muscle that has only one type of muscle fiber, and the size of all its motor neurons is fixed. Figure 3.4.3-a shows that force increases linearly with β, by definition of equation 3-12. Figure 3.4.3-b shows the expected distribution of force around the optimal active stretch, and also shows that the value of β does not affect the shape, β only affects the amplitude of the force-stretch relation.
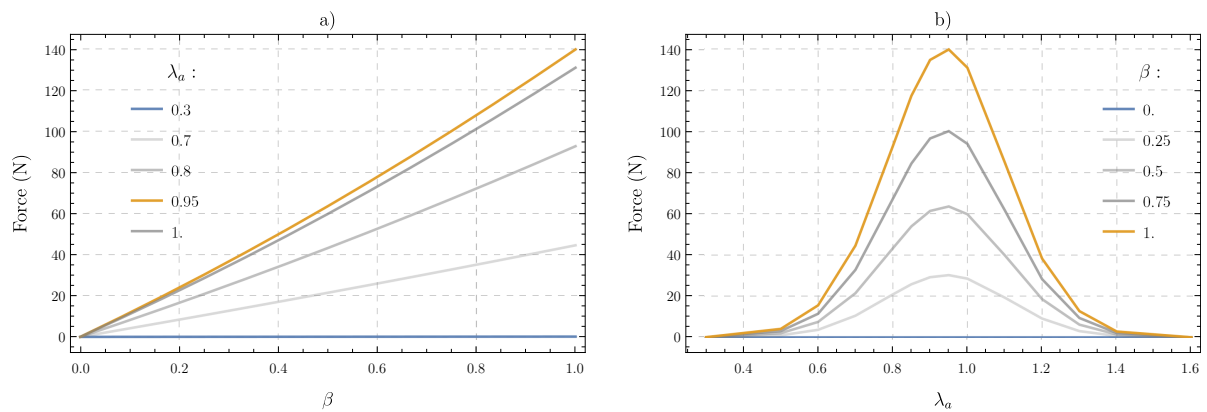
Figure 3.4.3: Active response of skeletal muscle. **a)** Force generated at fixed λ_a as a function of β. **b)** Force generated at fixed β as a function of λ_a.

3.5 Conclusion

There is a natural necessity of a connection between the mechanics of muscle tissue and the biological processes that ultimately dictate adaptation laws; however, in most cases, such a connection is blurry if not nonexistent. Regarding growth formulation, after developing a model for the biological process of protein **synthesis** in chapter 4, which is suitable for the description of a growth law, skeletal muscle hypertrophy is addressed in chapter 5. Regarding the active response formulation, there is room for an exploration of features related to muscle fiber-type distribution, for instance contraction speed, fatigability or maximum voluntary contraction. In particular, after developing a model for the biological process of protein-isoform **replacement** in chapters 6 and 7, maximum voluntary contraction will be addressed in chapter 8.

The passive and active responses of skeletal muscle tissue presented in this chapter agree with experimental observations and constitute the basic formulation to explore the adaptation features developed in this thesis.

Appendix

3.A Convergence analysis

Computation time (figure 3.A.1), tensile test response (figure 3.A.2) and the error on the maximum force of the active response (figure 3.A.3) were tested for different FEM meshes. Table 3.A.1 shows the parameters of the FEM structures simulated.

Table 3.A.1: Convergence test parameters. Each structured mesh was constructed by a number of columns, and each column contains a number of elements; total number of elements and nodes of the structure are also listed. Structures for tensile test and active response were both built using the numbers presented in this table.

Columns	Elements per column	Elements	Nodes
12	17	204	306
32	26	832	1107
60	35	2100	2628
96	44	4224	5085
140	53	7420	8694
192	62	11904	13671
252	71	17892	20232
320	79	25280	28240

The computation time test shows the characteristic fast increase with the number of elements, bear in mind that each step of the active response is computationally more expensive than a tensile step. The passive response test shows a relatively large variation in FPK, but all tested cases are within experimental deviations. The relative error in the maximum force (calculated between a refined mesh and the previous mesh presented in table 3.A.1) improves by less than 0.5% with each structure after 832 elements.
The results of the convergence test show that the active and passive responses converge to a stable solution.
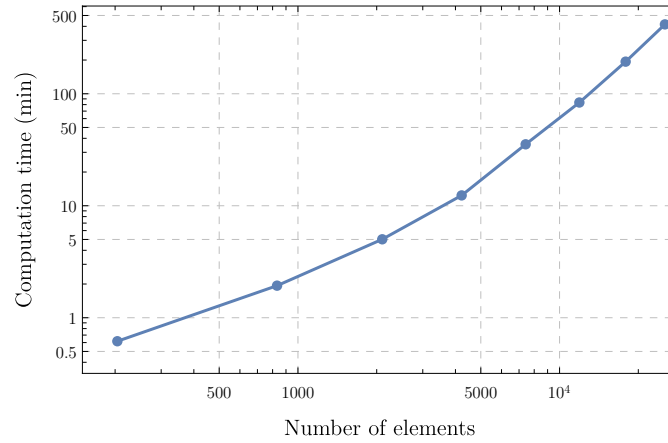
Figure 3.A.1: Time required for 200 steps of tensile test with increasing number of elements.
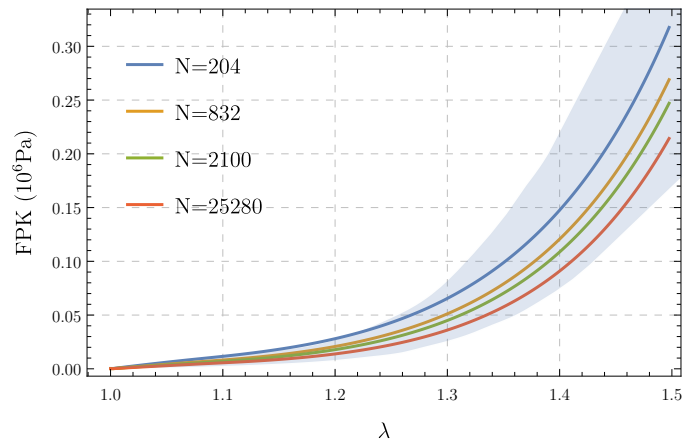
Figure 3.A.2: Passive response for different meshes. Results for all meshes lay within the experimental deviations reported by Calvo et al. [24]). (N is the number of elements).
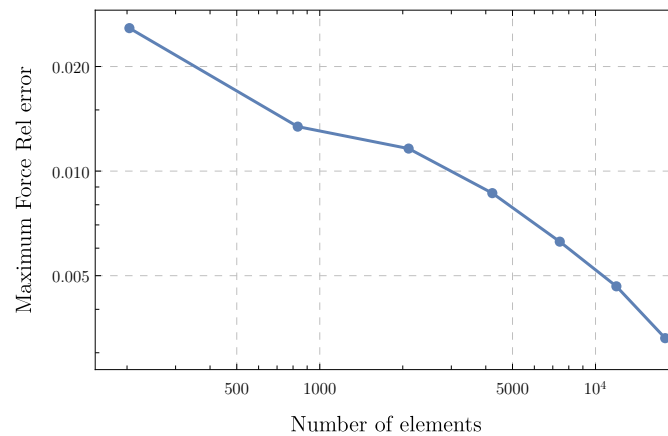
Figure 3.A.3: Error in the force produced by one mesh relative to the force produce by the following improved mesh.

4 Biochemical model for the IGF1-AKT signaling pathway [1]

4.1 Background

Skeletal muscle is the most adaptive tissue in the human body and it is also the main reservoir of protein. Among the factors that produce muscle adaptation, physical activity, which is strongly related to quality of life [108, 180], plays a major role. The reason for this is that physical activity triggers the biochemical response of groups of molecules involved in sets of interactions called signaling pathways [37, 141]; a different pathway mediates each aspect of the adaptation process. In particular, protein content is mediated by the IGF1-AKT signaling pathway, which in fact is one of the most studied [37, 141, 143, 15]. A brief description of the main interactions in this pathway is the following: insulin-like growth factor (IGF1) [2] induces the activation of serine/threonine kinase (AKT) [152], which is related to hypertrophy by the regulation of the mammalian target of rapamycin (mTOR) [70]; at the same time, AKT is related to atrophy via the Forkhead box transcriptions factor (FOXO) [174]; conclusively, hypertrophy is the outcome of protein synthesis, and atrophy is the outcome of protein degradation.

Since the interaction between molecules is known, mathematical models (that provide the possibility to control different features of the pathways) have been designed to test implications, explore limitations, and make predictions of the adaptation responses [46, 93]. However, a mathematical model for muscle adaptation would be beneficial to improve quality of life, if it gives the possibility to personalize a training protocol, and if -based on the knowledge of biochemical responses- it predicts the evolution of macroscopic characteristics such as size, strength, or fatigability.

As a starting point, this chapter presents a model for the adaptation process of muscle cross-sectional area (CSA) based on the IGF1-AKT signaling pathway. This chapter details the dynamical system that describes the time course of that adaptation process under different loading-activity scenarios; and it shows the applicability of the model by simulating the adaptation of the muscle CSA under particular training protocols.

---

[1]Most of the content of this chapter was published in [173], permission to use is provided in appendix 4.A.

4.2 Materials and Methods

This section is divided into two parts. In the first (4.2.1), the general aspects of the model are described; in the second (4.2.2), additional aspects required for different simulation scenarios are presented.

4.2.1 Dynamical model

This section presents the description of the dynamical model. The first part considers: the set of equations as well as the relation between the variables of the system and the molecules involved in the IGF1-AKT signaling pathway (4.2.1.1); the importance and meaning of the stability analysis (4.2.1.2); and the description of the initial conditions as well as the parameters required in the set of equations (4.2.1.3).

4.2.1.1 Set of equations

The purpose the model presented in this chapter is to state the main (and minimum) set of interactions between the components of the pathway that produce muscle adaptation, and it is not intended to describe the behavior of any component in particular.

A simplified mechanism of the IGF1-AKT signaling pathway was reviewed by Schiaffino [143]. Using that mechanism, a description of the inter-relations of the molecules is the following: IGF1 stimulates muscle hypertrophy [2, 73], and it induces the activation of AKT [150]. AKT is important in processes of cell growth and proliferation [102], but as AKT is actually a family of very similar molecules [141, 152], it is also related to growth retardation and muscle atrophy [51]. AKT positively regulates protein synthesis via mTOR [70, 51], and negatively regulates protein degradation via FOXO [142]. FOXO also diminishes protein synthesis by the inhibition of mTOR [135]. The inter-relation between those biochemical species can be direct or mediated by other species considered here as less important. The simplified pathway along with the variable names are presented in figure 4.2.1.

The model assumes that bouts of exercise (mechanical stresses) activate IGF1 [79], and IGF1 triggers the signaling pathway. In this model, the biochemical species involved in the IGF1-AKT pathway are considered populations that interact with each other, produce protein synthesis (or degradation), and control the number of muscle myofibrils.

In this model, the molecules behave as a system of interacting populations in a Lotka-Volterra system. Lotka-Volterra systems have been used to model interacting species outside the ecology domain; see for instance Pandiyan et al. and Sooknanan et al. [121, 153]. The equation system is the following:

$$\dot{x}_1 = x_1 \left(a_1(t) - b_1 x_1 \right) \tag{4-1a}$$
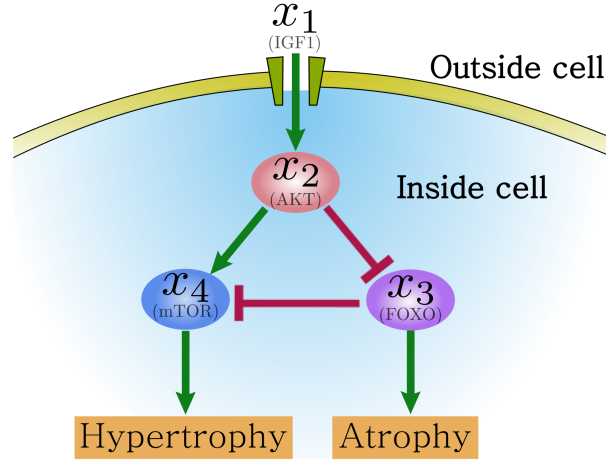
Figure 4.2.1: Reduced set of interactions based on the IGF1-AKT signaling pathway reviewed by [143]. Arrow heads indicate activation and flat heads indicate inhibition. The molecules IGF1, AKT, FOXO, mTOR are represented by the variables x_1, x_2, x_3, and x_4, respectively. In the simplified signaling pathway for muscle adaptation: x_1 promotes x_2; x_2 has a double role, on one side x_2 promotes x_4, and x_4 promotes hypertrophy; on the other side x_2 inhibits x_3, and x_3 promotes atrophy, but also inhibits x_4.

$$\dot{x}_2 = x_2 \left(a_2(t) - b_2\, x_2 + c_{21}\, x_1 \right) \tag{4-1b}$$

$$\dot{x}_3 = x_3 \left(a_3 - b_3\, x_3 - c_{32}\, x_2 \right) \tag{4-1c}$$

$$\dot{x}_4 = x_4 \left(a_4 - b_4\, x_4 + c_{42}\, x_2 - c_{43}\, x_3 \right) \tag{4-1d}$$

$$\dot{z} = f\left(x_3, x_4 \right). \tag{4-1e}$$

Where x_i is the population number of the *ith*-molecule; coefficient a_i is its intrinsic growth rate; b_i is its self-inhibition rate; and coefficient c_{ij} is the coupling strength between molecule i and molecule j. z is the population number of myofibrils, and the function $f(x_3, x_4)$, which depends on populations x_3 and x_4, is proposed as a function that controls the rate of change of myofibril population z (see equation 4-2). The time dependency of a_1 and a_2 will be addressed in section 4.2.2.

The rate of change of population x_1 is proportional to its own population; it is also proportional to a reduced intrinsic growth rate to include self-inhibition (Eq. 4-1a).

The rate of change of population x_2 is proportional to its own population, and it is also proportional to a term that includes intrinsic growth rate, a self-inhibition term and a promotion term guided by population x_1 (Eq. 4-1b).

The rate of change of population x_3 is described in the same way as population x_1, but the second term includes an inhibition term guided by population x_2 (Eq. 4-1c).

The rate of change of population x_4 is described in the same way as population x_1, but this time, x_4 is inhibited by population x_3 and promoted by population x_2 (Eq. 4-1d).

The rate of change of myofibril population z is a function that balances populations x_3 and x_4 (Eq. 4-1e). This function is defined as a piecewise function (equation 4-2).

$$f(x_3, x_4) = \begin{cases} 0 & \text{if} \quad z < z^{\min} \quad \text{or} \quad z > z^{\text{Max}} \\[2mm] 0 & \text{if} \quad x_4 < x_4^0 \quad \text{and} \quad x_3 < x_3^0 \\[2mm] k_1\left(x_4 - x_4^0\right) - k_2\left(x_3 - x_3^0\right) & \text{if} \quad x_4 > x_4^0 \quad \text{and} \quad x_3 > x_3^0 \\[2mm] -k_2\left(x_3 - x_3^0\right) & \text{if} \quad x_4 < x_4^0 \quad \text{and} \quad x_3 > x_3^0 \\[2mm] k_1\left(x_4 - x_4^0\right) & \text{if} \quad x_4 > x_4^0 \quad \text{and} \quad x_3 < x_3^0 \, , \end{cases} \tag{4-2}$$

where $z^{\min}$ and z^{Max} are the minimum and maximum values of the myofibril population; x_4^0 and x_3^0 are the threshold values of populations x_4 and x_3; and k_1 and k_2 are the rates of protein synthesis and protein degradation respectively.

In equation 4-2, the first line stands for the limitation of maximum and minimum sizes of a muscle. The second line indicates that when populations x_3 and x_4 are below some threshold values, the myofibril population does not change. Line three considers the case of populations x_3 and x_4 above their thresholds, which represents the balance of simultaneous protein synthesis and protein degradation. Line four eliminates the possibility of protein synthesis by considering that only x_3 is above its threshold. And finally, line five eliminates the possibility of protein degradation by considering that only x_4 is above its threshold.

4.2.1.2 Stability analysis

The self-inhibition terms make the equation system 4-1 non-linear, which could be unstable (i.e., under small variations of the initial conditions or parameters, the system response is unbounded). To find a set of parameters that produce stable solutions, a stability analysis was performed. The first step of the stability analysis is to find the singular points, which are the values at which the right-hand side of the set of equations becomes zero. The second step is to linearize the set of equations around those singular points and establish the characteristic matrix. The third step is to calculate the characteristic polynomial of the characteristic matrix. The final step is to find the roots (λ) of the characteristic polynomial; these roots determine the stability of the singular points.

The system is stable around the singular points if the real part of every λ is negative. This condition is met under a particular relation between the coefficients c_{ij} of the model and the

intrinsic growth rate functions $a_1(t)$ and $a_2(t)$; in other words, the condition for stability is an equation that the proper set of parameters of equation system 4-1 must fulfill.

4.2.1.3 Initial conditions and parameters

Homeostatic values of IGF1, AKT, FOXO, and mTOR acquired from experimental evidence [92, 10] were normalized and selected as initial conditions; whereas initial condition for the myofibril population was set to 1.0. The same set of initial conditions (table 4.2.1) was used throughout this study to represent a muscle in a homeostatic state previous to each loading-activity scenario; the loading-activity scenarios are described in the next section. All populations are expressed in arbitrary units (a.u.).

Parameters for equation system 4-1: Intrinsic growth rates, self-inhibition rates, and coupling strengths were fitted by a heuristic approach that was in agreement with the initial conditions, and also with the stability condition that can be seen in section 4.2.1.2. Parameters for equation 4-2: minimum and maximum value of the myofibril population come from experimental evidence [28, 84]; thresholds for x_3 and x_4 were selected at values close to their initial conditions; and the rates of protein synthesis and degradation were fitted. The whole set of parameters is shown in table 4.2.2.

Table 4.2.1: Initial conditions for equation system 4-1.

Init. Cond.	Value	Units	Reference
$x_1(0)$	1.000×10^{-2}	a.u.	[92]
$x_2(0)$	9.880×10^{-1}	a.u.	[10]
$x_3(0)$	4.318×10^{-1}	a.u.	[10]
$x_4(0)$	4.692×10^{-1}	a.u.	[10]
$z(0)$	1.000×10^{0}	a.u.	

4.2.2 Simulations

In the previous section, the dynamical system for the IGF1-AKT signaling pathway was described (equation 4-1). This pathway produces skeletal muscle adaptation provided that the pathway is triggered by mechanical stimulation (i.e., the dynamical system requires the introduction of an exercise input). The exercise input activates the pathway and will be directly associated to x_1; however, the evolution of the pathway depends on certain restrictions associated to x_2. These restrictions are represented here as four *loading-activity* scenarios: steady state, atrophy, hypertrophy, and recovery after hypertrophy (detraining). Since the time courses of x_1 and x_2 are different [11, 25], $a_1(t)$ and $a_2(t)$ are defined in different ways. The function $a_2(t)$ will be described in its respective loading-activity scenario,

Table 4.2.2: Parameters for the biochemical model. For equation system 4-1: intrinsic growth rates (a_i), self-inhibition rates (b_i), coupling strengths between species (c_{ij}). For the rate of change of the myofibril population (eq. 4-2): Minimum value $(z^{\min})$; maximum value (z^{Max}); threshold for x_3 (x_3^0); threshold for x_4 (x_4^0); rate of protein synthesis (k_1); and rate of protein degradation (k_2). a_{10} and a_{20} are reference values for functions $a_1(t)$ and $a_2(t)$.

Parameter	Value	Units	Reference
a_{10}	9.000×10^{-2}	hours^{-1}	fitted
a_{20}	4.875×10^{-1}	hours^{-1}	fitted
a_3	1.068×10^{-2}	hours^{-1}	fitted
a_4	4.635×10^{-3}	hours^{-1}	fitted
b_1	2.000×10^{0}	hours^{-1} (a.u.)$^{-1}$	fitted
b_2	5.000×10^{-1}	hours^{-1} (a.u.)$^{-1}$	fitted
b_3	2.000×10^{-2}	hours^{-1} (a.u.)$^{-1}$	fitted
b_4	1.000×10^{-2}	hours^{-1} (a.u.)$^{-1}$	fitted
c_{21}	2.846×10^{-1}	hours^{-1} (a.u.)$^{-1}$	fitted
c_{32}	2.000×10^{-3}	hours^{-1} (a.u.)$^{-1}$	fitted
c_{42}	1.139×10^{-3}	hours^{-1} (a.u.)$^{-1}$	fitted
c_{43}	2.500×10^{-3}	hours^{-1} (a.u.)$^{-1}$	fitted
$z^{\min}$	0.5000	a.u.	[28]
z^{Max}	1.300	a.u.	[84]
x_3^0	4.340×10^{-1}	a.u.	fitted
x_4^0	4.690×10^{-1}	a.u.	fitted
k_1	2.500×10^{-2}	hour^{-1}	fitted
k_2	1.900×10^{-2}	hour^{-1}	fitted

while the definition of the function $a_1(t)$ is the same for each loading-activity scenario and it is described below.

In this model, the exercise input is a function that shapes the intrinsic growth rate of x_1 (i.e., a_1 is defined as a function of time that represents a training protocol). This function (equation 4-3) incorporates intensity and training frequency according to any training protocol. It is assumed that $a_1(t)$ returns to the previous steady state as soon as the training session ends. After scaling the exercise signal, through a scale factor η, the training protocol enters into equation system 4-1 as the intrinsic growth rate $a_1(t)$.

$$a_1(t) = \begin{cases} \eta\, I\, F_{\max} & \text{During training time} \\ a_{10} & \text{During resting time} \end{cases} \tag{4-3}$$

Where $\eta = 2/50$ (hours $*$ kgf)$^{-1}$; I is the fraction of the maximum force ($F_{\max}$ in kgf) that the

muscle can produce; a_{10} is given in table 4.2.2; training and resting time define the training frequency, for instance, 1 hour every 48 hours.

Finally, the intrinsic growth rate of x_2 (a_2) is a function of time that is triggered by the $a_1(t)$ function (i.e., a_2 is triggered by a bout of exercise); but its subsequent behavior depends on the training (or loading) conditions according to the four different scenarios mentioned earlier. The next sections describe the three first scenarios, while the detraining case is considered in the validation section (section 4.3.3).All simulations were performed using a Runge-Kutta fourth-order method implemented in MATLAB R2015a (The MathWorks, Inc.).

4.2.2.1 Steady State

This model considers the steady state of the myofibril population as the result of minimum daily loading conditions that do not promote atrophy nor hypertrophy. The function $a_1(t)$ was set as 1.5 % of F_{max} (150 kgf, human quadriceps based on the experiments by Leger [92]). The function $a_2(t)$ was set at the constant value a_{20} given in table 4.2.2.

4.2.2.2 Atrophy: under bed rest and under therapy

The protein synthesis is inhibited in this case; therefore, the function $a_2(t)$ can only remain constant or decrease. $a_2(t)$ is considered as a decaying function such that population x_2 decreases in time; consequently, the myofibril population decreases as well. The model was tested for atrophy without training and for atrophy with training (therapy). In the latter, the role of each bout of exercise is to reset the rate of change of $a_2(t)$ to zero.

$$\frac{da_2}{dt} = -\frac{t}{f_{gA}} \exp\left[-\frac{t}{\tau_a}\right], \quad a_2(0) = a_{20} \tag{4-4}$$

where, $f_{gA} = 12.00 * 10^5 \text{ hours}^2$, $\tau_a = 690$ hours, a_{20} is given in table 4.2.2

This proposed behavior of $a_2(t)$ is based on experimental observations [92, 34] that show that AKT levels decrease in time under rest conditions.

4.2.2.3 Hypertrophy

In a healthy individual, the exercise input defined in equation 4-3 produces spikes in population x_1, which in turn produce spikes in population x_2 by means of function $a_2(t)$. Based on observations by Leger et al. and Louis et al. [92, 100], it is proposed that $a_2(t)$ increases for 12 hours and decreases to its previous level in 5 hours. A time delay of 12 hours between function $a_1(t)$ and population x_2 is also considered, so that a peak of x_1 occurs close to the

maximum value of x_2. $a_2(t)$ is defined by the following equation:

$$\frac{da_2}{dt} = \frac{1}{2}\left(-\frac{1}{\tau_h} - \frac{t - t_1}{\tau_h^2}\right)\exp\left[\frac{t - t_1}{\tau_h}\right], \quad a_2(0) = a_{20} \tag{4-5}$$

where τ_h = 6 hours, t_1 = 17 hours, a_{20} is given in table 4.2.2. In the case when no exercise signal is applied, $a_2(t) = a_{20}$.

The amplitude of the exercise input was based on the experiments by Leger et al. and Gorostiaga et al. [92, 65] on leg press training. In this chapter, bouts of exercise were simulated as pulses of 80% of $F_{\max}$ = 150 kgf, during a training time of one hour.

4.3 Validation

This section presents the methodology and results of the comparison between the model developed in this chapter and particular experimental studies. Specifically, the myofibril population of the model is compared to experimental measurements of cross-sectional area (CSA) in three of the four scenarios mentioned earlier: atrophy, hypertrophy, and detraining. The steady state scenario is presented, conveniently, in the simulation results section (4.4.2.1).

4.3.1 Validation of the atrophy scenario

Reduced muscle activity produces muscle atrophy: the duration of the inactivity period correlates to a decrease in the measurements of muscle volume, muscle CSA, and fiber CSA [130, 37, 164], as is shown in table 4.3.1 and figure 4.3.1. The model presented in this chapter used bed rest studies for validation up to 56 days of inactivity, while the model used spinal cord injury studies for validation from 42 up to 168 days of inactivity.

As required in equation 4-3, a simulation with an exercise input of intensity equal to zero was performed to simulate the atrophy scenario.

In figure 4.3.1 the different studies presented in table 4.3.1 are shown with different point styles; all the experiments considered for validation were performed on leg muscles. The results by Castro [28] validate the need of the saturation size $z^{\min}$ in equation 4-2, because every muscle has a different one. The match between the model developed in this chapter and the observations under bed rest condition is remarkable.

4.3.2 Validation of the hypertrophy scenario

Periodic high intensity training produces muscle hypertrophy: the duration of a high intensity training program correlates to an increase in muscle CSA, as presented in table 4.3.2 and figure 4.3.2. In particular, DeFreitas et al. [50] conducted an experiment in which subjects

Table 4.3.1: Atrophy validation data: Decrease in relative size (Rel. size) of muscle CSA as a function of the inactivity period. Each reference measured the CSA on different muscles: Quadriceps, Q; vastus lateralis, VL; soleus, SOL; gastrocnemius medialis, GM; quadriceps femoris, QF; vastus medialis VM. Most references measured the whole organ CSA, only two measured mean fiber CSA ($\star$). The effect of short term inactivity was measured under bed rest conditions ([†]), and the effect of long term inactivity was measured on spinal cord injury patients ([††]).

Rel. size	Inactivity (days)	Muscle	References
0.95	14	Q	[48, 83, 165] [†]
0.90	23	Q	[48] [†]
0.89	30	VL and SOL $\star$	[75] [†]
0.73	36	VL $\star$	[18] [†]
0.77	43	GM	[131] [†]
0.74	56	GM	[112] [††]
0.69	42	QF	[28] [††]
0.62	77	QF	[28] [††]
0.58	168	QF	[28] [††]
0.56	42	VM	[28] [††]
0.50	77	VM	[28] [††]
0.46	168	VM	[28] [††]

participated in training sessions on days 1, 3, and 5 of every week for 8 weeks; in addition to that, the intensity of training was approximately 80% of the one-repetition maximum force. For comparison purposes, the results by DeFreitas et al. [50] were normalized to the initial muscle CSA.

Simulations under three protocols similar to the experiment by the DeFreitas et al. [50] were performed. The simulations included 24 training sessions at 80% of F_{max}: (1) every two days, (2) every three days, and (3) on days 1, 3, and 5 of the week.

Figure 4.3.2 shows the comparison between the model and the experimental results by De-Freitas et al. [50]: Simulation results show that training every 2 days produces a faster growth and a bigger size; training every 3 days produces a slower growth as well as a smaller size; and training on days 1, 3, 5 of every week produces good agreement to the validation data.

4.3.3 Validation of the detraining scenario

Decreasing the intensity of a regular activity produces a reduction in muscle size. In particular, Leger et al. [92] observed the increase in CSA under high intensity training for 8 weeks
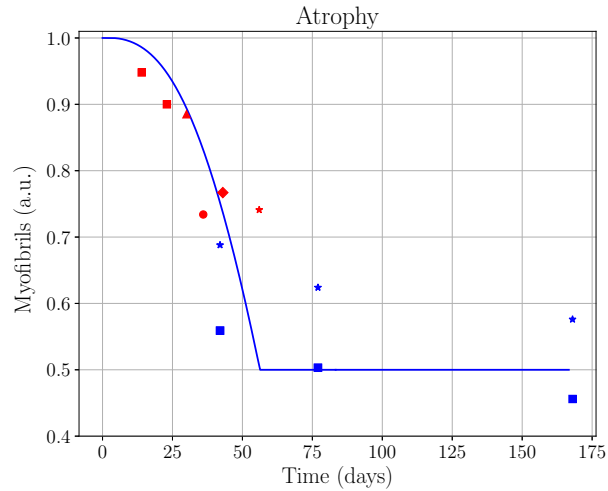
Atrophy

Figure 4.3.1: Comparison of experimental results vs. the model presented in this chapter for simulations of the atrophy scenario. Decrease in normalized CSA due to bed rest is presented in red (■ [48], ▲ [75], ● [18], ◆ [131], ★ [112]), and spinal cord injury is presented in blue (★ [28], ■ [28]); details are presented in table 4.3.1. Root mean squared error (RMSE), RMSE= 0.106.
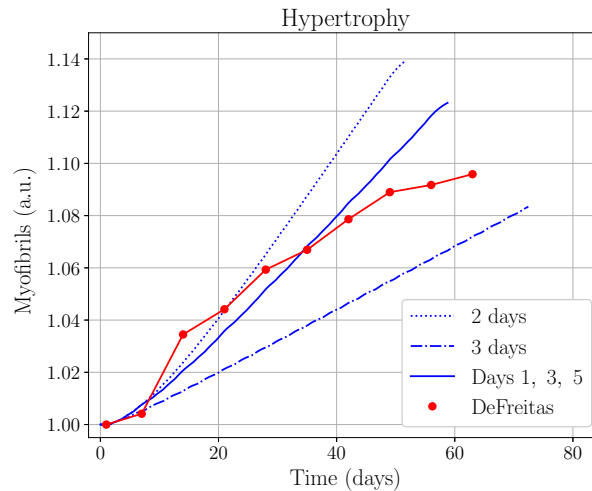
Hypertrophy

Figure 4.3.2: Comparison of experimental results vs. model simulations for the hypertrophy scenario. Hypertrophy results by DeFreitas et al. [50], three training protocols were used: training every 2 days (RMSE= 0.0193); training every 3 days (RMSE= 0.0261); and training on days 1, 3, and 5 of every week (used by DeFreitas et al., RMSE= 0.0114).

followed by a detraining period of 8 weeks. Training sessions took place 2 times per week for the first 4 weeks followed by 3 times per week for the last 4 weeks of training. The results showed an increase in CSA of about 10% after 8 weeks training, and a loss of half the gain

Table 4.3.2: Relative increase in muscle CSA due to high intensity training as a function of the activity period.

Rel. increase (%)	Activity (days)	References
0	1	[50]
0.4	7	[50]
3.5	14	[50, 148]
4.4	21	[50, 148]
5.9	28	[50]
6.7	35	[50, 148]
7.9	42	[50]
8.9	49	[50]
9.2	56	[50]
9.6	63	[50]

after 8 weeks of detraining.

A simulation of 15 training sessions at 80% of F_{max} every two days was performed, and then compared the maximum CSA (which occurs at certain time t_m) to the CSA after a time of $2\,t_m$.

Figure 4.3.3 shows how the myofibril population evolves during the 30 days of training protocol followed by 30 days of detraining. At the end of the 15 training sessions, the myofibril population continues growing for about 7 days, then it reaches a maximum, and finally it starts to decrease. The decrease in the myofibril population after the hypertrophy period is not as fast as an atrophic process. The model simulation produced an 8.3% increase in CSA; according to Leger et al. [92], the expected size after detraining is 4.15% smaller than the maximum size after training. The hypertrophy and decrease in size simulation results are similar to those reported by Leger et al. [92].

4.4 Results and discussion

This section starts by presenting and explaining the stability condition; then, the results of the simulations are provided in the same sequence as section 4.2.2.

4.4.1 Stability condition

The stability analysis shows that the dynamical system (eq. 4-1) always has a region of stability, since all parameters are positive by definition. The stability of equation system 4-1
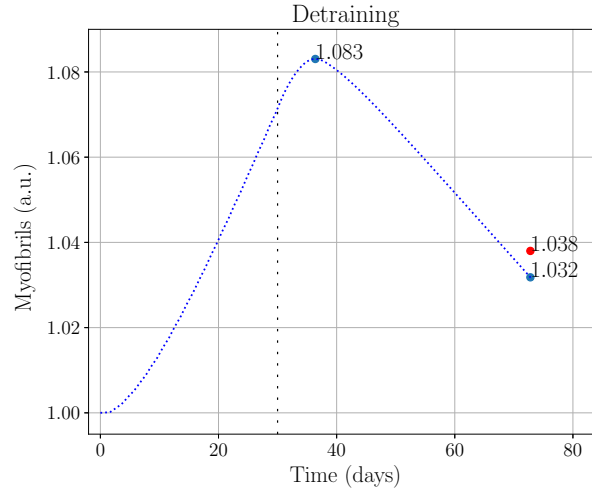
Figure 4.3.3: Comparison of experimental results vs. the model simulations for the detraining scenario. Expected results based on Leger et al. [92] observations (•); simulation results (⋯), reference points (•); end of the training time (⋮). According to Leger et al., a decrease in size of about half the gain is expected after a detraining time equal to the total training time; the decrease in size is calculated over the hypertrophied muscle. The relative error between the expected result and the model simulation is 0.6%.

occurs under the following condition:

$$L_{\min} < \frac{a_2(t)}{b_2} + \frac{c_{21}}{b_2}\frac{a_1(t)}{b_1} < \frac{a_3}{c_{32}} \tag{4-6}$$

with

$$L_{\min} = \max\left\{0, \frac{c_{43}\,a_3 - b_3\,a_4}{c_{43}\,c_{32} + b_3\,c_{42}}\right\}$$

For a given set of parameters, the upper and lower limits of the stability condition are fixed. The stability condition depends on: (1) the intrinsic growth rates $a_1(t)$, which defines the amplitude of the exercise signal, $a_2(t)$, which allows the system to evolve in a different time scale of the exercise signal, and a_3; (2) the self-inhibition rates b_2 and b_1; and (3) the coupling strengths c_{21} and c_{32}.

The coupling between x_3 and x_2 (c_{32}) strongly influences the upper limit of the stability condition. The lower the c_{32} value, the larger the upper limit to avoid positive λ values. Nonetheless, c_{32} should not be very small because x_3 determines the decrease in the myofibril population z (i.e., x_3 promotes atrophy).

Any set of parameters that contradicts equation 4-6 produces at least one positive λ and at least one negative singular point. Negative singular points are inaccessible, because only positive values for the variables are allowed in a population dynamics system. Thus, equation

system 4-1 is always stable provided that all parameters and initial conditions are greater than zero.

4.4.2 Simulation results

The model developed in this chapter was compared to experimental results in the validation section. This section presents some numerical examples of how the model predicts the evolution of the CSA in a muscle, considering the steady state, atrophy, and hypertrophy scenarios. First particular aspects of each scenario in relation to populations x_1, x_2, x_3, and x_4 are examined; then, the effects of different training protocols on the behavior of the myofibril population z are compared.

4.4.2.1 Steady state

The size of a skeletal muscle under sedentary conditions does not change in the time scale of months, unless a training program is developed. This means that the daily activity of a muscle is intense enough to avoid atrophy but not enough to produce hypertrophy. At this level of activity, the rate of growth of the five populations considered (the four biochemical families and the myofibril population) must be zero. This case is used to set a minimum value of the intrinsic growth rate of x_1.

Figure 4.4.1 shows how the biochemical populations x_1, x_2, x_3, x_4, and z evolve to their steady states. For x_1 and x_2, steady state populations are not close to the initial conditions due to their high intrinsic growth rate. x_1 and x_2 must respond faster than x_4 and x_3 because x_1 receives stimulus directly and x_2 is affected only by x_1. As x_3 and x_4 control the evolution of the myofibril population, the steady state populations x_3 and x_4 are close to their respective threshold. This implies that an increase or decrease in the daily activity promotes an adaptation process on the myofibril population but, since the system is stable, it returns to the steady state.

4.4.2.2 Atrophy

The atrophy case verifies the evolution of the populations when protein synthesis is restricted. Figure 4.4.2 shows the results of the dynamical system under atrophy conditions. These results are consistent with the following observation: the signaling pathway becomes active every time the muscle senses exercise via x_1; therefore, in the absence of a sustained exercise signal, population x_1 should decrease to zero.

When population x_1 decreases, population x_2 decreases as well. That decrease in population x_2 causes an increase in population x_3. Both, the increase in x_3 and the decrease in x_2 cause x_4 to decrease; as a consequence, the myofibril population decreases as well. Population z decreases until it reaches its minimum value ($z^{\min}$). The evolution of the variables of the
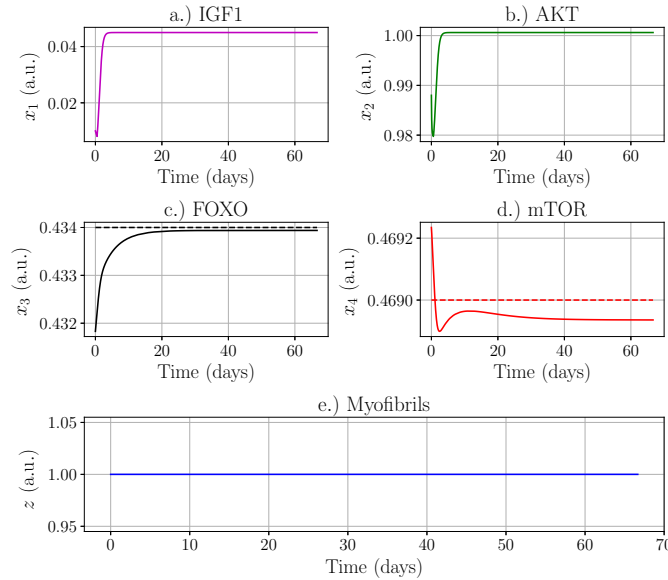
Figure 4.4.1: Steady state solution of the dynamical system (eq. 4-1). **a.)** IGF1 (population x_1), **b.)** AKT (population x_2), **c.)** FOXO (population x_3) and its threshold level (dashed line), **d.)** mTOR (population x_4) and its threshold level (dashed line), **e.)** Myofibrils (population z). All populations reach a steady state provided that no intense exercise is performed.

pathway is presented in figure 4.4.2, and the evolution of the myofibril population is shown in the continuous line of figure 4.4.3.

In a special case where muscle is not able to hypertrophy, such as in spinal cord injury, therapy is intended to avoid muscle tissue loss. According to the model developed in this chapter, x_1 is increased due to bouts of exercise. An increase in x_1 is followed by an increase in population x_2, and this change in population x_2 promotes the evolution of the system. Figure 4.4.3 shows the behavior of the populations in response to different therapy-training frequencies. Results show that therapy helps tissue to slow the atrophy process even in the case of low-therapy frequency: compare therapy every 6 days with the case of no therapy. According to the results in figure 4.4.3, the model suggests that therapy every two days leads to a muscle waste of only 10% in 84 days.

4.4.2.3 Hypertrophy

This section considers the evolution of the dynamical system in the case where none of the populations are restricted. Figure 4.4.4 shows that: first, $a_1(t)$ produces a delayed increase response in x_1 and triggers function $a_2(t)$; and second, the behavior of population x_2 reflects a superposition of $a_2(t)$ and x_1.

Populations evolve in a similar way as described in the atrophy case: x_1 increases due to exercise, and it produces an increase in x_2. This time, the increase in population x_2 causes
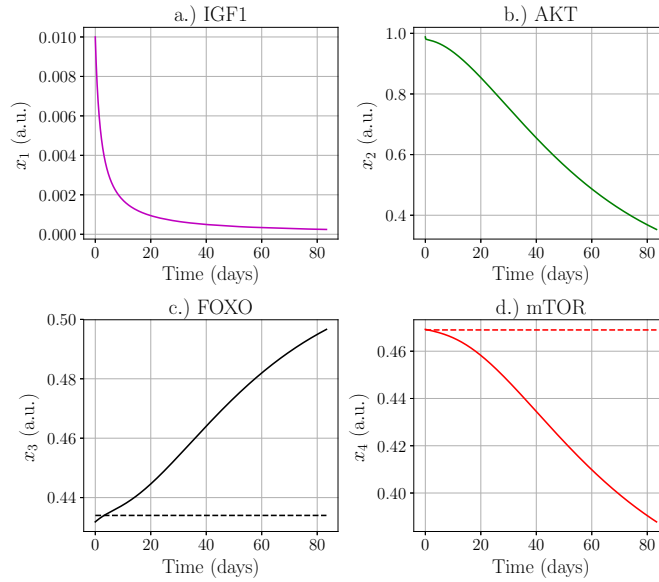
Figure 4.4.2: Evolution of the dynamical system under rest conditions. **a.)** population x_1 decreases to zero; **b.)** population x_2 decreases because x_1 regulates its behavior; **c.)** the increase in population x_3 promotes atrophy; **d.)** population x_4 decreases as a result of an increase in population x_3 and a decrease in population x_2. Dashed lines are the threshold for x_3 and x_4.
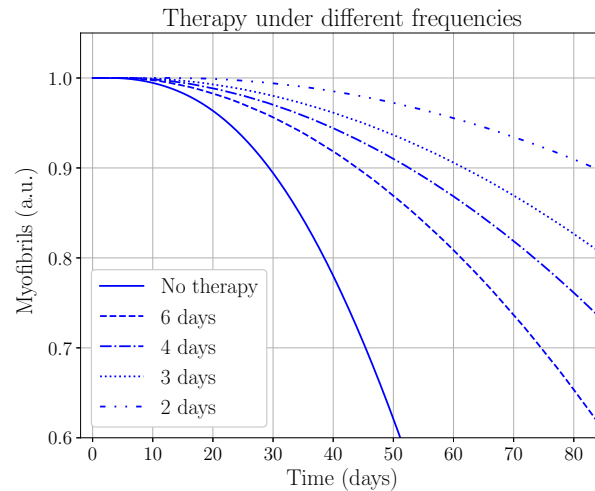
Figure 4.4.3: Evolution of the myofibril population for spinal cord injury and therapy loading conditions. Bouts of exercise every six, four, three, and two days. The model developed in this chapter shows that the atrophy effects of spinal cord injury (or atrophy) are reduced by therapy. Protein synthesis is blocked, but protein degradation is slowed by increasing the frequency of therapeutic exercise.

a decrease in population x_3. Finally, both the decrease in x_3 and the increase in x_2 cause x_4
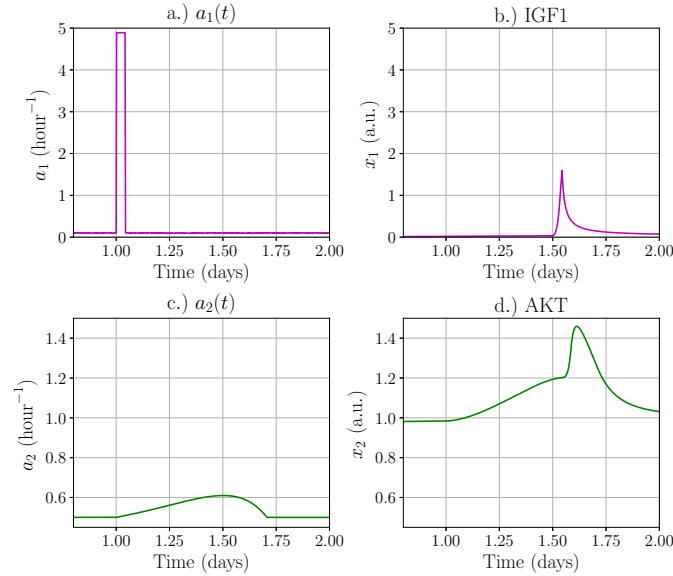
Figure 4.4.4: Behavior of the intrinsic growth rate functions. **a.)** a_1 represents a bout of exercise of a duration of an hour. **b.)** x_1 peaks 12 hours after the activation of the function a_2. **c.)** The function $a_2(t)$ does not peak during exercise; this allows x_2 to sustain the effects of exercise for a longer time than x_1. **d.)** According to the stability analysis, population x_2 peaks as a superposition of function a_2 and population x_1.

to increase; as a consequence, the myofibril population increases as well.

Hypertrophy is the result of repeated training [50, 63], the effect of training frequency are shown in figure 4.4.5a, a simulation of the increase in the myofibril population after training protocols of 15 bouts of exercise every day, every two, every four, and every five days is presented. As expected, hypertrophy is faster in the protocol of everyday training, but the case of training every two days produces similar results. The protocol of training every four days produces hypertrophy at a much slower and irregular pace. It is interesting to note that in the case of training every five days, hypertrophy is not produced. This last result is consistent with the common medical recommendation of practicing exercise at least three times a week (every two or three days) [180].

The model considers a maximum myofibril population that is based on experimental observations (table 4.2.2). However, the simulations results were far from that maximum size: the myofibril population was only 14% bigger than the initial population after 24 training sessions every two days (fig. 4.3.2), and about 11% after 15 training sessions every day (fig. 4.4.5). Although, according to the trend of the simulation results, the maximum size will be reached after a greater number of training sessions, experiments show that muscle growth reaches a plateau within 6 to 12 weeks of training depending on the muscle group [39]. The time to reach the plateau suggests that the rate of protein synthesis also adapts to exercise; chapter 5 addresses this feature.

Figures 4.4.5b to 4.4.5e show that as long as x_4 is above its threshold, x_3 is below its threshold; these figures also show that higher training frequencies allow x_4 to build above the threshold (figs. 4.4.5b and 4.4.5c), whereas an oscillation around it occurs at lower frequencies (figs. 4.4.5d and 4.4.5e).
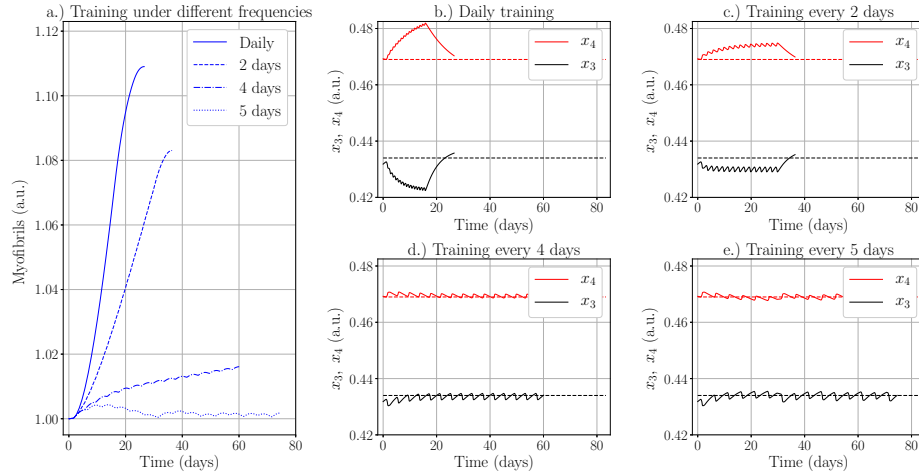
Figure 4.4.5: **a.)** Evolution of the myofibril population under different training frequencies. The oscillatory behavior of populations x_3 and x_4 to each corresponding frequency is shown in figures **b.)** to **e.)**. 15 training sessions were simulated for each training frequency. The dashed lines in figures **b.)** to **e.)** represent the thresholds of population x_3 and x_4.

4.5 Conclusion

A mathematical model for the IGF1-AKT signaling pathway was developed in this chapter. The model predicts the variation in muscle protein content under different activity conditions. The pathway was modeled using its 4 main molecules as variables in a dynamical system, and it was proposed that the pathway is triggered by an exercise signal. To differentiate the atrophy to the hypertrophy scenarios, a different behavior of only one parameter of the model was considered. Assuming that the protein content correlates to muscle cross sectional area, the model was validated by comparison to experimental data, and additional activity patterns were also simulated. The simulation results show that atrophy is reduced by the implementation of therapy as an exercise signal: the more frequent the therapy, the slower the atrophy effects; in the case of hypertrophy, cross sectional area increases at different pace depending on the frequency of training: the more frequent the training the faster the hypertrophy effects; the simulation results also show that training every five days is not frequent enough to produce hypertrophy.

The hypertrophy simulations results suggest that the protein synthesis rate should be affected by the increasing size of the muscle, otherwise the protein content would increase indefinitely.

This observation is addressed in the next chapter, where the IGF1-AKT model of this chapter is connected to the continuum mechanical model presented in chapters 2 and 3.

Appendix

4.A Published work permission to use

Most of the content of this chapter was published in:

A dynamical system for the IGF1-AKT signaling pathway in skeletal muscle adaptation

5 Multi-scale mechanobiological model for skeletal muscle hypertrophy

5.1 Background

Training exercise has an important effect on skeletal muscle as it is the main mechanism to increase protein content. Training exercise is related to the mechanical behavior of muscle, whereas the increase in protein content is related to the biological behavior.

From the biological perspective, protein synthesis is promoted by the IGF1-AKT signaling pathway [143, 141]. The most prominent relation in this pathway starts when insuline-like growth factor (IGF1) [2] promotes the serine/threonine kinase (AKT) [152]. After that, AKT promotes the mammalian target of rapamycin (mTOR) [70] and inhibits the forkhead box transcription factor (FOXO) [174]. Two outcomes can occur: hypertrophy or atrophy. If FOXO is inhibited, then mTOR activates protein synthesis to produce hypertrophy; while, if AKT is inhibited, then FOXO promotes protein degradation and the inhibition of mTOR to produce atrophy.

The regulation of protein content is key to preserve or improve the ability to generate force, which at a subcellular scale is explained by the sliding filament theory [69, 129, 81]. According to this theory, internal sarcomere constituents -actin and myosin- overlap and change the overlapping length while momentarily bound to one another; this short-lasting bound generates force and is known as cross-bridge [82, 133, 57, 138]. The force generation process starts when the nervous system sends electrical signals to muscle fibers triggering a muscle contraction [104, 89, 49].

Muscle contraction, from a mechanical perspective, is also known as active response. The force generated during contraction is a function of the fiber stretch that occurs during the actin and myosin overlap [64, 56, 161]. In contrast, a passive response occurs when a muscle is stretched without contracting. Both the active [71, 132] and passive [14, 168] responses of skeletal muscle tissue have been modelled as hyperelastic transversely isotropic materials.

In addition to the passive and active responses, the mechanical description also addresses the adaptive characteristics of living tissue through the mechanics of growth, in particular for cardiac tissue [60] and longitudinal skeletal muscle growth [181, 3]. Regarding the mechanical description of tissue growth, the multiplicative decomposition [136] of the deformation gradient into elastic and growth components plays a major role. The elastic component

requires the characteristic material response of the tissue (passive response), whereas the growth component requires the use of a factor known as growth multiplier [60] that lacks of a connection to any biochemical aspect of tissue adaptation.

As mentioned before, physical activity triggers a biochemical response that produces an increase in protein content; however, neither the hyperelastic mechanical response nor the growth models consider any biochemical basis for an increase in mass. Besides this biochemical basis, a model for skeletal muscle adaptation should address two other key characteristics: first, skeletal muscle adapts to intermittent yet regular training (in contrast to continuum-mechanics growth models that require continuous sustained strain or stress); and second, the time scale of skeletal muscle adaptation as an outcome of exercise training ranges from weeks to months (whereas the time scale of simulations on active and passive mechanical responses of muscle tissue ranges from seconds to minutes, and the time scale of simulations of tissue growth models agrees with that of muscle adaptation).

The aim of this chapter is to present a multi-scale mechanobiological model for skeletal muscle cross sectional area (CSA) adaptation. Starting with the models presented in chapters 3 and 4, this chapter describes the procedure to couple the biochemical model to the mechanical model by the definition of a growth multiplier. After that, the procedure to couple the mechanical model to the biochemical model by the definition of a feedback function is described. With the purpose of validation, a training protocol was simulated and the model predictions were compared to experimental data. Finally, a discussion of the results is presented.

5.2 Materials and Methods

Features related to different size scales of skeletal muscle tissue are mathematically modeled from two independent study fields: biochemistry and mechanics. A biochemical model describes features at the cellular scale, and a mechanical model describes features at the organ scale. The biochemical and mechanical multi-scale model of this chapter is based on the inter-relation between both fields.

Previous chapters presented the mechanical model (skeletal muscle passive and active responses in chapter 3), and the biochemical model (IGF1-AKT signaling pathway that produces muscle hypertrophy or atrophy in chapter 4). Briefly, the main outcome of the biochemical model (eq. 4-1) is the rate of change of population z, i.e. $f(x_3, x_4)$, and the main function of the mechanical model is the description of the deformations of muscle tissue due to strain, stress or growth. A change in size due to muscle hypertrophy or atrophy affects the mechanical response via the growth tensor that is described later in this section.

This section is divided into two parts: Mechanobiological model (section 5.2.1), and Numerical experiments (section 5.2.2). Section 5.2.1 presents the procedures to couple: first, the biochemical to the mechanical model, and second, the mechanical to the biochemical model;

section 5.2.2 presents particular aspects regarding parameters, initial conditions, exercise-training protocol and computational implementation.

5.2.1 Mechanobiological model

The concepts to interrelate the biochemical and mechanical models that compose the multi-scale mechanobiological model are described in this section.

To describe the coupling procedures between the independent models, two conceptual stages and two coupling functions are needed. First, the two stages are defined as follows: a *training period* that typically ranges from minutes to hours, occurs when external loading conditions stimulate the biochemical pathway, and allows the assessment of CSA and force according to the mechanical model; and a *growth period* that typically ranges from days to weeks, occurs after each training session, and promotes the evolution of the myofibril population z according to the biochemical model. The intention of the two functions, *growth multiplier* and *force-activation relation*, is to build a mathematical connection between the different scales of the independent models and will be briefly described in the paragraphs below. Details of the construction of the functions and the coupling procedures are presented in appendices 5.A and 5.B.

The growth of the muscle structure is characterized by the growth tensor $\mathbf{F_g}$, which, following a multiplicative decomposition [91, 136, 163], requires an elastic deformation $\mathbf{F_e}$ to ensure compatible configurations while the muscle grows:

$$\mathbf{F} = \mathbf{F_e}\,\mathbf{F_g} \tag{5-1}$$

The growth tensor $\mathbf{F_g}$ links the rate of change of myofibrils $f\left(x_3, x_4\right)$ to the increase in cross-sectional area $(\mathcal{A})$ of the muscle structure by using a growth multiplier $G\left(t\right)$ defined as:

$$G\left(t\right) = \frac{f\left(x_3, x_4\right)\Delta t}{\kappa\,\mathcal{A}\left(t - \Delta t\right)} + 1 \tag{5-2}$$

Details about the construction of the growth multiplier are presented in appendix 5.A.1. According to equation 3-14, assuming $\vartheta_L = 1$, in this chapter,

$$\mathbf{F_g} = \mathbf{F_g}(t) = \boldsymbol{e}_1 \otimes \boldsymbol{E}^1 + G\left(t\right)^{1/2}\left(\mathbb{1} - \boldsymbol{e}_1 \otimes \boldsymbol{E}^1\right), \tag{5-3}$$

where $G\left(t\right)$ (that replaces ϑ_A), defined by equation 5-2, produces an increase in the area transverse to vector $\boldsymbol{e}_1$ ($\boldsymbol{e}_1$ defines the direction of the muscle fiber).

The biochemical model is now coupled to the mechanical model by converting $f\left(x_3, x_4\right)$ (which results from the biochemical model in section 4.2.1) into the growth tensor (according to equations 5-2 and 5-3), and by operating the growth tensor over the current muscle

structure. Details of the implementation of this procedure are presented in appendix 5.A.2.

Now that the biochemical model is linked to the mechanical model, the mechanobiological model needs to close the feedback loop by linking the mechanical to the biochemical model. In this regard, the force-activation relation $F(\mathcal{A}, \beta)$ links the active response of the mechanical model to the rate of change of myofibrils $f(x_3, x_4)$ by means of the inverse function $\beta(\mathcal{A}, F)$. The procedures to build both the function $F(\mathcal{A}, \beta)$ and its inverse function $\beta(\mathcal{A}, F)$ are described in appendix 5.B.1.

The mechanical model is coupled to the biochemical model by modifying the protein synthesis rate (k_1 in equation 4-2). This modification uses the function $\beta(\mathcal{A}, F)$ as feedback; the concepts for implementing this procedure are presented in appendix 5.B.2.

In summary, the biochemical model is coupled to the mechanical model by means of the growth tensor, and the mechanical model is coupled to the biochemical model by means of the force-activation relation. A full algorithm of the computational model is shown in figure 5.2.1.
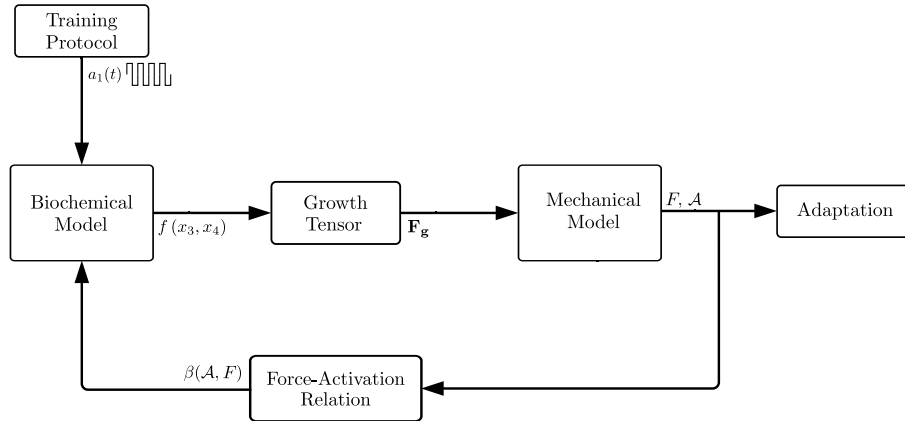
Figure 5.2.1: Algorithm for the mechanobiological model for muscle adaptation. f is the rate of change of the myofibril population, $\mathbf{F_g}$ is the growth tensor, F and $\mathcal{A}$ are the force and CSA of the updated muscle structure, $\beta(\mathcal{A}, F)$ is the inverse function of the *force-activation* relation at CSA $\mathcal{A}$.

5.2.2 Numerical experiments

Parameters and initial conditions of the independent models were presented in the previous chapters. Parameters for the biochemical model were presented section 4.2.1.3, and for the mechanical model were presented in section 3.4. The initially normalized myofibril population allows a proportionality constant $\kappa = 1/\mathcal{A}(0)$.

The implementation of the biochemical model considers a hypertrophy scenario (see section 4.2.2.3) with a training input based on the experimental protocol given in DeFreitas et al.

[50]. Subjects in that study performed a total of 24 1-hour sessions on days 1, 3, and 5 of every week. The intensity of training was approximately 80% of the one repetition maximum (1-RM) force. As defined in section 5.2.1, each 1-hour training session is a *training period*, while the time right after each training session is a *growth period*.

Equation system 4-1 was solved by means of a Runge-Kutta fourth-order method in a Fortran routine. The time step was 0.05 hours and the total time simulated was eight weeks.

The implementation of the mechanical model depends on the stage of the evolution process. First, the implementation during the growth period uses the growth multiplier given in equation 5-2, the growth tensor given by equation 5-3, and the activation parameter $\beta = 0$. Second, during the training period, the growth tensor is equal to the identity tensor, and the activation parameter first increases from 0 to 1 and then decreases back to 0.

The mechanical response of the tissue was simulated by means of a UEL subroutine, implemented in Fortran, linked to the solving procedures in the specialized software ABAQUS 3DEXPERIENCE R2017x (Dassault Systemes USA, Waltham, MA).

The CSA evolution from the mechanobiological model will be compared to the adaptation results obtained by DeFreitas et al. [50]. In their study, the CSA of human right thigh muscles was measured every week by using a peripheral quantitative computed tomography.

5.3 Results and discussion

The mechanobiological model in section 5.2.1 was tested under the numerical experiments described in section 5.2.2. The main result of the numerical experiments was the increase in CSA of the muscle structure at the end of three different stages of the algorithm, namely: first, at the end of the biochemical model; second, at the end of the mechanical model before the implementation of the feedback from the mechanical to the biochemical model; and third, at the end of the mechanical model after the feedback was included (see figure 5.2.1).

The first two stages show that the CSA of the muscle structure differs from the myofibril population of the biochemical prediction, as seen in figure 5.3.1. This difference is explained by the elastic response of the material that enforces compatible configurations. In this regard, since the mechanical properties of the muscle tissue do not change due to adaptation processes, the elastic deformation contribution of the deformation gradient (eq. 5-1) does not depend on the biochemical parameters. Hence, the difference between CSA and biochemical prediction shown in figure 5.3.1 cannot be avoided because the biochemical model only controls the growth tensor contribution of the deformation gradient.

Before the results of the third stage, the function $\beta(\mathcal{A}, F)$ is required (this function is the inverse relation of the force-activation relation and the link from the mechanical to the biochemical model). Function $\beta(\mathcal{A}, F)$ (figure 5.3.2), obtained following the procedure described in appendix 5.B.1, shows that a larger muscle requires a smaller activation to produce a fixed force.
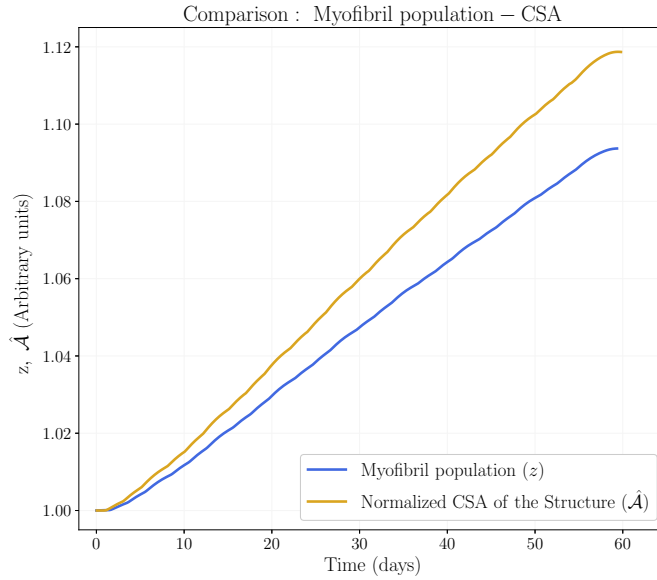
Figure 5.3.1: Cross Sectional Area and myofibril population comparison. These results were obtained by considering full activation ($\beta = 1$) for the whole training protocol, and no feedback from the mechanical to the biochemical model.
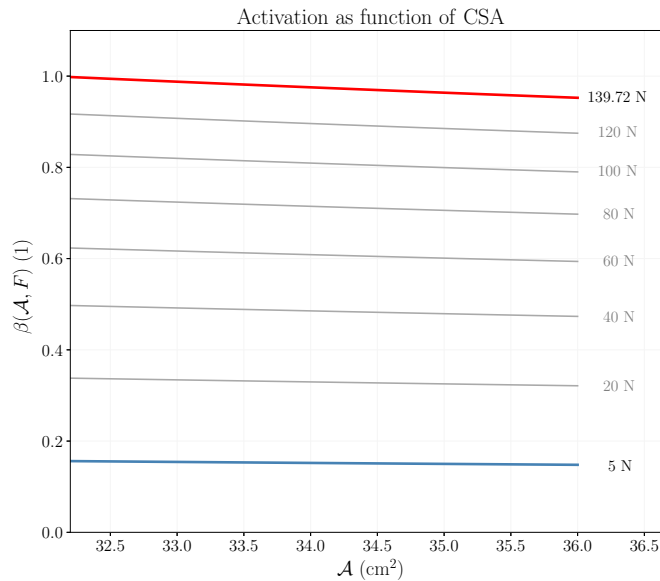
Figure 5.3.2: Activation level β as a function of the CSA $\mathcal{A}$ for different force levels. The activation required to produce a fixed force decreases as the CSA of the structure increases.

Assuming an increasing CSA, the following observations about function $\beta(\mathcal{A}, F)$ justify the necessity to feedback the biochemical model: first, the decrease in the activation required to produce a fixed force implies that the muscle tissue receives a decreasing intensity of

stimulus if the training load is fixed during the training protocol; second, the variation on the activation required with lighter loads is almost negligible and supports the recommendation of training with intermediate to high loads; and third, the variation on the activation required with heavier loads is noticeable and supports the recommendation of training with increasing loads. These observations can be related to early neuronal adaptation, which can occur before significant hypertrophy happens; however, since the model ignores the neuronal variable, further analysis is necessary.

Now, the CSA after stage three, which includes the function $\beta(\mathcal{A}, F)$ as feedback, is considered. In the biochemical model, the size of the myofibril population z is strongly dominated by the size of population x_4. However, it was assumed that population x_4 should remain close to its threshold x_4^0 to have steady-state solutions; therefore, the mecanobiological model included the feedback directly into the protein synthesis rate k_1 (eq. 4-2) rather than in the equation for the rate of change of x_4. The modified protein synthesis rate k_1 is given by:

$$k_1 = k_{10} * \left(d_1\, \beta\left(\mathcal{A}, F\right) - d_2 \right) \tag{5-4}$$

where k_{10} is the k_1 value used in the biochemical system without feedback, and dimensionless parameters d_1 and d_2 allow to adjust the strength of the coupling; in the simulations of this chapter: $d_1 = 25.664$, and $d_2 = 23.987$.

Figure 5.3.3 shows a comparison of the ratio k_1/k_{10} of the biochemical system alone, and the same ratio using the coupling relation $\beta(\mathcal{A}, F)$ as feedback. At the initial CSA, the coupling relation produces a greater value of k_1 than the value of k_{10}. A greater value of k_1 produces a faster growth rate during the first weeks of training in agreement with experimental results (fig. 5.3.4). The parameter k_1 decreases below k_{10} while CSA increases; the decrease in the value of k_1 implies a decrease in growth rate.

Figure 5.3.4 shows the mechanobiological model results when the feedback is used in k_1, and also a comparison with experiments. The simulation results show that muscle grows faster during the early days of the training period, and the growing speed decreases with time even when training is continued. This means that the protein storing rate decreases as the protein content increases until eventually a maximum muscle size is reached. In the mechanobiological model, the protein synthesis rate was initially set constant (before the feedback implementation); when the biochemical system was fed back directly in the protein synthesis rate (according to equation 5-4) the mechanobiological model matches in size and shape the experimental results. Therefore, it is reasonable to argue that the muscle adaptation feedback affects directly the protein synthesis level. In addition, the mechanobiological model shows that a muscle cannot grow indefinitely when driven only by exercise.

Finally, some aspects of the experimental data in figure 5.3.4 are discussed. Experiments show that muscle grows even in the early days of a training period. According to Seynnes and DeFreitas [148, 50], the early increase in CSA can be considered as hypertrophy; but Damas and coworkers [44] argue that a major contribution could be related to edema. To
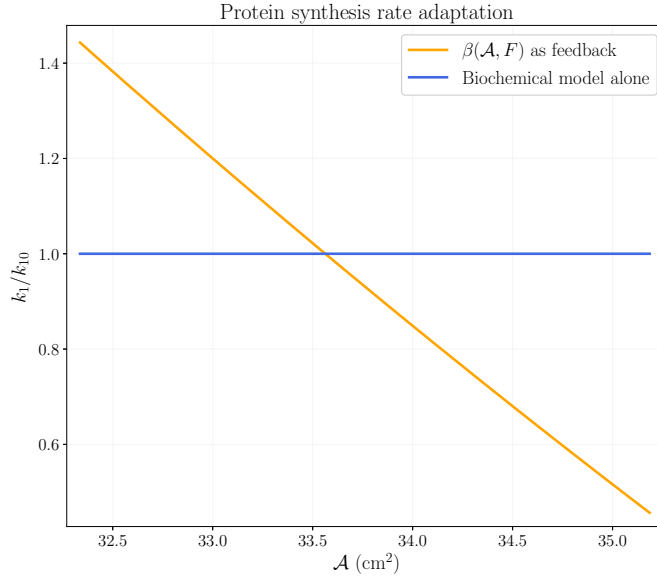
Figure 5.3.3: Protein synthesis rate k_1 given by equation 5-4, at parameters d_1 = 25.664 and d_2 = 23.987. Here, the growth rate k_1 of the original biochemical system eq. 4-1 is compared to the modified value of k_1 using the feedback from the mechanical response given by equation 5-4.

solve the edema observation, Stock and coworkers [162] measured the CSA increase under a concentric-only training; they showed that hypertrophy is small but detectable during the first training sessions. The increase in CSA is similar in all cases, even when the training protocol avoids edema. Thus, it is possible to argue that, although the mechanobiological model ignores muscle damage and considers isometric contraction, the simulation results are in good agreement to regular and concentric-only training.

5.4 Conclusion

In this chapter a multi-scale mechanobiological model for muscle CSA adaptation was proposed. Starting at the biochemical base of the IGF1-AKT signaling pathway to predict how the protein content inside a muscle fiber evolves, a growth multiplier and subsequently a growth tensor were defined; the multiplier and the tensor allowed to connect the cellular scale of the adaptation to the organ scale by means of the mechanics of growing tissue. Furthermore, the characteristic adaptation in force allowed to build a function that describes how the activation of a muscle changes during the adaptation process. This chapter proposed that this activation function affects the protein synthesis rate, and in this way the activation function connects the organ scale to the cellular scale. The results of the multi-scale mechanobiological model for the CSA adaptation presented in this chapter show a
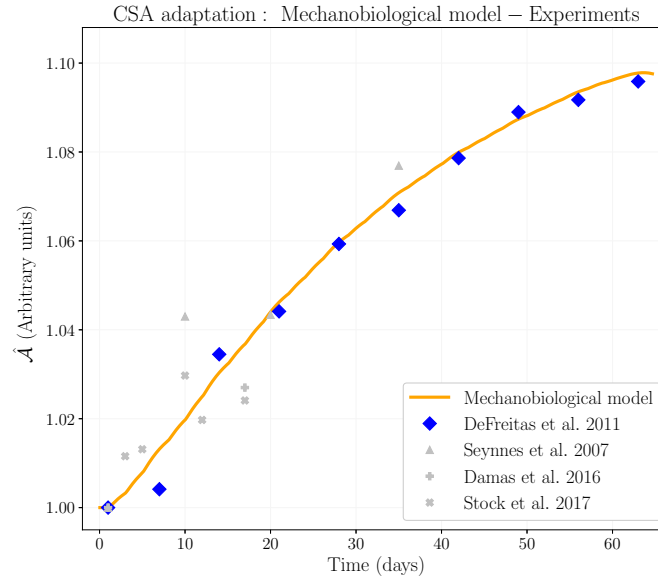
Figure 5.3.4: Normalized CSA adaptation due to training. Experimental results compared to the mechanobiological model simulations. The activation function shown in figure 5.3.2 was used to feedback equation system 4-1. The modified protein synthesis rate was defined in equation 5-4, and replaces the constant value of the protein synthesis rate in function $f(x_3, x_4)$ defined through equation 4-2. The training protocol of DeFreitas et al. [50] was simulated, and parameters d_1 and d_2 were fitted to minimize the RMSE.

remarkable agreement to experiments.

Exercise training also triggers the evolution of the protein-isoform content specific for each fiber type (the protein-isoform content relates to fiber type distribution), but the mechanisms that produce protein increase and protein-isoform replacement are different. The next chapter addresses the calcineurin-NFATc signaling pathway that is key in the promotion of protein-isoform replacement.

Appendix

5.A Coupling the biochemical to the mechanical model

Muscle structure at the organ scale adapts according to signals at the biochemical scale. In this appendix, the construction the growth multiplier that couples scales, and the procedure to update the muscle structure are presented.

5.A.1 Constructing the growth multiplier

Sections 3.1 and 3.2 presented the mechanical response of muscle as a continuous material, and section 4.2.1 presented the mathematical description of the IGF1-AKT signaling pathway; however, those descriptions are independent of one another. Here the growth multiplier is introduced; the multiplier links the rate of change of myofibrils $f(x_3, x_4)$ to the increase in CSA of the continuous material.

If myofibrils are added in parallel, the CSA of a muscle fiber increases; therefore, it is assumed that the myofibril population z is proportional to the CSA of muscle ($\mathcal{A}$):

$$z(t) = \kappa \, \mathcal{A}(t) \tag{5.A.1}$$

Where κ is the proportionality constant in myofibrils/cm^2. Assuming that $z(t = 0) = z_0$, and $\mathcal{A}(t = 0) = \mathcal{A}_0$, then $\kappa = z_0 / \mathcal{A}_0$.

As muscle tissue is assumed as a nearly incompressible material, the mass density of the tissue will be considered constant. From a mechanical perspective, the CSA at time t is equal to the growth multiplier at time t acting on the CSA at time $t - \Delta t$

$$\mathcal{A}(t) = G(t) \, \mathcal{A}(t - \Delta t) \tag{5.A.2}$$

From the biochemical perspective, the myofibril population is the outcome of the biochemical system (eq. 4-1)

$$\frac{dz}{dt} = f(x_3, x_4)$$

A small increment in z is:

$$\Delta z = f(x_3, x_4) \, \Delta t \tag{5.A.3}$$

The evolution of z is linked to $\mathcal{A}$ by replacing eq. 5.A.1 in the definition of a differential of z:

$$\Delta z = z(t) - z(t - \Delta t)$$
$$= \kappa \mathcal{A}(t) - \kappa \mathcal{A}(t - \Delta t)$$

Using the mechanical evolution of $\mathcal{A}$ given by eq. 5.A.2:

$$\Delta z = \kappa G(t) \mathcal{A}(t - \Delta t) - \kappa \mathcal{A}(t - \Delta t)$$
$$= \kappa (G(t) - 1) \mathcal{A}(t - \Delta t)$$

From this,

$$G(t) = \frac{\Delta z}{\kappa \mathcal{A}(t - \Delta t)} + 1$$

and finally, using the biochemical evolution of z given by eq. 5.A.3:

$$G(t) = \frac{f(x_3, x_4) \Delta t}{\kappa \mathcal{A}(t - \Delta t)} + 1 \tag{5.A.4}$$

$G(t)$ is the growth multiplier of the muscle transverse to the fibers. This implies that the transverse components of the growth tensor are modulated by this growth multiplier. In equation 5.A.4, Δt is the time increment of the geometry of the muscle via the mechanical model. It is important to note that the time scale of the biochemical evolution is not necessarily equal to the mechanical part, because, for the mechanical evolution, Δt is not an incremental step for an ordinary differential equation, whereas the set of differential equations for the biochemical part (eq. 4-1) require a small time step (dt) for convergence.

5.A.2 Updating the muscle structure with the growth tensor

The simulation starts at day 0 with a growth tensor equal to the identity tensor. At day 1 the training protocol function $a_1(t)$ (defined in equation 4-3) stimulates the biochemical model for the first time, such stimulation lasts a training period.
The implementation of the mechanobiological model continues as follows:

1. After a training period, the populations of molecules in the biochemical model evolve according to the system of equations presented in section 4.2.1; the solution of the system is stored, and in this way, $f(x_3, x_4)$ is a function of time.

2. During the growth period, the rate of change of the population of myofibrils ($f(x_3, x_4)$ function) at time t is converted into the growth tensor $\mathbf{F_g}(t)$ according to equations 5.A.4 and 5-3.

3. According to the kinematics of finite growth [60], $\mathbf{F_g}(t)$ is applied to the current muscle structure in order to generate the updated structure.

4. The time t is incremented; the process goes back to step 2 if a growth period is occurring, or to step 1 if a new training period is going to stimulate the system. In the latter case, the last stored state of the variables of the biochemical model is used as a new set of initial conditions for equation system 4.2.1.

5.B Coupling the mechanical to the biochemical model

Biochemical parameters adapt according to muscle size and strength. In this appendix, the construction of the force-activation relation that couples scales, and the procedure to update the biochemical model are presented.

5.B.1 Constructing the force-activation relation

The CSA of the structure changes as a result of applying the growth tensor over the current structure during the growth period, and every updated muscle structure can generate a different force. The structure right **before** a training period is subjected to an activation cycle of the mechanical model (according to section 3.4.2) to evaluate how the force generation is affected by the adapting structure: the mechanical model runs over different values of the activation parameter (β) and calculates the corresponding force (F); as β increases from 0 to 1, the force F increases. This relation is called *force-activation* relation. In what follows, the CSA of the structure stored **before** a training period will be simply referred to as CSA. A feedback function ($\beta = \beta(\mathcal{A}, F)$) is required to build the link from the mechanical to the biochemical model. For a given force (F) and a given CSA ($\mathcal{A}$), the feedback function describes how the activation (β) changes. To address this aim, the following procedure was implemented:

- For each CSA, a set of points from the *force-activation* relation is obtained. A quadratic fit for the inverse relation *activation-force* is calculated (see figure 5.B.1):

$$\beta\left(F\right) = a_{\mathcal{A}} + b_{\mathcal{A}} \, F + c_{\mathcal{A}} \, F^2,$$

  where the subindex $\mathcal{A}$ means that the coefficient depends on a fixed value of CSA.

- Using each CSA and its corresponding coefficients, sets $\{\mathcal{A}, a_{\mathcal{A}}\}$, $\{\mathcal{A}, b_{\mathcal{A}}\}$, $\{\mathcal{A}, c_{\mathcal{A}}\}$ are built.

- A quadratic fit for each set is calculated:

$$
\begin{aligned}
a(\mathcal{A}) &= a_0 + a_1\,\mathcal{A} + a_2\,\mathcal{A}^2 \\
b(\mathcal{A}) &= b_0 + b_1\,\mathcal{A} + b_2\,\mathcal{A}^2 \\
c(\mathcal{A}) &= c_0 + c_1\,\mathcal{A} + c_2\,\mathcal{A}^2
\end{aligned}
\tag{5.B.1}
$$

- The functions defined in equation 5.B.1 allow to have an explicit activation function:

$$\beta\left(\mathcal{A}, F\right) = a(\mathcal{A}) + b(\mathcal{A})\,F + c(\mathcal{A})\,F^2, \tag{5.B.2}$$
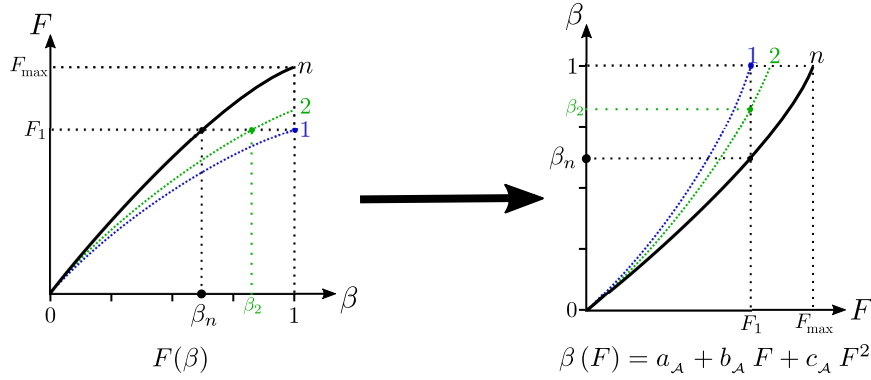
Figure 5.B.1:   *Force-Activation* relation $F(\beta)$. Force F increases as the activation β increases from 0 to 1. $F(\beta)$ changes as a result of muscle tissue adaptation (each curve is numbered according to the training session and corresponds to a different CSA). The muscle is able to produce the force F_1 at full activation $\beta = 1$ in the first training session; due to adaptation, the muscle requires a smaller activation β_n to produce the same force after n training sessions. The sketch on the right shows that, for each different CSA, a curve $\beta(F)$ is fitted by a quadratic function; therefore, there are sets of coefficients: $\{\mathcal{A}, a_{\mathcal{A}}\}$, $\{\mathcal{A}, b_{\mathcal{A}}\}$, $\{\mathcal{A}, c_{\mathcal{A}}\}$.

In summary, from the *force-activation* relation, the function $\beta(F)$ is built by a quadratic fit. The coefficients of the $\beta(F)$ function depend on the CSA and allow to built functions $a(\mathcal{A})$, $b(\mathcal{A})$ and $c(\mathcal{A})$ also by quadratic fits. The quadratic function for $\beta(F)$ and the quadratic functions $a(\mathcal{A})$, $b(\mathcal{A})$ and $c(\mathcal{A})$ are combined into the full activation function $\beta(\mathcal{A}, F)$ that allows to calculate the activation β that generates a given value of force F at a given CSA $\mathcal{A}$ of the muscle structure. Figure 5.B.2 shows a diagram of the procedure to build the $\beta(\mathcal{A}, F)$ function.

The mechanobiological model assumes that the adaptation of the activation (β) affects the evolution of the biochemical system. Therefore, the *Activation* function is the link from the mechanical model to the biochemical model that allows to have a closed loop for the mechanobiological system.

5.B.2 Updating the rate of protein synthesis with the force-activation relation

In the mechanobiological model, the link from the biochemical to the mechanical model is the growth tensor ($\mathbf{F_g}$). In addition, the relation between *Activation*, CSA, and force ($\beta(\mathcal{A}, F)$) is the link from the mechanical to the biochemical model. However, as seen in
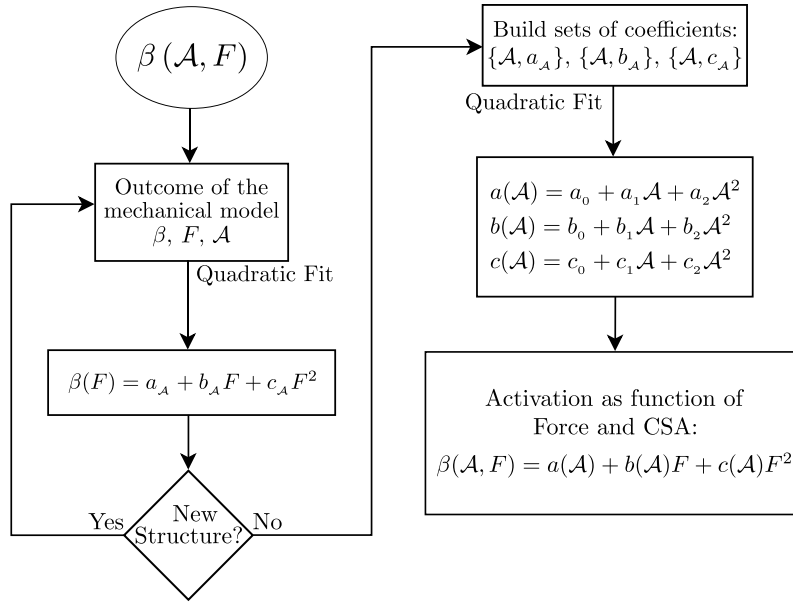
Figure 5.B.2: Procedure to calculate the activation level β required to produce a given force F with a given CSA $\mathcal{A}$ of the muscle structure.

equation system 4-1, there are many possibilities to be affected by the adaptation process; for instance, the growth rate of each molecule or the coupling coefficients. Nonetheless, in this model it is proposed that the major impact of the muscle structure adaptation (link from the mechanical to biochemical model), should be in the rate of change of the myofibril population ($f\left(x_3, x_4\right)$, eq. 4-2), specifically in the rate of protein synthesis k_1.

6 Biochemical model for the NFATc signaling pathway

6.1 Background

Training exercise produces skeletal muscle adaptation at the myofiber scale, as well as at the organ scale. Some features of the adaptation were discussed in previous chapters: myofiber protein amount was addressed in chapter 4, and muscle cross section area was addressed in chapter 5. Features related to myofiber type, and maximum voluntary contraction adaptation require a myofiber mechanism of specific protein-isoform synthesis; such mechanism depends on muscle activity patterns, involves the nuclear factor of activated T cells (NFATc), and ultimately switches the myofiber gene program to target characteristics of one fiber type or another.

The adaptability of skeletal muscle tissue has been studied at two levels (namely fiber type and protein-isoform content) under *chronic low frequency stimulation* (CLFS) [54, 99]. Evidence shows that fiber properties adapt according to the frequency of the signal and the pattern of stimulation. The role of the stimulation pattern is to evoke the effects of endurance training by keeping moderate sustained concentrations of free cytosolic Ca^{2+}, or to evoke the effects of resistance training by producing high short-duration concentrations of free cytosolic Ca^{2+}. Ca^{2+} concentration is key to regulate the calcineurin-NFATc signaling pathway, which is a mechanism related to fiber type transformation [33, 97, 144].

Only moderate sustained concentrations of free Ca^{2+} (produced by endurance training) are able to activate the calmodulin-calcineurin (CaM-CaN) complex; then, the active CaM-CaN complex produces the dephosphorylation of NFATc, which finally translocates to the nucleus. Once in the nucleus, NFATc promotes the gene regulation of slow type proteins; on the contrary, the gene regulation of fast type proteins occurs when the CaM-CaN complex is inactive or blocked [145].

In the long term, the adaptation of the fiber type characteristics produces a shift in muscle fiber type such that an increase in the number of myofibers of the fast type (that occurs when myofibers of the slow type shift to fast type) produces force adaptation, whereas an increase in the number of myofibers of the slow type (that occurs when myofibers of the fast type shift to slow type) produces fatigability adaptation [128].

Force and fatigability adaptation are the main target of most training protocols; however, limitations imposed by the fiber type distribution at the organ scale receive little attention.

The aim of this chapter is to provide a mechanism that, starting from a stimulation protocol, produces the NFATc signal required to trigger the gene program of fiber type transformation that guides the myofiber distribution adaptation. Based on the calcineurin-NFATc signaling pathway a dynamical model to describe the time course of dephosphorylated NFATc in the nucleus is presented in this chapter.

6.2 Materials and Methods

This section is divided into two parts, section 6.2.1 describes the general aspects of the calcineurin-NFATc model; section 6.2.2 presents initial conditions, parameters and additional aspects required for different simulation scenarios and validation.

6.2.1 Dynamical model

This section presents the description of the dynamical model. Section 6.2.1.1 presents the relation between the variables of the system and the molecules involved in the calcineurin-NFATc signaling pathway, as well as the set of equations of the model; section 6.2.1.2 presents the functions required for the implementation of the set of equations.

6.2.1.1 Set of equations

The function of the calcineurin-NFATc pathway was presented by [33]. A brief description of the pathway, and the set of equations to model the pathway are presented below; a scheme of the pathway is presented in figure 6.2.1.

Free Ca^{2+} activates calmodulin, and activated calmodulin can associate with calcineurin to form the activated Calmodulin-Calcineurin (CaM-CaN) complex. The amount of this complex decreases (or deactivates) when it interacts with cytosolic NFATc that exists in its phosphorylated state; i.e. the CaM-CaN complex dephosphorylates NFATc. Dephosphorylated NFATc can translocate to the nucleus where is phosphorylated and translocated back to the cytosol [33, 97].

The dynamics of the pathway is described by two compartment models: first, a compartment model for Ca^{2+}; and second, a compartment model for NFATc.

The Ca^{2+} compartment model is the following:

$$\dot{y}_1 = -k_1\,y_1 + k_2\,y_2 + \mathrm{f}(t)$$
$$\dot{y}_2 = -k_2\,y_2 + k_1\,y_1\ ,$$

(6.2.1)

where y_1 is the free Ca^{2+} concentration, y_2 is the activated CaM-CaN complex concentration, and $\mathrm{f}(t)$ is a function to resemble cytosolic Ca^{2+} release and uptake. y_1 favours the increase in y_2 at a rate k_1; because of this, y_2 increases at the same rate that y_1 decreases.
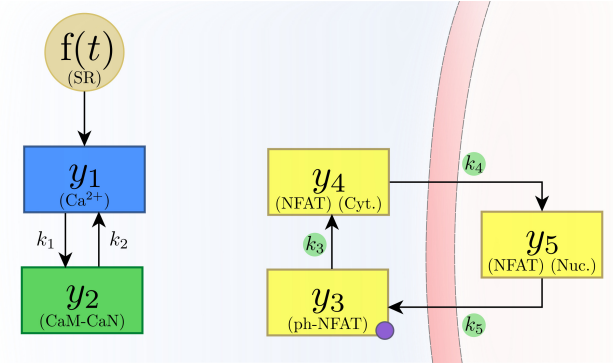
Figure 6.2.1: Reduced set of interactions based on the calcineurin-NFATc signaling pathway reviewed by [33]. The molecules: Ca^{2+}, activated CaM-CaN, phosphorylated NFATc, dephosphorylated NFATc in the cytosol, and dephosphorylated NFATc in the nucleus are represented by the variables y_1, y_2, y_3, y_4, and y_5, respectively. y_1 activates y_2, and y_2 controls the transition rates of the NFATc compartments: y_2 promotes the transition of NFATc from y_3 to y_4, which can translocate to the nucleus to become y_5. y_5 is phosphorylated and returned to the cytosol.

y_2 deactivates at a rate k_2, and y_1 increases at the same rate that y_2 decreases.

The NFATc compartment model is the following:

$$\dot{y}_3 = -k_3\, y_3 + k_5\, y_5 \tag{6.2.2a}$$
$$\dot{y}_4 = -k_4\, y_4 + k_3\, y_3 \tag{6.2.2b}$$
$$\dot{y}_5 = -k_5\, y_5 + k_4\, y_4 \ , \tag{6.2.2c}$$

where y_3 is the amount of phosphorylated NFATc in the cytosol, y_4 is the amount of dephosphorylated NFATc in the cytosol, and y_5 is the amount of dephosphorylated NFATc in the nucleus; k_3 is the rate of dephosphorylation of y_3, k_4 is the translocation rate of y_4 to the nucleus, and k_5 is the rate of phosporilation and translocation of y_5 to the cytosol.
Based on the saturation of NFATc in the nucleus found by Liu et al. [97], in this model, the total amount of NFATc (y_N) available in a myofiber remains constant:

$$y_N = y_3 + y_4 + y_5 \ . \tag{6.2.3}$$

Inserting y_4 from equation 6.2.3 into equation 6.2.2b leads to:

$$\dot{y}_4 = \ (k_3 + k_4)\, y_3 + k_4\, (y_N - y_5) \ . \tag{6.2.4}$$

This equation shows that y_4 is completely defined by y_3 and y_5; thus, by replacing y_4 from

equation 6.2.3 into equation 6.2.2c, equation system 6.2.2 is reduced to just two equations:

$$\dot{y}_3 = -k_3\,y_3 + k_5\,y_5 \tag{6.2.5a}$$

$$\dot{y}_5 = -(k_4 + k_5)\,y_5 + k_4\,(y_N - y_3)\ . \tag{6.2.5b}$$

The coupling between equation system 6.2.1, and 6.2.5 is proposed to be in the transition rates k_3, k_4, and k_5, because the dynamics of NFATc depends on the activation of the CaM-CaN complex [169, 160] (i.e. the transition rates depend on the behavior of y_2). The dependency of the transition rates is addressed in the next section.

6.2.1.2 Specialization of the model

The implementation of the calcineurin-NFATc signaling pathway model, requires the definition of the calcium release and uptake function $f(t)$, and the transition rate functions of the NFATc compartment model k_3, k_4 and k_5. These functions are described below.

Electrical stimulation triggers the release of Ca^{2+} from the sarcoplasmic reticulum (SR) to the cytosol; under sustained stimulation, the total amount of Ca^{2+} in the cytosol is high (between 100 and 300 nM in fibers of slow type [33]) relative to the passive state (about 60 nM [176, 32]); once the stimulation finishes, Ca^{2+} is removed from the cytosol by the action of calcium pumps. The duration of Ca^{2+} release and uptake ranges from 20 to 100 ms, with a release rate from 0 to 150 nM/ms, and an uptake rate from 0 to −25 nM/ms [110].

The model presented in this chapter considers cytosolic Ca^{2+} as a squared function with a varying duration that depends on the stimulation pattern. $f(t)$ is a function that quickly increases the availability of cytosolic Ca^{2+} when stimulation is turned on, and quickly removes cytosolic Ca^{2+} when stimulation is turned off.

$$\int_0^t f(t')\,dt' = \begin{cases} 0 & t < t_{on} & \text{before stimulus is on,} \\[2mm] y_1^M & t_{on} < t < t_{off} & \text{stimulus is on,} \\[2mm] 0 & t_{off} < t & \text{after stimulus is off,} \end{cases} \tag{6.2.6}$$

where y_1^M is the total amount of Ca^{2+} released from SR, t_{on} is the time when stimulus is turned on, and t_{off} is the time when stimulus is turned off.

As it was mentioned before, the coupling from the Calcium compartment model to the NFATc compartment model is proposed in the transition rates of the NFATc compartment model. Those transition rates are based on the measurements of nuclear NFATc reported by [97]; evidence shows that nuclear dephosphorylated NFATc evolves in three phases: first, NFATc increases while stimulus is on; second, NFATc holds its concentration for about 10

minutes after stimulus is turned off (memory); and third, NFATc decreases after the memory phase; additionally, both continuous and pulsed stimulation are able to bring nuclear NFATc to saturation.

Based on the three phases of nuclear NFATc, k_3 and k_5 are functions defined by three phases accordingly, and k_3 includes the saturation condition; for simplicity, k_4 was set as proportional to k_3:

$$k_3(y_2, t) = \begin{cases} k_{3u} & \text{if} & \dot{y}_2 > 0 \\ k_{3m} & \text{if} & \dot{y}_2 < 0 & \text{and} & t' < t_m \\ k_{3d} \exp\left(-\frac{t'}{\tau_d}\right) & \text{if} & \dot{y}_2 < 0 & \text{and} & t' > t_m \\ 0 & \text{if} & y_5 > y_5^M \end{cases} \tag{6.2.7}$$

$$k_4(y_2, t) = \alpha\, k_3(y_2, t) \,, \tag{6.2.8}$$

$$k_5(y_2, t) = \begin{cases} k_{5u} & \text{if} & \dot{y}_2 > 0 \\ k_{5m} & \text{if} & \dot{y}_2 < 0 & \text{and} & t' < t_m \\ k_{5d}\left(1 + \frac{t'^{\nu}}{t_{1/2}^{\nu} + t'^{\nu}}\right) & \text{if} & \dot{y}_2 < 0 & \text{and} & t' > t_m \end{cases} \tag{6.2.9}$$

where k_{3u} and k_{5u} are the transition rates during the increasing phase of y_5 that occurs while y_2 increases; k_{3m} and k_{5m} are the transition rates when a quick drop of y_2 occurs, they act during the memory phase of y_5, and allow y_5 to increase at a slower pace when a pulsed stimulation pattern is used; k_{3d} and k_{5d} define the maximum values of the transition rates that act during the decreasing phase of y_5; y_5^M is the saturation level of NFATc; α is a proportionality constant between k_4 and k_3; t' is the time immediately after stimulus is switched off $(t - t_{off})$; t_m, τ_d, $t_{1/2}$, and ν are parameters related to the duration of the memory phase.

6.2.2 Numerical experiments

Numerical values of the parameters for equations systems 6.2.1, 6.2.5, and equations 6.2.6, 6.2.7 and 6.2.9 are listed in table 6.2.1. Initial conditions are listed in table 6.2.2.

In the previous section, the dynamical system for the calcineurin-NFATc signaling pathway was described (equations 6.2.1 and 6.2.5). Recall that sustained low-amplitude Ca^{2+} oscillations are required to trigger the pathway, and that these oscillations are originated in cycles of Ca^{2+} release and uptake. The Ca^{2+} oscillations that led to the NFATc behavior reported by [97] were obtained by the use of three electrical stimulation patterns: a 30 minutes continuous stimulation, a 30 minutes pulsed stimulation, and a 2 hours pulsed stimulation; in this work, those Ca^{2+} oscillations are shaped by the function $f(t)$.

Table 6.2.1: Parameters and transitions rates for equation systems 6.2.1 and 6.2.5, and functions 6.2.6, 6.2.7, and 6.2.9.

Parameter	Value	Units	Reference
y_1^M	250.0	nM	[32]
y_5^M	100.0	a.u.	[97]
t_m	1.250	min	fitted
τ_d	8.00	min	fitted
$t_{1/2}$	15.00	min	fitted
ν	5.00	a.u.	fitted
k_1	0.1375	min^{-1}	fitted
k_2	0.7000	min^{-1}	fitted
k_{3u}	0.0400	min^{-1}	fitted
k_{3m}	0.0326	min^{-1}	fitted
k_{3d}	0.0150	min^{-1}	fitted
α	1.10	a.u.	fitted
k_{5u}	0.00	min^{-1}	fitted
k_{5m}	0.00134	min^{-1}	fitted
k_{5d}	0.00403	min^{-1}	fitted

According to the definition of f(t) given in equation 6.2.6, the Ca^{2+} amplitude is given by y_1^M (see table 6.2.1). For simulation porpuses, an illustration pattern is used to describe the behavior of the system, and the stimulation patterns used by [97] (continuous and pulsed) are used for validation. The parameters t_{on} and t_{off} of equation 6.2.6 are defined in table 6.2.3; basically, the continuous pattern has a fixed amplitude for 30 minutes, whereas the illustration and pulsed patterns are squared signals repeated a certain number of times (Cycles).

All simulations were performed using a Runge-Kutta fourth-order method implemented in MATLAB R2015a (The MathWorks, Inc.).

6.3 Results and discussion

The results of the illustration stimulation pattern are presented in section 6.3.1 and are divided in three sections: first, the behavior of the compartment model for Calcium (section 6.3.1.1); second, the transition rate functions (section 6.3.1.2); and third, the compartment model for NFATc (section 6.3.1.3). Finally, the results of the continuous and pulsed stimulation patterns are presented in section 6.3.2.

Table 6.2.2: Initial conditions for equation systems 6.2.1 and 6.2.5.

Init. Cond.	Value	Units	Reference
$y_1(0)$	60.0	nM	[32]
$y_2(0)$	10.0	nM	fitted
$y_3(0)$	196.3	a.u.	fitted
$y_4(0)$	0.0	a.u.	fitted
$y_5(0)$	26.3	a.u.	[97]
y_N	222.6	a.u.	fitted
$k_3(y_2, 0)$	0.0	min^{-1}	fitted
$k_5(y_2, 0)$	0.0	min^{-1}	fitted

Table 6.2.3: Stimulation pattern for illustration and validation. Continuous and pulsed stimulation patterns are based on the experiments of [97], the total time under stimulation (ST) is $(Active + Rest) * Cycles$. $Active$ is defined as $t_{\text{off}} - t_{\text{on}}$ (t_{on} and t_{off} refer to eq. 6.2.6); $Rest$ refers to the time lapse before a new stimulation starts; $Cycles$ is the number of squared stimulation pulses; and $Recover$ refers to the observation time after stimulation.

Stimulation	Active	Rest	Cycles	ST (min)	Recover (min)
Illustration	5 min	10 min	3	45	15
Continuous	30 min	–	1	30	210
Pulsed	5.0 s	45 s	36	30	210
2 h pulsed	5.0 s	45 s	144	120	35

6.3.1 Illustration results

The purpose of this section is to show how function f(t) defined in eq. 6.2.6 was implemented, and to show how the Calcium compartment model links to the NFATc compartment model by means of the transition rate functions k_3 and k_5.

6.3.1.1 Calcium compartment model

Figure 6.3.1 shows the behavior of f(t), total calcium, cytosolic calcium, and activated CaM-CaN complex of the Ca^{2+} compartment model.

A positive short-duration pulse of function f(t) stimulates the y_1 compartment (fig. 6.3.1a) and produces a sudden increase in the total calcium concentration (fig. 6.3.1b). The negative short-duration pulse of function f(t) produces a sudden drop in the total calcium concentration. Between the positive and negative pulses of f(t), the total amount of calcium is

sustained at a high concentration that is distributed between cytosolic Ca^{2+} (fig. 6.3.1c) and the activated CaM-CaN complex (fig. 6.3.1d).
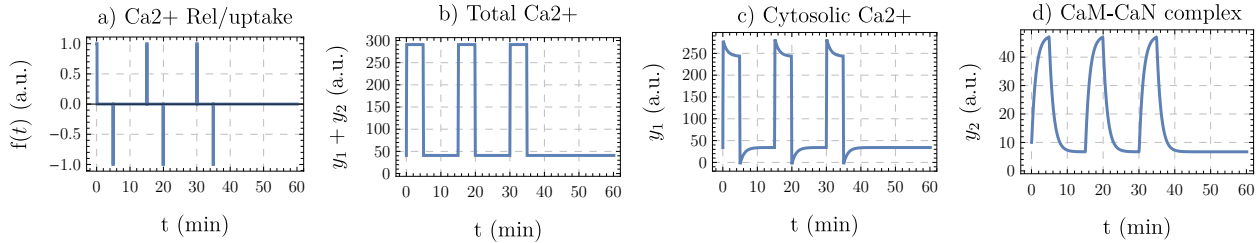
Figure 6.3.1: Ca^{2+} compartment model simulation. **a)** Normalized f(t); **b)** total Ca^{2+} released and uptaken ($y_1 + y_2$); **c)** free cytosolic Ca^{2+} (y_1); **d)** activated CaM-CaN complex (y_2). Notice that y_1 and y_2 are in phase with f(t).

Figures 6.3.1c and 6.3.1d show that there is enough y_1 available for many other cellular functions of the contraction mechanism. Those functions are not relevant in this model because the Ca^{2+} compartment model is only required to control the transition rate functions of the NFATc compartment model.

6.3.1.2 Transition rate functions

As mentioned before, in this model the transition rates of the NFATc compartment model are functions of y_2. Compare figure 6.3.1d with figure 6.3.2; as soon as y_2 increases, k_3 jumps from 0 to its maximum value (fig. 6.3.2a), the change in k_3 allows the transition of y_3 to its dephosphorylated state y_4; k_5 remains inactive during the increasing phase of y_2, because y_5 must be dephosphorylated in the nucleus before going back to the cytosol (fig. 6.3.2b). The sudden drop in y_2 produces an instantaneous change in k_3 and k_5, and those values remain constant during the memory phase of NFATc. After the memory phase, k_3 decreases avoiding the transition of y_4 to y_5 (because k_4 is proportional to k_3), and k_5 increases promoting the transition of y_5 to y_3.

6.3.1.3 NFATc compartment model

The dynamics of the transition rates allow the transition of NFATc from y_3 to y_4 for a longer time than the increasing phase of y_2. This prolonged transition is required for the memory phase of NFATc and can be noticed by comparing figure 6.3.3a with figure 6.3.1d: y_3 decreases at a fast pace during the increasing phase of y_2, and decreases at a slower pace when y_2 is decreasing; if a new stimulus is not received soon enough, y_3 starts to increase. Figures 6.3.3b and 6.3.3c show that y_4 and y_5 increase faster or slower during the increase or decrease of y_2, respectively. Notice that although y_2 shows an oscillatory behavior, y_5 accumulates; the accumulation of y_5 is key to the delayed effect of exercise: adaptation is
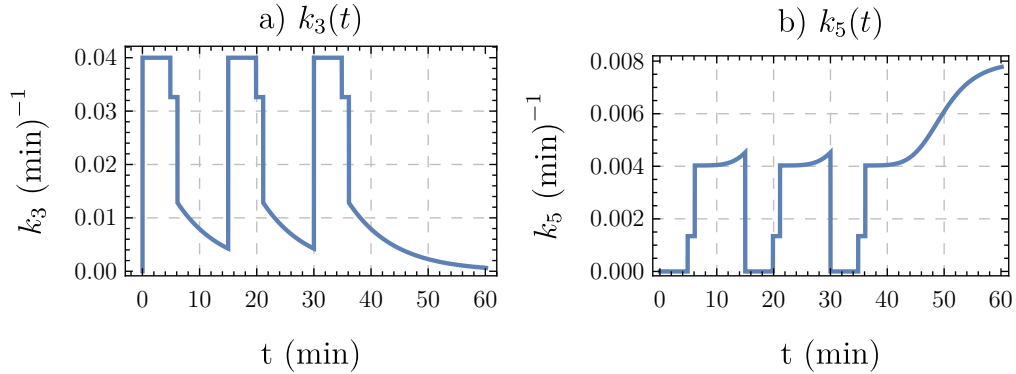
Figure 6.3.2: Transition rates functions: **a)** transition rate from y_3 to y_4 (k_3), **b)** transition rate from y_5 to y_3 (k_5). k_3 has its maximum value during the increasing phase of y_2, k_3 decreases during the decreasing phase of y_2. k_5 behaves opposite to k_3. The relative amplitudes of k_3 and k_5 allow the accumulation of y_5 during stimulation (nuclear NFATc increases), and the increase of y_3 after stimulation (cytosolic phosphorylated NFATc increases).

triggered by exercise, but its effects are noticeable after repetition of the stimulus and last longer than the stimulation period.
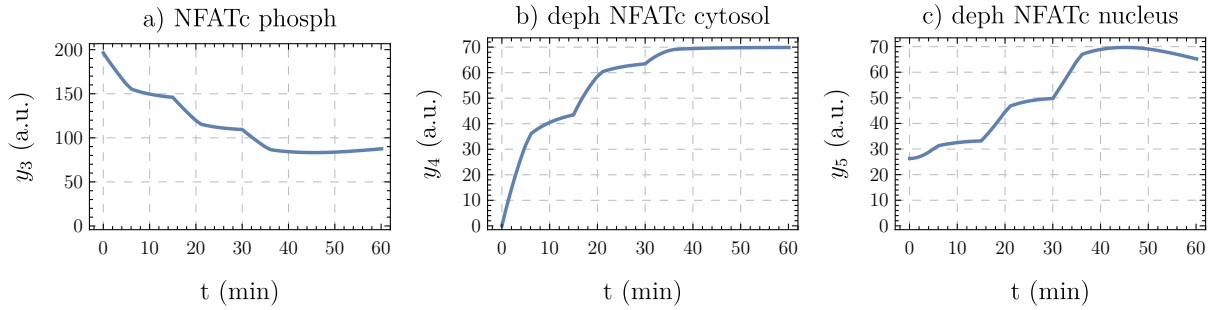
Figure 6.3.3: NFATc compartment model simulation. **a)** phosphorylated NFATc in the cytosol (y_3); **b)** dephosphorylated NFATc in the cytosol (y_4); **c)** dephosphorylated NFATc in the nucleus (y_5). Notice the cumulative effect produced by the repetition of the stimulation; also notice that after some minutes without stimulation, phosphorylated NFATc increases, and nuclear NFATc decreases.

6.3.2 Validation results

Figure 6.3.4 shows the remarkable agreement between the model and the experimental evidence during the increase, memory and early decrease phases of y_5. Only the continuous pattern matches the y_5 decrease after 80 minutes of observation.

The increasing phase of y_5 allows the fitting of k_{3u} using the continuous stimulation pattern, and the fitting k_{3m} using the pulsed stimulation pattern. Notice that the increasing phase

of y_5 is slower or faster depending on the values of k_{3u} and k_{3m}; clearly, if $k_{3u} = k_{3m}$ the simulation results of the continuous and pulsed stimulation would have the same increasing dynamics without any effect of the time between peaks of stimulation.
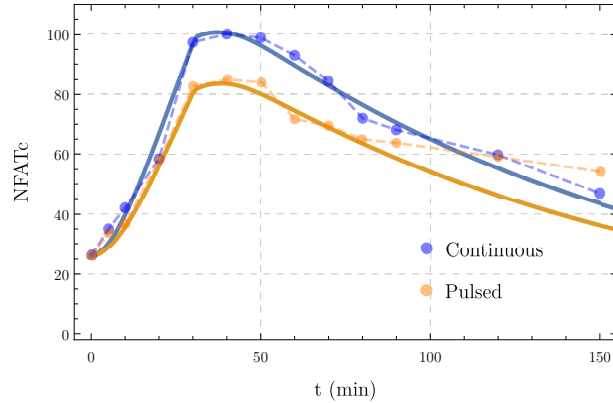
Figure 6.3.4: NFATc in the nucleus, experiment (point-dash) compared to simulation results (continuous line). The same set of parameters was used for both stimulation patterns.

The memory effect after 30 minutes of stimulation is evident in both continuous and pulsed stimulation patterns (see fig. 6.3.4), and those results could be interpreted as a saturation level that depends on the stimulation pattern; the results of the 2 hours pulsed stimulation eliminate that possibility.

Figure 6.3.5 shows a comparison of the experiments using 30 minutes and 2 hours pulsed stimulation, and the simulation results. Pulsed stimulation for 2 hours shows that NFATc reaches a saturation level of the same amplitude of the continuous stimulation, but pulsed stimulation requires about 10 minutes more than the continuous stimulation to reach saturation; the model simulation matches very well the saturation delay.

The saturation delay suggests that low intensity stimulation requires more stimulation time to produce the results of the continuous stimulation, that delay also suggests the existence of an optimal intensity/duration ratio that maximizes the benefits of training: too high intensity would produce high amplitude calcium transients of insufficient duration to activate the calcineurin-NFATc pathway; whereas too low intensity would require longer training sessions to reach nuclear NFATc saturation.

6.4 Conclusion

The model for the calcineurin-NFATc signaling pathway presented in this chapter allows an excellent approximation of the regulatory mechanism to control the myofiber gene program that transforms the protein isoform content and ultimately the myofiber distribution of a muscle. The next chapter uses the nuclear NFATc evolution triggered by exercise and proposes a model for the transformation of protein isoforms.
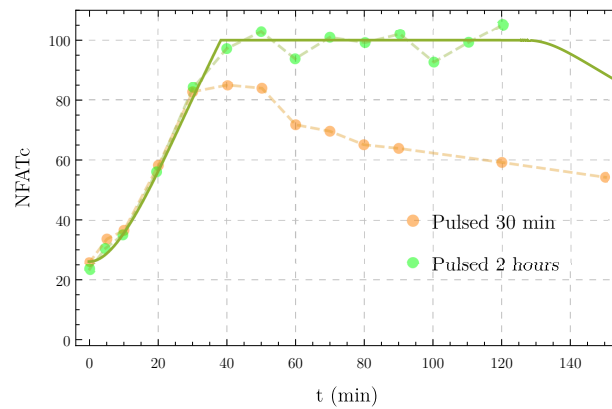
Figure 6.3.5: Nuclear NFATc after 30 minutes, and two hours pulsed stimulation. Evidence shows that the saturation level is independent of the stimulation pattern (compare to saturation due to continuous stimulation in figure 6.3.4). The model simulation (continuous green line) reaches saturation in very good agreement to experiments.

7 Gene program: MLCf transition

7.1 Background

Brown et al. [21, 22] studied the changes in the concentration of myosin light chain (MLC) isoforms in tibialis anterior muscles of rabbits under 10 weeks continuous stimulation at 10 Hz, and the recovery for 6 weeks after stimulation. During the 10 weeks under stimulation, results show that the transformation of the total MLC of fast isoform (MLCf) follows three well defined phases: a slow decrease during the first 3 weeks, a fast decrease during the following three weeks, and finally, a slow decrease for the last 4 weeks. During the 6 weeks of recovery, results show two phases: a fast increase of MLCf during the first 3 weeks, and a slow increase during the following 3 weeks. These experiments demonstrate the gradual transition of muscle-fiber characteristics under the simplest stimulation patterns: full time stimulation or no stimulation at all.

More interesting stimulation patterns were investigated by Lopez-Guajardo et al. [98, 99]. They studied the steady state of the properties of rabbit muscle fibers after 6 weeks of two different stimulation procedures: procedure A [98], which used stimulation patterns with fixed amount of pulses every 24 hours; and procedure B [99], which used stimulation patterns varying *duty*, defined as the percentage ratio of time with stimulation (t_{on}) divided by time without stimulation (t_{off}) plus time with stimulation (duty = $100\% * t_{on}/(t_{off}+t_{on})$). Procedure A included 5 groups of rabbits. One group was continuously stimulated at 5 Hz for 24 hours, and four groups were stimulated at 10 Hz under different stimulation patterns: 30 seconds on followed by 30 seconds off; 30 minutes on followed by 30 minutes off; 12 hours on followed by 12 hours off; and continuous 24 hours. Notice that the 10 Hz 24 hours stimulation pattern contains a double amount of pulses compared to any of the other patterns.

Procedure B also included 5 groups of rabbits. Each group was stimulated at 10 Hz for 30 minutes, but each group had a different time without stimulation: 0.5 h, 1.5 h, 3.5 h, 11.5 h, and 23.5 h, with duties: 50.0%, 25.0%, 12.5%, 4.2%, and 2.1%, respectively.

Figures 7.1.1 and 7.1.2 show the total myosin light chain of fast and slow fibers (MLCf and MLCs) of procedures A and B respectively. First, notice that the MLCf and MLCs are mirror images of each other; and second, notice that the MLC content of the continuous stimulation pattern (depicted as t_{on} = 1440 min in figure 7.1.1a, as duty = 100% in figure 7.1.2a, and t_{off} tends to zero in figures 7.1.1b and 7.1.2b) is opposite to the MLC content of the control group (which was free of electrical stimulation but also free to move, depicted as t_{on} tends to zero in figures 7.1.1a, as duty = 1% in figure 7.1.2a, and t_{off} = 1440 min in figures

7.1.1b and 7.1.2b). Both procedures demonstrate that electrical stimulation produces the transformation of the MLC content from fast to slow isoforms: MLCf content starts close to 100% and decreases to less than 20%, and MLCs content starts close to zero and increases to more than 80%.
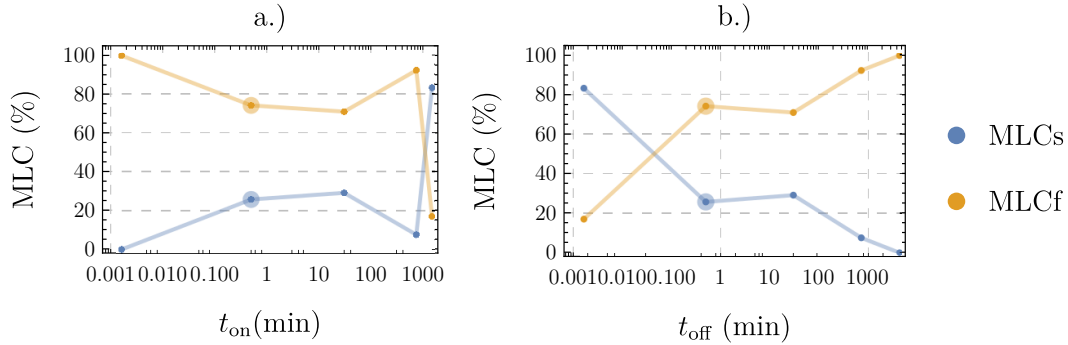
Figure 7.1.1: Myosin light chain of fast and slow-type (MLCf and MLCs) transition due to electrical stimulation, experiments by Lopez Guajardo et al. procedure A [98]. MLCs and MLCf isoforms after 6 weeks of stimulation as a functions of: **(a)** stimulation time (t_{on}) as presented in [98], and **(b)** time with stimulation off (t_{off}). The 30s-on followed by 30s-off data are specially marked to notice that this stimulation pattern is the only one that used less than 30 minutes of stimulation.

The aim of procedure A (figure 7.1.1a) was to use a fixed number of pulses, but this approach simultaneously changes t_{on} and t_{off}; notice that in procedure A, all stimulation patterns represent 50% duty, except the continuous stimulation pattern.
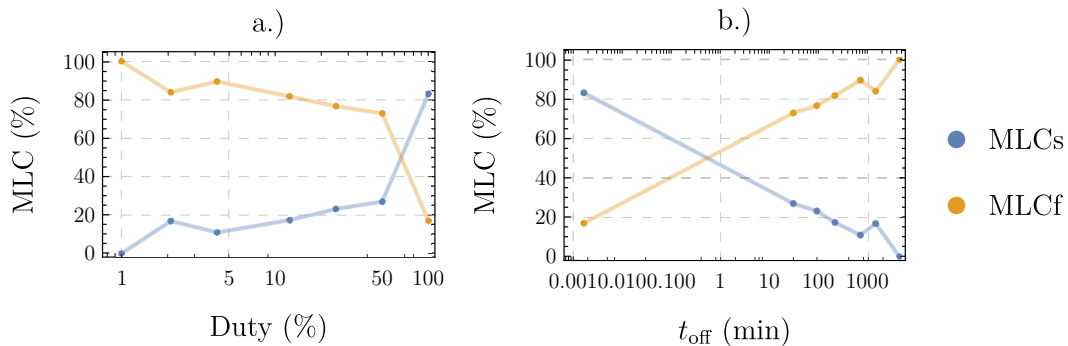
Figure 7.1.2: Myosin light chain of fast and slow-type (MLCf and MLCs) transition due to electrical stimulation, experiments by Lopez Guajardo et al. procedure B [99]. MLCs and MLCf isoforms after 6 weeks of stimulation as a functions of: **(a)** duty as presented in [99], and **(b)** time with stimulation off (t_{off}).

Figure 7.1.2a shows a clear trend when duty is used as the control variable; however, all stimulation patterns in procedure B used t_{on} = 30 min, which means that the actual variable was t_{off}. Figures 7.1.1b and 7.1.2b show the experimental results as functions of t_{off};

notice that the trends are clearer for both procedures, and also notice that there is only one stimulation pattern that used t_{on} of less than 30 minutes.

Figure 7.1.3 shows a comparison of MLCf of procedures A and B as functions of t_{off}. Two aspects must be noted: first, the t_{on} = 12 hours followed by t_{off} = 12 hours (of procedure A) produced almost the same MLCf of the t_{on} = 30 minutes followed by t_{off} = 11.5 hours (procedure B); second, the t_{on} = 30 seconds followed by t_{off} = 30 seconds is particularly far from the data trend, but produced almost the same results of the t_{on} = 30 minutes followed by t_{off} = 30 minutes.

The first aspect mentioned in the previous paragraph is justified by the evidence presented in [97]; according to those results, nuclear NFATc reaches a maximum after 30 minutes of continuous stimulation, once the maximum NFATc is reached, any stimulation longer than 30 minutes is equivalent to the 30 minutes stimulation pattern as long as t_{off} is fixed. The second aspect mentioned in the previous paragraph may be justified also by the evidence presented in [97]: nuclear NFATc will reach saturation using pulsed stimulation provided that t_{off} is shorter than the memory phase (see section 6.2.1.2).

The linear trend in semi-log scale (figure 7.1.3) will be used as a starting point to model the steady state of MLCf. The aim of this chapter is to provide a mechanism that, starting from a stimulation protocol, produces the respective MLCf transformation that results from sustained electrical stimulation.
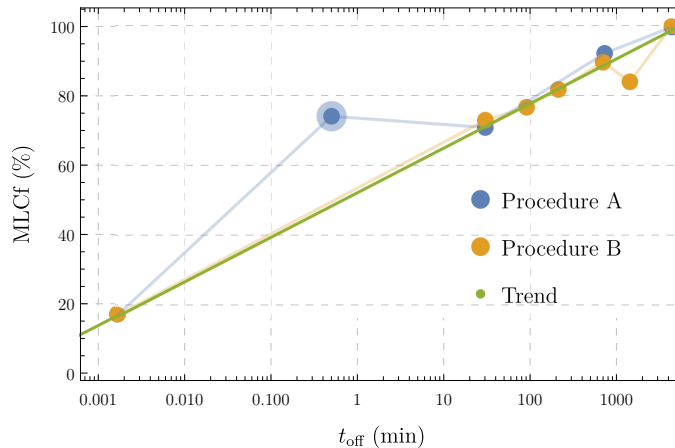
Figure 7.1.3: Myosin light chain of fast (MLCf) transition due to electrical stimulation [98, 99] as functions of time without stimulation (t_{off}), each data point is the MLCf content after 6 weeks of stimulation. Notice that only the 30s stimulation deviates from the trend, and also the only procedure with less than 30 minutes of stimulation. The smallest value of MLCf at the left is the 24 hours continuous stimulation, the greatest value at the right is the control non-stimulated group.

7.2 Materials and Methods

This section is divided into two parts. The first part contains the mathematical description of the model for MLCf transition (section 7.2.1), and the second part contains details of the simulation implementation and validation (section 7.2.2).

7.2.1 Dynamical model for MLCf transition

The model developed in this section assumes that the MLCf evolution (summarized in figure 7.1.3) is the steady state of a logistic behavior. This section is divided in 4 parts: first a short description of the logistic model for the evolution of the MLCf is presented (section 7.2.1.1); second, considerations for the description of the transient response are proposed in the carrying capacity of the logistic model (section 7.2.1.2); third, the nuclear NFATc found in the previous chapter is introduced to control the gene program that resets the carrying capacity (section 7.2.1.3); and fourth, parameters and initial conditions are listed (section 7.2.1.4).

7.2.1.1 Logistic behavior of the MLCf

The dynamics of a logistic system is suitable for the MLCf evolution, assuming that each individual muscle fiber will transform its MLCf content to a steady state value:

$$\frac{dN}{dt} = r\,N\left(1 - \frac{N}{K}\right), \qquad N(0.) = N_0, \tag{7.2.1}$$

where N is the current MLCf content, N_0 is the initial MLCf of the fiber, r is the growth rate, and K is the carrying capacity of N (that is simply the targeted steady state of N). Figure 7.1.3 shows that the targeted steady state of MLCf depends on the stimulation pattern; hence, the carrying capacity of equation 7.2.1 should reproduce the experimental results shown in figure 7.1.3.

7.2.1.2 Adaptive Carrying Capacity

Considering stimulation patterns such as those used by Lopez-Guajardo et al. [99], two targets have to be considered: target during time without stimulation, and target during time with stimulation. The target during time without stimulation depends on how long the stimulation is off before a new stimulus is applied (t_{off}); whereas the target during time with stimulation depends on how long the stimulation is on (t_{on}). In principle, no stimulation produces total transformation of MLCs into MLCf, whereas continuous stimulation produces the maximum transformation possible of MLCf into MLCs.

Target during time without stimulation

The data trend in figure 7.1.3 is simply:

$$K_{\mathrm{M}}(t_{\mathrm{off}}) = \nu \log\left(\frac{t_{\mathrm{off}}}{t_0}\right) \tag{7.2.2}$$

where K_{M} is the steady state of MLCf content of a muscle fiber after 6 weeks of stimulation as a function of t_{off} in minutes (assuming $t_{\mathrm{on}} > 30$ minutes); ν is the slope of the trend in semi-log scale; and t_0 is the value of t_{off} that produces the maximum transformation of MLC content from typically fast to typically slow isoform.

The trend function 7.2.2 is useful to predict the steady state of MLCf under a prolonged periodic-stimulation pattern, i.e. each data point in figure 7.1.3 requires a fixed stimulation pattern (fixed t_{off}) for at least 6 weeks. A more general function should predict the MLCf content even in the case of a changing pattern, i.e. in the case of a nonperiodic-stimulation pattern; in other words, from the perspective of a muscle fiber, t_{off} is always unknown and, as a consequence, the steady state of MLCf (which is the value of K_{M}) is also unknown.

The more general function mentioned above has to be consistent with equation 7.2.2; therefore, in the case of periodic stimulation, the average general function has to produce the same steady state than the $K_{\mathrm{M}}(t_{\mathrm{off}})$ prediction, this is:

$$\frac{1}{t_{\mathrm{off}} - 0} \int_0^{t_{\mathrm{off}}} K_{\mathrm{g2}}(t)\, dt = K_{\mathrm{M}}(t_{\mathrm{off}}) \tag{7.2.3}$$

where $K_{\mathrm{g2}}(t)$ is the carrying capacity of equation 7.2.1 during time without stimulation, which provides the transient MLCf value from the perspective of the muscle fiber; and t_{off} is the time that the fiber spends without stimulation (t_{off} resets the behavior of the muscle fiber's machinery each time that a new stimulus is applied). Figure 7.2.1 sketches the difference between $K_{\mathrm{g2}}(t)$ and $K_{\mathrm{M}}(t_{\mathrm{off}})$

A rescaled version of K_{M} is a simple general function consistent with 7.2.3:

$$K_{\mathrm{g2}}(t) = K_{\mathrm{M}}(e\,t) \tag{7.2.4}$$

where e is the Euler's number.

Target during time with stimulation

In this case, the carrying capacity needs to target a fixed minimum MLCf that is reached only if the stimulation is long enough. This minimum value of MLCf is approached through the function:

$$K_{\mathrm{g1}}(t) = K_{\mathrm{M}}(t_I), \qquad t_I = \begin{cases} t_{21} \exp\left(-t/\tau\right) & \text{if } t_I < t_{0I} \\ t_{0I} & \text{if } t_I \geq t_{0I} \end{cases} \tag{7.2.5}$$
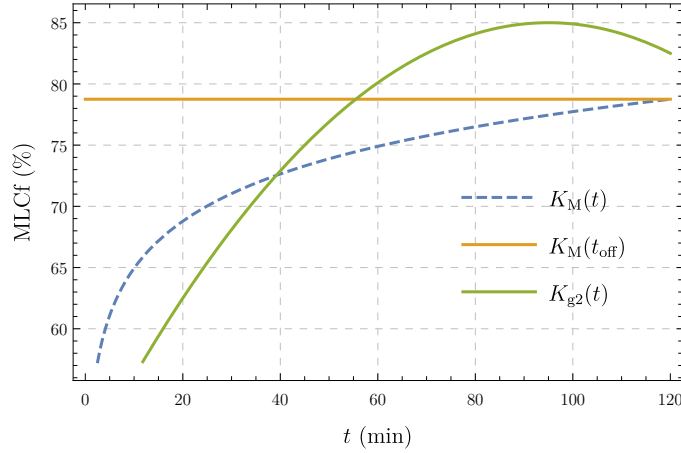
Figure 7.2.1: Sketch of the targeted MLCf content of a muscle fiber under stimulation. Function $K_{\mathrm{M}}(t)$ (defined in equation 7.2.2) is an increasing function that only defines the targeted value $K_{\mathrm{M}}(t_{\mathrm{off}})$. At any time $t < t_{\mathrm{off}}$, a muscle fiber targets to the function $K_{\mathrm{g2}}(t)$, which is a function such that its averaged value is equal to $K_{\mathrm{M}}(t_{\mathrm{off}})$. In this sketch, $t_{\mathrm{off}} = 120$ min.

where $K_{\mathrm{g1}}(t)$ is the carrying capacity of equation 7.2.1 during time with stimulation; t_{21} is such that $K_{\mathrm{M}}(t_{21})$ targets the MLCf threshold between fibers type I and type IIA (see table 7.2.3); τ is a characteristic time related to the continuous decrease of the targeted MLCf; and t_{0I} is such that $K_{\mathrm{M}}(t_{0I})$ is the minimum value of MLCf mentioned previously.

Equations 7.2.2, 7.2.4, and 7.2.5 provide the targeted value of the MLCf of a muscle fiber, and define the general carrying capacity of equation 7.2.1.

Recall that MLCf is the kind of protein typically found in muscle fibers of the fast type. Also recall, that the synthesis of protein requires a gene-program signaling that in the case of muscle fibers is related to the NFATc signaling pathway presented in chapter 6.

The nuclear NFATc concentration is used as a signal to switch the gene program (GP) targeting muscle-fiber properties of the fast or the slow type, thus the GP switching is a convenient signal to control the carrying capacity:

$$K_{\mathrm{gm}}(t) = \begin{cases} K_{\mathrm{g1}}(t) & \text{if} \quad \text{GP favours type I} \\ K_{\mathrm{g2}}(t) & \text{if} \quad \text{GP favours type II} \end{cases} \tag{7.2.6}$$

The next section explains how the gene program switching is defined, and how it relates to the adaptive carrying capacity.

7.2.1.3 Gene Program switch

The behavior of the nuclear NFATc is assumed to be independent on the number of repeated stimulations; because of that, the nuclear NFATc function found in chapter 6 is simply arranged in a periodic way. The passive *state* of the gene program favours the production of properties of type II fibers (GP = 0), only when a sustained stimulus is applied, the gene program switches to favour type I (GP = 1). The gene-program switch is controlled by the rate of change of nuclear NFATc ($\dot{y}_5$), and changes to GP= 1 according to the following rules:

- $\dot{y}_5$ is positive or zero.
- $\dot{y}_5$ is decreasing.
- $\dot{y}_5 < \dot{y}_5^*$.

$\dot{y}_5^*$ is a triggering rate of change. Figure 7.2.2 shows how the GP switches in relation to the NFATc signal. Remark that the gene-program switching is not synchronized to the stimulation pattern due to the triggering rate $\dot{y}_5^*$, and the memory effect of the nuclear NFATc.
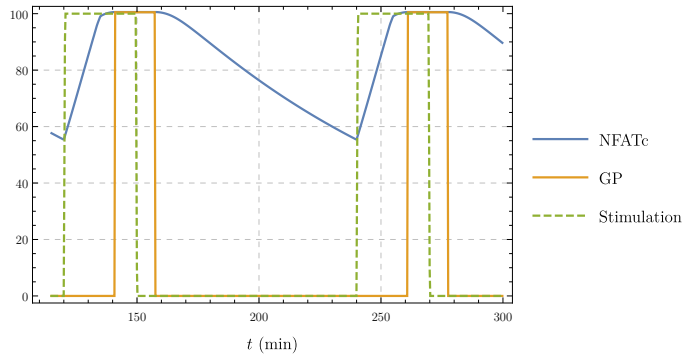
Figure 7.2.2: Gene program (GP) switching signal; GP = 0 favours type II fibers, GP = 1 favours type I fibers (GP re-scaled to 100 for an easy observation of its relation to NFATc). The increasing concentration of nuclear NFATc is not enough to switch the GP. When the rate of change of NFATc is decreasing and, at the same time, is smaller than a triggering value (before NFATc reaches its maximum value), the GP switches to 1 and holds the new state until NFATc starts to decrease.

7.2.1.4 Parameters and initial conditions

The transition model for MLCf (equation 7.2.1) requires two parameters: r and K. r is a state-dependent parameter defined according to the GP state and the fiber type, see table 7.2.1; and K (defined in equations 7.2.2, 7.2.4 and 7.2.5) requires several parameters, see table 7.2.2. The triggering rate of change required for the gene program switch is also listed in table 7.2.2.

Table 7.2.1: Growth rate for MLCf (equation 7.2.1). The MLCf transition observed by Brown et al. [22] suggests a growth rate that depends on the current MLCf content but also the target of the transition: continuous stimulations favours type I fibers, no stimulation favours type II fibers.

GP	MLCf range	r	Units	Reference
favours type I	100 - 85	$0.018 * 10^{-6}$	min^{-1}	fitted
	85 - 20	$0.60 * 10^{-6}$	min^{-1}	fitted
	20 - 0	$0.50 * 10^{-6}$	min^{-1}	fitted
favours type II	0 - 60	$75.5 * 10^{-6}$	min^{-1}	fitted
	60 - 100	$20.5 * 10^{-6}$	min^{-1}	fitted

Table 7.2.2: Parameters for the adaptive carrying capacity function, and triggering rate of change for gene-program switch.

Equation	Parameter	Value	Units	Reference
7.2.2	ν	$13.13 * 10^{0}$	1.	fitted
7.2.2	t_0	$84.48 * 10^{-6}$	min	fitted
7.2.5	t_{21}	0.0028	min	table 7.2.3
7.2.5	τ	10.5	min	fitted
7.2.5	t_{0I}	$91 * 10^{-6}$	min	fitted
	$\dot{y}_5^*$	$84 * 10^{-3}$	min^{-1}	fitted

A correlation between fiber type and MLCf content is assumed based on two statements: first, results by Lopez-Guajardo [99] show an indirect correlation between MLCf and tetanic force -the bigger the amount of MLCf the greater the tetanic force; second, results by McDonagh [107] show a relation between force and fiber type -type IIB are the strongest and type I are the weakest. The indirect correlation between fiber type and MLCf, and the results shown in [22, 99] lead to the following fiber type classification: fibers with MLCf content of more than 85% are type IIB; fibers with a MLCf content between 20% and 85% are type IIA; and fibers with a MLCf content of less than 20% are classified as type I.

For the purposes of simulation, the MLCf content is considered as a continuous variable in each individual muscle fiber. In a pool of N_f fibers, the total MLCf content is simulated in three stimulation scenarios: Continuous stimulation, recovery after stimulation, and periodic stimulation (details of the stimulation pattern are described in the next section). The fiber-type classification according to the MLCf content, and the initial fiber distribution for each stimulation scenario is presented in table 7.2.3.

Table 7.2.3: Fiber type classification according to MLCf content, and initial fiber distri-
bution in the continuous stimulation pattern (CS), recovery after continuous
stimulation (R), and periodic stimulation (PS). Simulations used a pool of
N_f = 100 fibers.

MLCf % [22, 99]	Type	CS % [22]	R % [22]	PS % [99]
0 - 20	I	0	90	7
20 - 85	IIA	0	10	32
85 - 100	IIB	100	0	61

7.2.2 Simulations and Validation

As mentioned in the previous section, three stimulation scenarios were used for validation:
first, continuous stimulation; second, recovery after stimulation; and third, periodic stimula-
tion. Brown et al. [22] studied the time course of MLCf transformation during 10 weeks of
continuous stimulation (first scenario), and during the 6 weeks that followed the cessation of
stimulation (second scenario); Lopez-Guajardo et al. [99] studied the steady state of MLCf
after 6 weeks of stimulation using different periodic stimulation patterns (third scenario).

In the first scenario, the GP continuously favours type I fibers; hence, the carrying capacity is
given by equations 7.2.2 and 7.2.5, and the evolution of the MLCf content of each individual
fiber is given by equation 7.2.1.
In the second scenario, the GP continuously favours type II fibers; this time, the carrying
capacity is given by equations 7.2.2 and 7.2.4, and the evolution of the MLCf content of each
individual fiber is given by equation 7.2.1.
The third scenario requires a stimulation pattern, and the simulation process follows three
steps: first, the stimulation pattern gives rise to a repetition pattern of the nuclear NFATc
(see figure 7.2.3); second, the NFATc pattern produces a GP switching signal following
the rules of section 7.2.1.3; and third, the GP switching signal guides the evolution of the
adaptive carrying capacity (see figure 7.2.4) that regulates the behavior of the MLCf given
by equation 7.2.1.
For validation purposes, each stimulation pattern used in Lopez-Guajardo's procedure B [99]
was tested (t_{on} = 30 minutes, t_{off} = 0.5 h, 1.5 h, 3.5 h, 11.5 h, and 23.5 h), and two additional
patterns: t_{off} = 10 min and 8 min were also simulated.
All simulations were performed using a Runge-Kutta fourth-order method implemented in
MATLAB R2015a (The MathWorks, Inc.).

7.3 Results and discussion

The simulations results of continuous stimulation and recovery after stimulation are pre-
sented in section 7.3.1. An analysis of the transient response is presented in section 7.3.2,
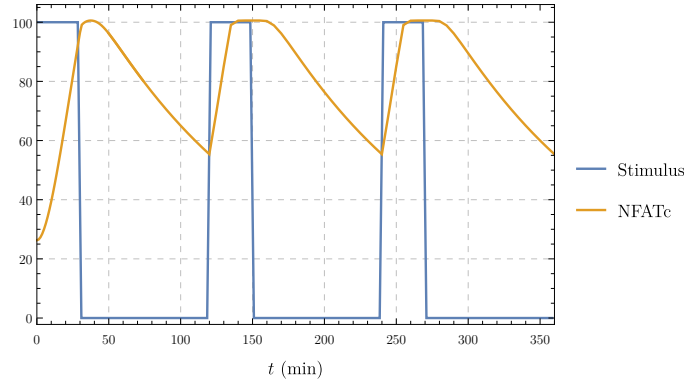
Figure 7.2.3: NFATc pattern. The NFATc behavior shown in chapter 6 is extrapolated into a periodic pattern. The amplitude of NFATc increases up to a saturation limit during t_{on}; NFATc holds the saturation amplitude due to the memory effect; finally, after the memory effect, NFATc decreases during the remaining part of t_{off}.
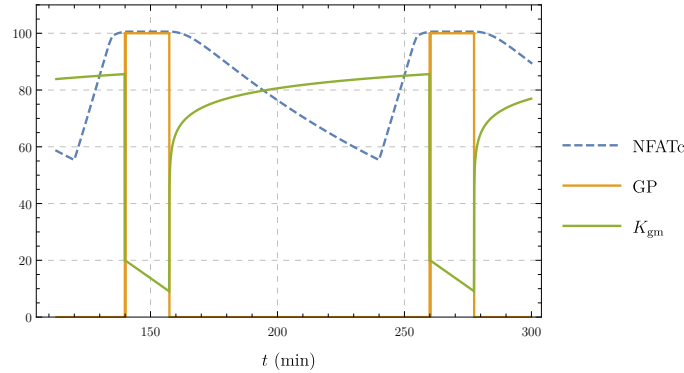
Figure 7.2.4: GP switching (GP re-scaled) and adaptive carrying capacity (K_{gm}). A GP-switch from 1 to 0 resets the K_{g2} function defined by equation 7.2.4, and the carrying capacity increases constantly while GP = 0 (favours type II fibers). A GP-switch from 0 to 1 resets the K_{g1} function defined by equation 7.2.5, and the carrying capacity decreases while GP = 1 (favours type I fibers).

and the steady state results are presented in section 7.3.3.

7.3.1 Continuous stimulation and recovery

The simulation results of the continuous stimulation (first scenario) are presented in figure 7.3.1, and the results of the recovery after stimulation (second scenario) are presented in figure 7.3.2.

The slow transformation of MLCf during the first three weeks of continuous stimulation is modelled by a very small growth rate (see table 7.2.1). This characteristic suggests that the properties of type IIB muscle fibers tend to remain constant under normal every day activities, and justifies the different transition rates according to muscle fiber classification.

The fast transformation after the first three weeks of continuous stimulation is modelled by a high growth rate (see table 7.2.1). This characteristic suggests the presence of transition fibers, which share characteristics of both type I and type IIB; because of that, transition fibers adapt faster than type IIB or type I fibers.

The slow transformation observed in the last four weeks, is modelled by a smaller growth rate (see table 7.2.1). This slower change indicates that the transformation of MLCf reached a more stable fiber type.
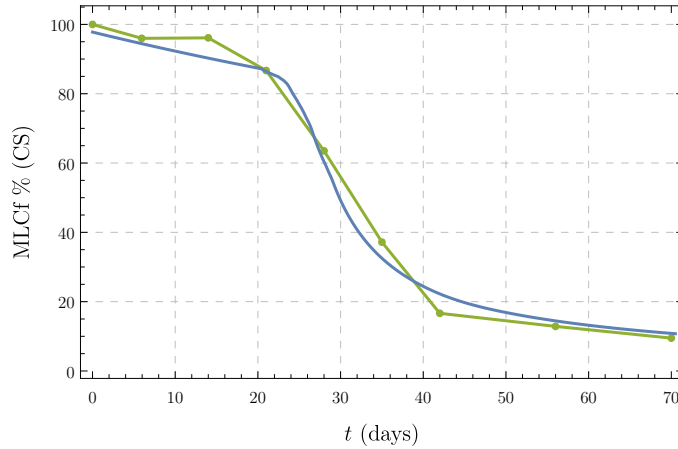
Figure 7.3.1: MLCf evolution under continuous stimulation for 10 weeks, experimental results (green) compared to simulation (blue). Results by Brown et al. [22] were used to fit the parameters shown in table 7.2.1 when GP continuously favours type I fibers.
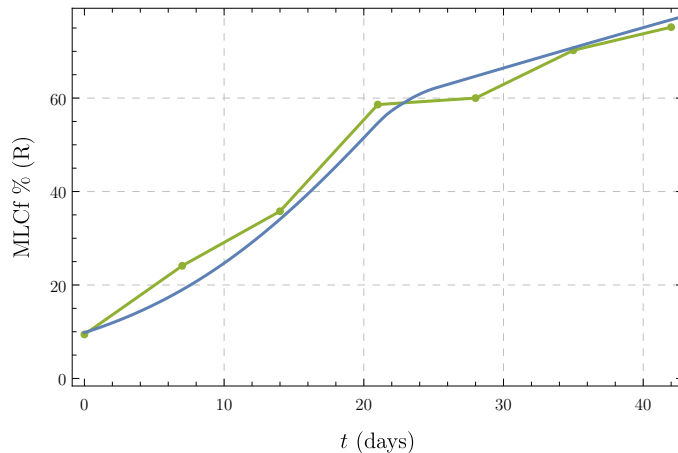
Figure 7.3.2: Recovery of the MLCf content after 10 weeks of continuous stimulation, experimental results (green) compared to simulation (blue). Results by Brown et al. [22] were used to fit the parameters shown in table 7.2.1 when GP continuously favours type II fibers.

The recovery scenario shows only two phases: a fast transformation during the first three

weeks followed by a slower transformation during the last three weeks. These characteristics are modelled by different growth rates (see table 7.2.1).

Although the growth rates of the stimulation and recovery processes are expected to be different, the change in growth rate is expected at the same MLCf levels in both scenarios. This inconsistency is explained by a lack of synchronization in the transition of individual fibers. This lack of synchronization happens because the recovery process occurs while the animals are free of electrical stimulation but are also free to perform normal daily activities; this means that some fibers are stimulated.

7.3.2 Transient response simulation results

Figure 7.3.3 shows the behavior of MLCf under stimulation patterns with t_{on} = 30 min and t_{off} = 23.5 h, 1.5 h, and 10 min. Results show that the shorter t_{off}, the longer the state with GP= 1, because NFATc decreases less with shorter t_{off} values, and then NFATc requires less time to reach its threshold. Figure 7.3.3 also shows the effect of the adaptive capacity: MLCf decreases during both GP= 1 and GP= 0 for the first 20 hours after stimulation, an increase in MLCf occurs when the time without stimulation (GP= 0) is longer than 20 hours (see figure 7.3.3a); MLCf remains almost constant for about 20 minutes even though GP= 1 (7.3.3b and c). MLCf decreases due to GP= 1 only if t_{off} is short relative to t_{on} (see figure 7.3.3c).
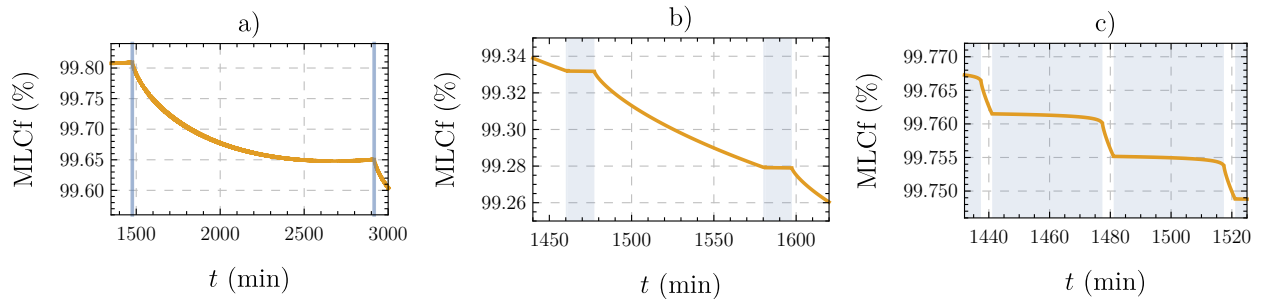
Figure 7.3.3: Transient MLCf evolution of an initially type IIB fiber under different stimulation patterns with t_{on} = 30 min, and a.) t_{off} = 23.5 h, b.) t_{off} = 1.5 h, and c.) t_{off} = 10 min; shaded blue areas indicate GP= 1. In figure a., GP= 1 lasts very shortly, and its effect is to reset the trend of the adaptive carrying capacity: MLCf decreases for up to 20 hours, and recovers (slowly increases) thereafter until a new resetting stimulus is received. In figure b., GP= 1 lasts about 20 minutes, but MLCf decreases due to the adaptive carrying capacity rather than the time with GP= 1. In figure c., GP= 1 lasts about 35 minutes, this is enough to clearly promote a MLCf decrease during GP= 1.

The long term evolution of MLCf under t_{on} = 30 min / t_{off} = 1.5 h is shown in figure 7.3.4. Figure 7.3.4a shows the MLCf evolution of a collection of fibers, where three aspects are

key: first, the initial MLCf value affects how long the adaptation process requires; second, fibers below steady state change their MLCf content faster than fibers above steady state; and third, all fibers tend to the same steady state. Figure 7.3.4b shows the average MLCf; notice that MLCf increases due to the fast transition of fibers below steady state, reaches a maximum due to the switch in the growth rate (see table 7.2.1) of fibers that change from type I to type IIA, and then it decreases towards steady state. Of course, the average MLCf behavior depends on the initial distribution of fibers.
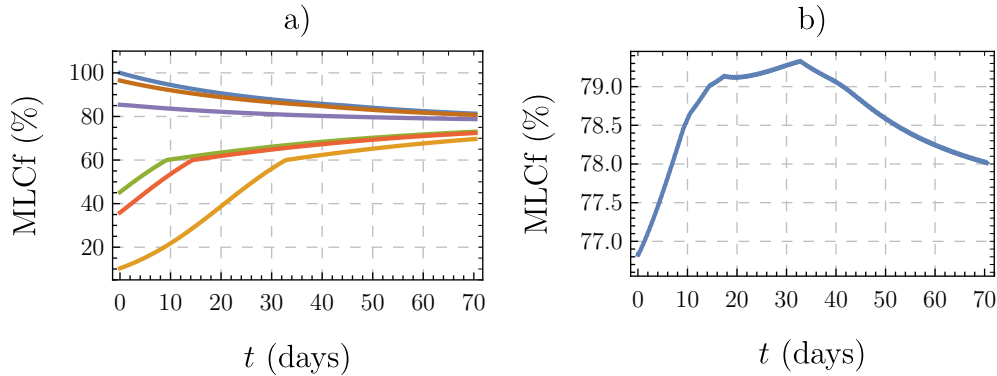
Figure 7.3.4: Evolution of MLCf under t_{on} = 30 min, t_{off} = 1.5 h. a.) Collection of individual fibers. b.) Average MLCf. MLCf of individual fibers evolve monotonously, whereas average MLCf reaches a maximum before approaching steady state. Notice that more than 6 weeks are necessary to reach steady state.

7.3.3 Steady state simulation results

Figure 7.3.5 shows a comparison between the experimental results of Lopez-Guajardo [99] and the simulations of the model presented in this chapter. The match between experimental data and simulation results using t_{off} within the range of 8 to 1410 min (23.5 h) is remarkable. Any stimulation pattern with t_{on} = 30 min and t_{off} smaller than 8 minutes is equivalent to the continuous stimulation pattern, because of the memory effect of nuclear NFATc. The memory effect allows a constant NFATc amplitude at the saturation limit, and a fixed GP state favouring type I fibers. In contrast, patterns with t_{off} slightly longer than the extension of the memory effect (simulated data points with t_{off} = 10 and 8 minutes in figure 7.3.5) produce MLCf with two characteristics: first, those results deviate from the experimental trend of t_{on} = 30 min; second, those results have the same MLCf content of stimulations patterns with t_{on} = 30 s / t_{off} = 30 s [98], continuous 2.5 Hz, and continuous 5.0 Hz [166]. Regarding continuous stimulation with different frequencies, recall that the experiments by Lopez-Guajardo et al. were obtained with electrical stimulation at 10 Hz; also recall, that nuclear NFATc accumulates at the same saturation level when using pulsed stimulation or continuous stimulation [97] (see chapter 6). The two previous observations, together with
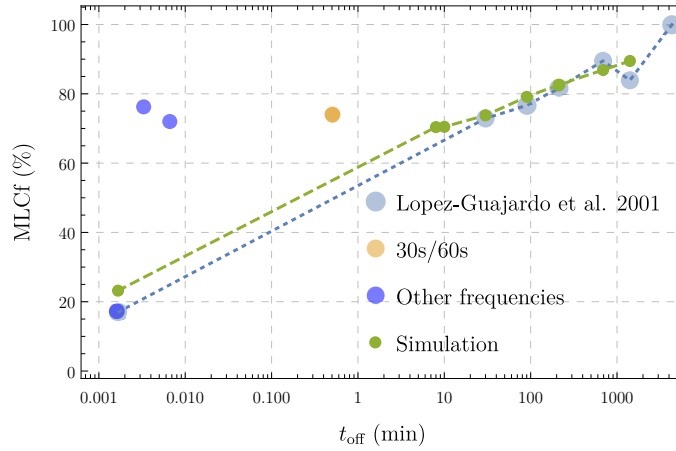
Figure 7.3.5: Averaged MLCf content after 6 weeks of periodic stimulation. Comparison between experimental results [99] and simulations. The two additional patterns t_{off} = 10 and 8 min produced a MLCf content in agreement with the results of the stimulation pattern with t_{on} = 30 s / t_{off} = 30 s reported in [98], and the results of continuous stimulation using frequencies of 2.5, and 5 Hz reported in [166] (for those frequencies, t_{off} is the respective period in minutes).

evidence shown in figure 7.3.5, allow to say that: first, there is a minimum frequency whose stimulation can be considered continuous, below that frequency, any stimulation acts as pulsed stimulation (see data points with t_{on} = 30 s / t_{off} = 30 s, and continuous 2.5 Hz and 5.0 Hz); and second, there is a balance between t_{on} and t_{off} in **minutes** that allows a fixed GP state and a total transformation even though stimulation is not 24 hours continuous (in agreement to the NFATc saturation produced by pulsed stimulation).

A direct simulation of protocols with t_{on} in the scale of seconds is not possible under the implementation developed for the simulations presented in this chapter; however, the model itself is suitable.

Effect of the parameters r, $\dot{y}_5^*$ and τ

According to the continuous stimulation and recovery results, in this model, parameter r affects how fast the steady state is reached, but the steady state value remains independent of r. The switching values of r are noticeable if most of the fibers in a muscle are of the same type (as shown in figures 7.3.1 and 7.3.2), and also in individual fibers (as shown in figure 7.3.4a); the trace of the switching values of r is lost in an averaged MLCf of a muscle with an initially wide distribution of fibers (as shown in figure 7.3.4b).

Parameter $\dot{y}_5^*$ affects the steady state of MLCf. Parameter $\dot{y}_5^*$ directly defines the instant when GP switches from 0 to 1; in that way, $\dot{y}_5^*$ directly affects the time that GP favours type I characteristics: the longer GP favours type I, the shorter GP favours type II; the steady state results from the balance of time favouring type I and time favouring type II

characteristics.

Figure 7.3.6 shows that MLCf is almost unaffected by τ under periodic stimulation with t_{off} greater than 90 minutes. The effect of τ is stronger in stimulation patterns with t_{off} smaller than 30 minutes. The patterns with t_{off} = 10 and 8 minutes are expected to produce the same MLCf results because of the memory effect reported by [97], this occurs with τ values smaller than 10.5 minutes and justifies the value listed in table 7.2.2.
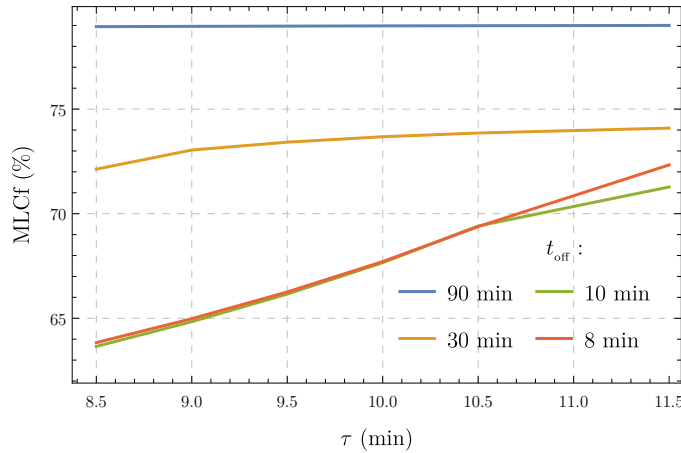
Figure 7.3.6: MLCf as a function of τ after 42 days of periodic stimulation patterns with different t_{off} values. According to these results, τ is important when t_{off} is about the same size of the memory effect of NFATc (about 10 minutes).

7.4 Conclusion

The transition of the MLCf isoform under electrical stimulation was modeled as a logistic behavior with an adaptive carrying capacity and a state-dependent growth rate. The carrying capacity adapts guided by the saturation of NFATc in the nucleus, which in turn depends on the times with and without stimulation; and the growth rate depends on the saturation of NFATc and the current state of MLCf of individual fibers. The model was tested under different stimulation protocols and the match between experiments and simulations is remarkable.

Evidence shows that other characteristics of myofibers evolve along with MLCf, in particular tetanus force. The model for MLCf evolution developed in this chapter will be used to model single-fiber force evolution through the adaptation of the specific force. Specific force adaptation and its inclusion in the continuum mechanical model of muscle active response will be presented in the next chapter.

8 Maximum isometric tension adaptation

8.1 Background

Mechanical characteristics such as force generation, contractile velocity, and fatigability are crucial in physical performance and correlate to sustained activity patterns. At the muscle fiber scale, -with the exception of fatigability that highly correlates to mitochondrial content [151, 17], but is out of the scope of this chapter and will not be addressed any further- those characteristics are determined largely by the molecular-level interactions of the contractile protein-filaments myosin and actin [111], and these interactions correlate to the protein isoform content of MLC and MHC that adapt to stimulation patterns as described in chapter 7.

The great number of possible combinations and proportions of MLC and MHC isoforms suggests a continuum of mechanical properties as functions of the protein isoform content [158, 155]; in particular, a correlation between specific force and MLCf content (as modeled in chapter 7) may be expected. Here, a distinction is required: the ratio peak force to cross sectional area (CSA) of **individual fibers** is frequently called specific force [170], whereas the ratio maximum voluntary contraction (MVC) to CSA of a **whole muscle** is called specific strength or simply MVC/CSA [85]. Notice that the continuum mechanics active response requires the definition of the maximum isometric tension parameter σ_o (see equation 3-11), which is fundamentally a homogenized specific force.

A fixed value of the maximum isometric tension σ_o was the basis of the model for the muscle active response presented in chapter 3. That model assumes a single muscle fiber type, which, for the purposes of short term muscle response, is equivalent to the homogenization of a distribution of muscle fiber types whose individual properties are fixed; however, fiber type distribution and contractile characteristics (which are functions of the protein isoform content) adapt as a long-term effect of exercise [127, 157].

Contractile characteristics of single fibers such as twitch force, and specific force increase in order I < IIA < IIB [170, 45, 111]; although the same order is accepted for CSA, there are conflicting results: some experiments show smaller CSA in type II fibers [45, 115], some others show smaller CSA in type I fibers [23, 107]; notice that these results account for steady state characteristics and overlook any connection to activity patterns.

Activity patterns and the gene program for protein replacement are related through the NFATc signaling pathway. Different activity levels produce different NFATc responses: resistance training (high intensity) blocks the translocation of NFATc to the nucleus, and the gene program signals the production of type IIB characteristics; endurance training (prolonged moderate to low intensity) allows the translocation of NFATc to the nucleus, and promotes type I characteristics; daily activities (low intensity) are unable to trigger the NFATc signaling pathway, and in this way, low intensity activities also promote type IIB characteristics. A full transformation of muscle fibers to type IIB as a consequence of low intensity activities is blocked by small pieces of RNA called micro RNA (miRNA) [29].

The particular group of miRNAs that affects cardiac and skeletal muscle is called myomiRNA, and its function is regulated by exercise training (endurance, or resistance) [106, 116]. The impact of myomiRNA variability was demonstrated by Davidsen et al. [47] in a 12 weeks resistance training program. They selected the participants with greater hypertrophy gains in one group (high responders), and the participants with lower gains in another group (low responders); they showed that some myomiRNA levels before and after the program were significantly different in low responders, whereas those myomiRNA levels were unchanged in high responders.

The aim of this chapter is to incorporate the evolution of the protein isoform adaptation (MLCf content) due to exercise into the maximum isometric tension parameter of the muscle active response model and to study its effects on MVC. A brief modification of the MLCf transition model (due to the myomiRNAs action) is considered, a specific-force function is proposed, and the homogenization of the specific force is presented.

8.2 Materials and Methods

The MLCf transition model requires a small modification motivated by the myomiRNA effect, this modification is presented in section 8.2.1. Thereafter, the two main assumptions to describe the evolution of the maximum isometric tension of a whole muscle are presented: first, an evolution of the specific force according to the MLCf content of individual fibers (section 8.2.2); and second, the homogenization of the maximum isometric tension that correlates fiber distribution and fiber-type specific force (section 8.2.3). This section also presents the parameters and initial conditions required for the evolution of the maximum-isometric-tension model (section 8.2.4), and finally the general description of the simulation procedure (section 8.2.5).

8.2.1 Memory effect due to myomiRNA action

The difference in myomiRNA levels between high and low responders [47] suggests a memory period that could explain how long it takes to reach a new fiber-distribution steady state. After a bout of high intensity or resistance training, the synthesis of proteins of type IIB

fibers occurs during the memory period; once the memory period is over, myomiRNAs block the protein synthesis avoiding the transformation of all fibers to type IIB, even though the gene program naturally signals the production of type IIB proteins. According to Nielsen et al. [116], the training memory period is about 48 hours.

The inclusion of this memory parameter only affects the MLCf transformation in cases of stimulation protocols with more than 48 hours without stimulation; because of this, the results obtained in chapter 7 remain unaffected.

To include the memory parameter (τ_{mem}) in the model for MLCf transition (presented in chapter 7), a simple solution is possible: if the time without stimulus is smaller than τ_{mem}, then function K_{g2} targets the MLCf value given by equation 7.2.4; if not, K_{g2} targets the initial MLCf of the fiber.

8.2.2 Specific force as a function of MLCf

A muscle fiber with 0% MLCf exhibits the smallest specific force ($\sigma_{\min}$), whereas a muscle fiber with 100% MLCf exhibits the greatest specific force ($\sigma_{\max}$). A muscle fiber with a MLCf content x exhibits a specific force σ_x. In this chapter, a sigmoidal function is proposed as the relation between σ_x and x:

$$\frac{\Delta\sigma_x}{\Delta\sigma_{\mathrm{R}}} = \frac{1}{1 + \left(\frac{x_{50}}{x}\right)^b}, \tag{8.2.1}$$

where $\Delta\sigma_x$ is the variation in the specific force ($\sigma_x - \sigma_{\min}$) for a given MLCf content x (x ranging from 0 to 100%), $\Delta\sigma_{\mathrm{R}}$ is the range of variation of specific force ($\sigma_{\max} - \sigma_{\min}$), x_{50} is the MLCf content that produces half $\Delta\sigma_{\mathrm{R}}$, and b is the cooperativity parameter. Rearranging for σ_x:

$$\sigma_x = \sigma_{\min} + \frac{\Delta\sigma_{\mathrm{R}}}{1 + \left(\frac{x_{50}}{x}\right)^b}. \tag{8.2.2}$$

This equation proposes that the specific force of a single muscle fiber changes continuously with the continuous increase (or decrease) of its MLCf content, and will be used to define an average specific force for each fiber type. The average specific force combined with the fiber distribution accounts for the maximum isometric tension adaptation.

8.2.3 Maximum isometric tension transition

The active SEF in equation 3-11 assumes a fixed value of the maximum isometric tension σ_o. This is valid under the assumption of homogenized properties of the muscle tissue, which is

equivalent to consider only one type of fiber:

$$\sigma_o = \sigma_k \frac{a_k \, n_k}{A_{tot}}, \tag{8.2.3}$$

where σ_k is the specific force that characterizes an individual fiber of type k, a_k is the cross sectional area of that fiber, n_k is the number of fibers of type k in the muscle, and A_{tot} is the total cross sectional area (CSA) of the muscle structure. In this case (only one fiber type), the product $a_k \, n_k$ is equal to the total CSA.

Now, to include the distribution of fibers in a muscle structure, a superposition of each fiber-type contribution leads to:

$$\sigma_o = \sigma_o(n_k, a_k) = \sigma_I \frac{a_I \, n_I}{A_{tot}} + \sigma_{IIA} \frac{a_{IIA} \, n_{IIA}}{A_{tot}} + \sigma_{IIB} \frac{a_{IIB} \, n_{IIB}}{A_{tot}}, \tag{8.2.4}$$

where the three fiber types (I, IIA, and IIB) are combined. Notice that the fraction $\frac{A_{tot}}{a_k}$ is the maximum number of fibers type k that a particular muscle can have; and, recalling that a given muscle can increase its size but not the total number of fibers, then the fraction $\frac{A_{tot}}{a_k}$ is simply the total number of fibers of the muscle N_{tot} (which is fixed independent on the fiber type). With that:

$$\sigma_o = \sigma_I \frac{n_I}{N_{tot}} + \sigma_{IIA} \frac{n_{IIA}}{N_{tot}} + \sigma_{IIB} \frac{n_{IIB}}{N_{tot}}. \tag{8.2.5}$$

This last equation is in agreement to the maximum isometric tension in equation 3-11, but offers the possibility to explore increments in maximum force due to training that are not a consequence of size increase but to adaptation at the fiber scale. In other words, the increment in force that results from exercise training is not necessarily proportional to the increase in CSA; the non-linearity in the relation between force and CSA can be explored through the adaptation of the fiber distribution and fiber-type specific force.

The fiber distribution numbers n_I, n_{IIA}, and n_{IIB}; and the set of fiber-type specific forces σ_I, σ_{IIA}, and σ_{IIB} are briefly described below.

Fiber distribution

Any particular muscle contains a fiber distribution adapted specifically to the activity level of the muscle [45]. A sustained change in the activity level of a muscle leads to adaptations at the protein scale that ultimately produce an adaptation of the fiber distribution, and this adaptation affects the maximum isometric tension as proposed in equation 8.2.5.

The evolution of the fiber distribution is obtained from the evolution of the MLCf presented in chapter 7. At any particular time, the fiber distribution is simply the number of fibers within each MLCf range presented in table 7.2.3.

Fiber-type specific force

The fiber distribution allows the calculation of an average MLCf for each fiber type. This average results from the MLCf content of all fibers within each range presented in table 7.2.3. The average MLCf defines the fiber-type specific force through equation 8.2.2.

8.2.4 Parameters and initial conditions

Table 8.2.1 presents the parameters for equation 8.2.2, and the initial fiber distribution required for the maximum isometric tension (equation 8.2.5). The maximum isometric tension also requires the initial fiber-type specific forces that result from the initial MLCf of each fiber.

The initial MLCf content of each fiber was assigned as a random number within the MLCf ranges defined in table 7.2.3. For instance, the initial MLCf of fibers type I are 50 (table 8.2.1) random numbers between 0 and 20 (table 7.2.3).

Table 8.2.1: Specific force parameters for equation 8.2.2, and initial fiber distribution. (*the value of $\sigma_{\max}$ lies within the ranges reported by [111, 178]).

Parameter	Value	Units	Reference
$\sigma_{\min}$	100	mN/mm^2	[111, 178]
$\sigma_{\max}$	155.7*	mN/mm^2	fitted
x_{50}	75.70	1.	fitted
b	11.50	1.	fitted
n_{I}	50	1.	[178]
n_{IIA}	33	1.	[178]
n_{IIB}	17	1.	[178]

8.2.5 Simulations and Validation

The simulations performed in this chapter are a composition of all the models presented in this thesis: a training input triggers the IGF1-AKT and NFATc signaling pathways (chapters 4 and 6); the outcome of IGF1-AKT pathway is used as input for the growth tensor to produce CSA increase (chapter 5), and the outcome of the NFATc pathway is used as input for the MLCF transition to produce the evolution of the fiber MLCf content (chapter 7) and fiber distribution. The fiber MLCf content and fiber distribution allow the calculation of the evolving maximum isometric tension (σ_o) that is stored in a lookup table; each value in the lookup table represents the updated σ_o value at the simulation time step of the mechanobiological model. Finally, the updated CSA, and maximum isometric tension allow the simulation of the changes in MVC (chapter 3) that result from training exercise.

All parameters and initial conditions were described in the corresponding sections of each chapter, except the initial fiber distribution that was described in the previous section.

For validation purposes, the experimental protocol used by DeFreitas et al. [50] to study the effects of resistance training was summarized in section 4.3.2 (training on days 1, 3, and 5 of every week for 8 weeks), and the results of the MVC normalized to the initial MVC are presented in table 8.2.2.

Table 8.2.2: Increase in muscle CSA, MVC, and relative MVC (Rel-MVC) due to high intensity training as a function of the activity period. Experimental results from DeFreitas et al. [50].

Activity (days)	CSA (cm²)	MVC (N)	Rel-MVC (%)
1	145.0	720.1	0
7	145.6	728.5	1.2
14	150.0	732.1	1.7
21	151.4	745.4	3.5
28	153.6	775.1	7.6
35	154.7	808.0	12.2
42	156.4	825.3	14.6
49	157.9	830.6	15.4
56	159.3	865.2	20.2
63	158.9	892.3	23.9

The dynamical equations of the NFATc signaling pathway and MLCf transition were solved by a Runge-Kutta fourth-order method implemented in MATLAB R2015a (The MathWorks, Inc.); the lookup table was stored in a file that was used to update the maximum isometric tension at each time step of the mechanobiological simulation. The mechanobiological model was simulated using a UEL subroutine, implemented in Fortran, linked to the solving procedures in the specialized software ABAQUS 6.10 (Dassault Systemes USA, Waltham, MA).

8.3 Results and discussion

Section 8.3.1 shows the results of MVC and MVC/CSA of the model using fixed maximum isometric tension; these results demonstrate that CSA increase using uniform constant fiber characteristics are not enough to explain MVC gains during a resistance training period. Section 8.3.2 presents the evolution of fiber distribution and average MLCf type to emphasize that these characteristics play an important role in the evolution of the whole organ characteristics. Section 8.3.3 presents the results of MVC and MVC/CSA using the evolution of fiber characteristics and a comparison to experimental measurements. Finally, hypertrophy results using different values of the memory effect are presented in section 8.3.4.

8.3.1 MVC due to CSA increase

According to the results of chapter 7, MLCf adapts under chronic low frequency stimulation; and according to the results of chapter 5, CSA adapts under high intensity training. Although it is reasonable to say that MLCf adapts under high intensity training, first it is necessary to show that CSA increment produces a MVC increment (figure 8.3.1a), but that increment is smaller than what experiments show; also, the ratio MVC/CSA suggests that the increase in CSA is not enough to account for the increase in MVC (figure 8.3.1b).
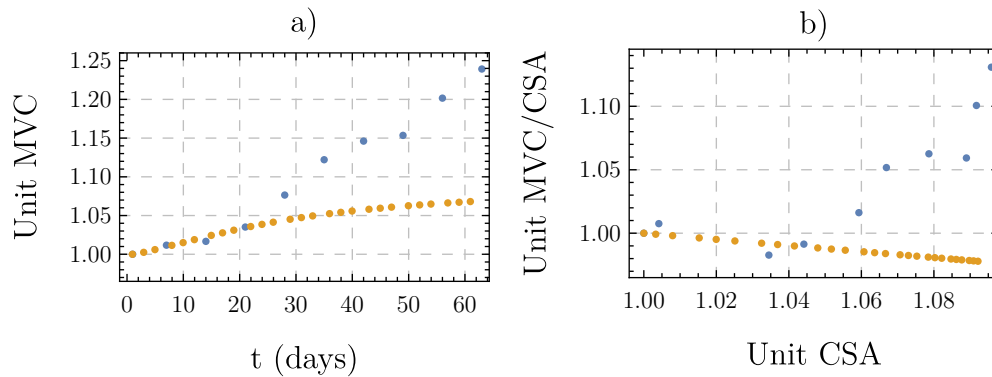
Figure 8.3.1: MVC and MVC/CSA adaptation due to training exercise considering fixed maximum isometric tension; simulation in orange, experiment by DeFreitas in blue. a.) MVC increases during the extension of the training protocol but accounts for only a third of the experimental results. b) the ratio MVC/CSA as a function of CSA shows that CSA is not dominant in MVC adaptation.

Figure 8.3.1 demonstrates that MVC is not proportional to CSA, and demonstrates the need of incorporating fiber type characteristics as described in section 8.2.3.

8.3.2 Fiber distribution and average MLCf type

Figure 8.3.2a shows that fiber distribution changes fast during the first week; then, fiber distribution remains stable during the following four weeks; and finally, type IIA fibers slowly transform to type IIB after the fifth week.

Figure 8.3.2b shows the evolution of the average MLCf of each fiber type. The average MLCf of type I fibers increases during the first 10 days, then it quickly drops because all type I fibers reached the threshold to classify as type IIA. A decrease in the average MLCf of type IIA fibers occurs because some type I fibers and a few type IIB fibers reach their thresholds faster than others, these fibers produce an increase in the number of type IIA fibers, but the total MLCf of type IIA fibers increases slower than the number of fibers. By the end of the fifth week, the MLCf content of type IIA and IIB fibers approaches a steady state.

Figures 8.3.2a and b show that, after the fifth week, type IIB fibers contain the same amount of MLCf in average although the number of fibers increases; whereas, type IIA fibers increase
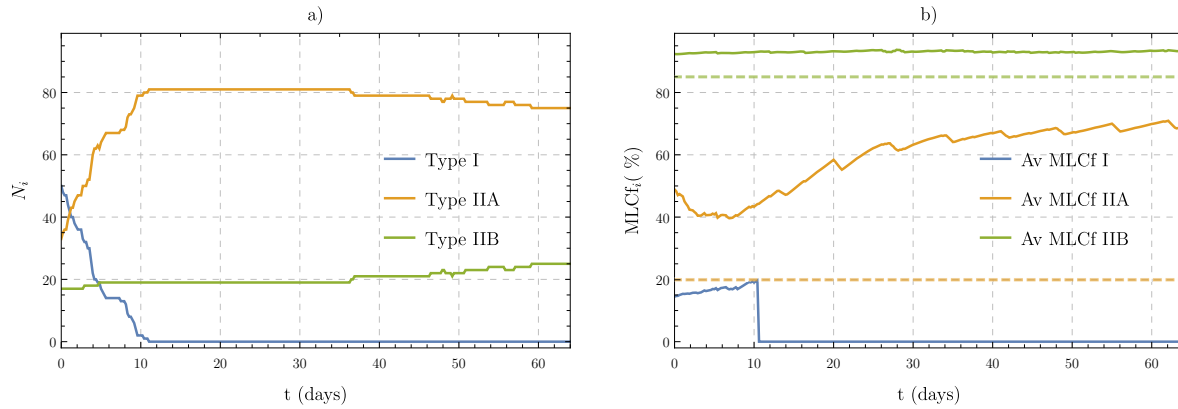
Figure 8.3.2: Fiber distribution and average MLCf type. a.) Type I fibers transform quickly to type IIA; some type IIA fibers transform to type IIB in the first week, and continue to transform only after the fith week. b.) The average MLCf of type IIA displays a wide variability because of a fast increase in number of fibers and a relative slower increase in MLCf; after the third week, average MLCf of type IIA continues to increase at a decreasing pace. Dashed lines indicate MLCf thresholds.

their MLCf in average although the number of fibers decreases.

Regarding fiber distribution, some experiments show that, during resistance training, the population of type IIB fibers actually decreases [96, 27]; in contrast, fast isokinetic/high velocity contraction training shows that the population of type IIB fibers may increase [119]. Although both resistance and fast isokinetic training are high intensity training, they produce a different fiber-type adaptation, and suggest that three exercise categories should be considered in modeling skeletal muscle adaptation: resistance, fast isokinetic, and endurance. Thus, the increase or decrease in the number of type IIB fibers could be explained by an activity-specific mechanism that operates at the myofiber level and differentiates each stimulus as one of the three categories. Such mechanism may be related to neuromuscular function, as well as to myomiRNA activity and is out of the scope of this thesis.

8.3.3 MVC due to CSA and specific force adaptation

Table 8.3.1 presents a comparison of some experimental and simulation characteristics regarding MVC and specific force adaptation. A few aspects to notice are: first, absolute values of CSA and MVC are not targets of the model, because the CSA of the simulation is smaller than the experimental CSA by design of the FEM structure; second, the ratios of experimental to simulation MVC and CSA are comparable, but suggest a nonlinearity; third, maximum isometric tension values (simulation σ) are within experimental specific force range (experimental σ); and fourth, σ values are about three times greater than MVC/CSA, but the experiment to simulation ratio suggests a linearity between them.

Figure 8.3.3 shows the simulation results of MVC and MVC/CSA normalized to their initial

Table 8.3.1: Absolute-value ranges of experimental measurements and simulation results of MVC and specific force adaptation. Experimental σ is specific force, and simulation σ is the maximum isometric tension (defined in section 8.2.3). The ratio (experiment/simulation) compares middle values of each characteristic.

	MVC (N)	CSA (cm²)	MVC/CSA (mN/mm²)	σ (mN/mm²)
Experimental	720 - 892	145 - 159	49.7 - 56.2	93 - 179
Simulation	140 - 171	32.34 - 35.36	43.2 - 48.3	108.8 - 126.8
Ratio	5.18	4.49	1.16	1.15

values. These results are the combination of growth (that results from protein synthesis) and fiber properties adaptation (that results from MLCf transition). A comparison of MVC in figures 8.3.1a and 8.3.3a shows that MLCf adaptation is responsible for more than 60% of the total MVC increase. Regarding the first three weeks of adaptation, experimental evidence shows two aspects: first, figure 8.3.3a shows that MVC increased in each measurement; and second, figure 8.3.3b shows that MVC/CSA is smaller than its initial value when unit CSA values are under 1.05 (increases in CSA under 5%). These two observations suggest that CSA increases faster than MVC during the first three weeks of adaptation.
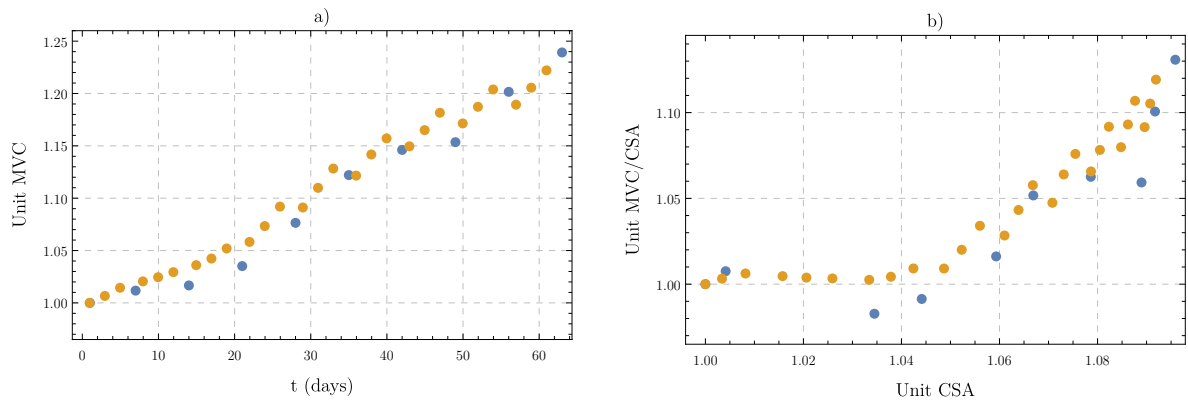
Figure 8.3.3: Evolution of MVC, and MVC/CSA as a function of CSA (MVC, CSA, and MVC/CSA normalized to initial values); simulation in orange, experiment by De-Freitas [50] in blue; compare to figure 8.3.1a and b. Simulation results show a very good agreement to experiments after the inclusion of fiber type and specific force adaptation.

The initial fast increase in CSA suggests that the effects of protein synthesis and protein isoform replacement occur in different time scales: the MVC correlates better to CSA increase during the first three weeks (see figure 8.3.1a, and also simulation results on unit MVC/CSA in figure 8.3.3b, which is almost constant when unit CSA is under 1.05); and after those three weeks, MVC correlates better to the combination of CSA and specific force adaptation (see figure 8.3.3a).

A comparison between unit MVC/CSA in figures 8.3.1b and 8.3.3b demonstrates the dramatic effect of considering the adaptation of single fiber characteristics at the protein level.

8.3.4 Variation of the memory-effect parameter

Results presented so far were obtained with τ_{mem} = 48 hours, figure 8.3.4 shows that a variation of τ_{mem} produces different hypertrophy results. Greater τ_{mem} values allow synthesis and replacement of type IIB proteins for longer times, and as a consequence, MLCf transforms faster relative to smaller τ_{mem} values. The simple incorporation of the parameter τ_{mem} in the MLCf transition model predicts that variations of the parameter are only detectable after three weeks of training, this is a consequence of the sigmoidal function for specific force proposed in equation 8.2.2: when the MLCf content increases, specific force increases only if MLCf approaches x_{50}.
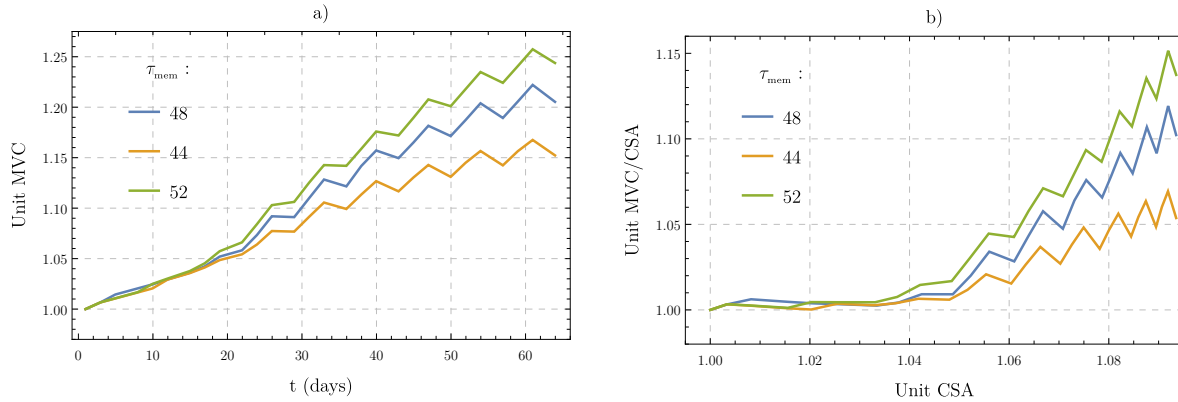
Figure 8.3.4: Effect of memory parameter due to myomiRNA activity on unit MVC (a), and unit MVC/CSA as function of CSA (b). Greater τ_{mem} produces greater MVC, and MVC/CSA; this result is consistent with the differentiation between high and low responders found by Davidsen et al. [47].

Recall that the memory effect was motivated by the work on myomiRNA function and training adaptation reported by Davidsen et al. [47]; their results show a considerable difference in the one-repetition maximum force (leg press and leg extension) between high and low responders, but a statistical difference in MVC was not concluded; in contrast, single fiber CSA results are radically and statistically different (the increase in CSA is about three times greater in high responders relative to low responders). This evidence suggests that the miRNA function affects protein synthesis in a greater extent than protein isoform replacement, and is also supported by the effect of miRNA fuction on the IGF1-AKT signaling pathway reported by many studies [118, 149, 26]. In consequence, to have a better approximation of the memory effect, both the MLCf transition model and IGF-AKT signaling pathway model require a way to incorporate miRNA activity; to this end, a time course

of the hypertrophy adaptation of high and low responders is necessary but has not been reported in the literature.

8.4 Conclusion

Protein isoform replacement and fiber distribution adaptation were incorporated in a new model for the evolution of the specific force of single myofibers. The assumption of a continuous evolution of mechanical characteristics of myofibers guided by the evolution of protein isoform replacement leads to an excellent approximation of MVC adaptation produced by exercise training; according to the model developed in this chapter, the increase in CSA accounts for only one third of the total MVC, the other two thirds are explained by the evolution of single fiber specific force.

One particularity of the protein isoform replacement is that a total replacement of proteins to type IIB isoform is hard to produce even though the myofiber gene program naturally targets type IIB characteristics. This observation was addressed by the incorporation of a memory effect conceptually based in the myomiRNA activity, and simulations show that a variation of this parameter produces different hypertrophy effects in agreement to experimental observations.

The model and results presented in this chapter are the composition of all the particular models of previous chapters, and is far from being a complete model for skeletal muscle adaptation. In particular a cellular mechanism to distinguish different kinds of training requires special attention.

9 Conclusions

This research aimed to mathematically model muscle adaptation starting with cellular processes that are triggered by physical activity. Muscle adaptation occurs by the interaction of many of those processes and in different time scales and length scales. By considering two key aspects of the adaptation process (protein synthesis and gene-program switch), this research found good agreement to hypertrophy and fiber type characteristics resulting from an exercise training signal. Muscle size was used as feedback to improve the match between experimental data and simulation on muscle cross sectional area (CSA), and fiber distribution was used to improve the match on maximum voluntary contraction (MVC).

A 3-dimensional idealized muscle structure was modelled to quantify macroscopic characteristics of skeletal muscle such as CSA and MVC. Using existing continuum mechanical models, the passive and active responses of skeletal muscle were obtained by the implementation of a hyperelastic material, whose strain energy function has a passive and an active contribution. This approach proved to be convenient to reproduce the force vs stretch material behavior of muscle tissue in both passive and active responses. In addition to CSA and Force, the continuum mechanical description is necessary to test the models for growth, and fiber shifting that were developed in this thesis.

A new model for skeletal muscle adaptation based on the IGF1-AKT signaling pathway was presented in this thesis. The fundamental idea is that the biochemical species of the pathway interact in a dynamical model; this interaction produces a balance between protein synthesis and protein degradation. In the long term, the protein balance promotes muscle hypertrophy or muscle atrophy according to an exercise training input. The model was validated by comparing it to experimental reports, and the model's applicability was demonstrated by showing numerical examples that represent physical activity in different scenarios. In spite of its simplicity (because many details of the exercise protocol and details of the signaling pathway were not considered), the model developed in this thesis produces a remarkable agreement to validation data in the atrophy case, and reasonable results in the hypertrophy case and numerical examples.

The IGF1-AKT model and the continuum mechanical model were coupled in a new mechanobiological model designed to explore effects of protein content on the mechanical behavior of tissue. This mechanobiological model is triggered by an exercise training protocol, and predicts how the protein content of the muscle evolves; the increase in protein content is then converted into a growth tensor that produces changes in the 3D structure, and those changes allow the quantification of CSA and force adaptation. The strategy consisted in

calculating the changes in the force - activation response for updated structures (obtained by the increasing size due to the increasing protein content), then calculating the required activation to produce a fixed force, and then updating the protein synthesis rate accordingly. The mechanobiological model shows that, to produce a given force, the activation changes during the extension of the training period: with a sufficiently long training period a muscle requires less activation to produce the fixed force. This reduction in the required activation agrees with training recommendations such as intensity and loading increase to target the highest protein synthesis possible. The use of the mechanobiological model to validate CSA in the hypertrophy case demonstrates a big improvement relative to the IGF-AKT model alone.

Protein content is one of many characteristics that are affected by exercise; in fact, each muscle fiber type is affected differently by exercise; in this regard, the IGF-AKT signaling pathway is not specific enough, and another pathway needs to be considered: the Calcineurin - NFATc signaling pathway.

A new model for the Calcineurin - NFATc signaling pathway was built with the aim to address fiber differentiation. This pathway is triggered by sustained physical activity and produces an increased level of NFATc in the nucleus. Nuclear NFATc is a key factor to activate or deactivate the gene program for specific muscle fiber characteristics, and thus, the Calcineurin-NFATc signaling pathway plays an important role in muscle fiber shifting. Evidence of the nuclear NFATc time course was used for validation of the model, and an excellent agreement between the Calcineurin - NFATc model and experimental results was found under two stimulation scenarios: continuous 30 minutes stimulation and pulsed stimulation. Nuclear NFATc saturates in both scenarios, and this saturation can be used to switch the gene program of muscle fibers.

The gene-program switch that results from the NFATc saturation allows to target characteristics of type I or type II fibers. Of the many characteristics that evolve with different sustained stimulation patterns, myosin light chain of the fast type (MLCf) showed a clear trend compatible with the evolution of a logistic behavior: in the long term, MLCf reaches a steady state known as carrying capacity. In this thesis, an adaptive carrying capacity was modelled in a way that the MLCf is a function of the time **without** stimulation when the gene program favours type II characteristics, but it is a function of the time **under** stimulation when the gene program favours type I characteristics. The model was validated for different scenarios including non-stimulation, continuous 24 h stimulation, and periodic stimulation; the modelled MLCf content showed a remarkable agreement compared to experimental evidence.

MLCf was then used to model the evolution of the single-fiber specific force, which usually is assumed as a fiber type characteristic. Adaptation in fiber characteristics at the protein level may occur simultaneously with the adaptation of single-fiber protein content, but the protein isoform replacement and the protein content are related to different biochemical processes. In this thesis, the protein content was addressed by the IGF-AKT signaling

pathway model, and the protein isoform replacement was addressed by the NFATc pathway together with the MLCf transition models. With the aim to match experimental evidence in MVC adaptation, a continuum adaptation of the single-fiber specific force as a function of MLCf was proposed. The MLCf content was used to classify fibers as type I, IIA or IIB, and then a homogenization of the specific force was used to update the maximum isometric tension of the muscle tissue at the organ scale. Very good match between normalized MVC and MVC/CSA was found, and the model demonstrates that MVC adaptation is the result of a combination between fiber sizes and characteristics at the protein level that are more detailed than fiber type classification.

A good understanding of muscle function is available, but most of muscle-function modeling focuses on muscle contraction, which occurs in the time scale of seconds; in contrast, the aim of this thesis was to model the cumulative effects of exercise that are only observable in the time scale of weeks. Because of the difference in time scales, many important aspects of muscle contraction were oversimplified and others overlooked, for instance Ca^{2+} function, recruitment patterns, and fatigability; also, the effects of training to fatigue, blood flow restriction, or even relative training intensity were overlooked in this work. The models and strategy developed in this thesis leave room for the incorporation of those and many other aspects of muscle function and physical training.

Muscle function is also an intensive field of research in continuum mechanics, but the modelling strategy proposed in this thesis differs from the regular approach in continuum mechanics because this thesis gives more importance to the biological processes that control cellular functions (through signaling pathways) rather than targeting a purely mathematical description that overlooks the complexity and specificity of biochemical process of living tissue.

Bibliography

[1] ABBOTT, Karen L. ; FRIDAY, Bret B. ; THALOOR, Deepa ; MURPHY, TJ ; PAVLATH, Grace K.: Activation and cellular localization of the cyclosporine A-sensitive transcription factor NF-AT in skeletal muscle cells. En: *Molecular biology of the cell* 9 (1998), Nr. 10, p. 2905–2916

[2] ADAMS, Gregory R. ; McCUE, Samuel A.: Localized infusion of IGF-I results in skeletal muscle hypertrophy in rats. En: *Journal of Applied Physiology* 84 (1998), Nr. 5, p. 1716–1722

[3] ALTAN, Ekin ; ZÖLLNER, Alexander ; AVCI, Okan ; RÖHRLE, Oliver: Towards modelling skeletal muscle growth and adaptation. En: *Pamm* 16 (2016), Nr. 1, p. 921–924. – ISSN 16177061

[4] ANDERSEN, Per ; HENRIKSSON, Jan: Training induced changes in the subgroups of human type II skeletal muscle fibres. En: *Acta physiologica scandinavica* 99 (1977), Nr. 1, p. 123–125

[5] BARANY, Michael: ATPase activity of myosin correlated with speed of muscle shortening. En: *The Journal of general physiology* 50 (1967), Nr. 6, p. 197–218

[6] BARANY, Michael: ATPase activity of myosin correlated with speed of muscle shortening. En: *The Journal of general physiology* 50 (1967), Nr. 6, p. 197–218

[7] BARNARD, R J. ; EDGERTON, V R. ; FURUKAWA, TETSUO ; PETER, JB: Histochemical, biochemical, and contractile properties of red, white, and intermediate fibers. En: *American Journal of Physiology-Legacy Content* 220 (1971), Nr. 2, p. 410–414

[8] BARTOO, Marc L. ; POPOV, Viktor I. ; FEARN, Lisa A. ; POLLACK, Gerald H.: Active tension generation in isolated skeletal myofibrils. En: *Journal of Muscle Research & Cell Motility* 14 (1993), Nr. 5, p. 498–510

[9] BAUMANN, Hugo ; CAO, Kezhen ; HOWALD, Hans: Improved resolution with one-dimensional polyacrylamide gel electrophoresis: myofibrillar proteins from typed single fibers of human muscle. En: *Analytical biochemistry* 137 (1984), Nr. 2, p. 517–522

[10] BICKEL, C S. ; BICKEL, C S. ; SLADE, Jill ; SLADE, Jill ; MAHONEY, Ed ; MAHONEY, Ed ; HADDAD, Fadia ; HADDAD, Fadia ; DUDLEY, Gary a. ; DUDLEY, Gary a. ;

ADAMS, Gregory R. ; ADAMS, Gregory R. ; SCOTT, C ; SCOTT, C: Time course of molecular responses of human skeletal muscle to acute bouts of resistance exercise. En: *Journal of Applied Physiology* 4560 (2005), p. 482– 488

[11] BICKEL, C S. ; BICKEL, C S. ; SLADE, Jill ; SLADE, Jill ; MAHONEY, Ed ; MAHONEY, Ed ; HADDAD, Fadia ; HADDAD, Fadia ; DUDLEY, Gary a. ; DUDLEY, Gary a. ; ADAMS, Gregory R. ; ADAMS, Gregory R. ; SCOTT, C ; SCOTT, C: Time course of molecular responses of human skeletal muscle to acute bouts of resistance exercise. En: *Journal of Applied Physiology* 4560 (2005), p. 482– 488

[12] BIJALWAN, Ashutosh ; PATEL, BP ; MARIESWARAN, M ; KALYANASUNDARAM, Dinesh: Volumetric locking free 3D finite element for modelling of anisotropic visco-hyperelastic behaviour of anterior cruciate ligament. En: *Journal of biomechanics* 73 (2018), p. 1–8

[13] BILLETER, Rudolf ; HEIZMANN, Claus W. ; HOWALD, Hans ; JENNY, Eduard: Analysis of myosin light and heavy chain types in single human skeletal muscle fibers. En: *European Journal of Biochemistry* 116 (1981), Nr. 2, p. 389–395

[14] BLEILER, Christian ; CASTAÑEDA, Pedro P. ; ROEHRLE, Oliver: A microstructurally-based, multi-scale, continuum-mechanical model for the passive behaviour of skeletal muscle tissue. En: *Journal of the mechanical behavior of biomedical materials* 97 (2019), p. 171–186

[15] BONALDO, Paolo ; SANDRI, Marco: Cellular and molecular mechanisms of muscle atrophy. En: *Disease models & mechanisms* 6 (2013), Nr. 1, p. 25–39. – ISBN 1754–8411

[16] BONET, Javier ; WOOD, Richard D.: *Nonlinear continuum mechanics for finite element analysis.* Cambridge university press, 1997

[17] BOOTH, Frank W. ; BALDWIN, Kenneth M.: Muscle plasticity: energy demand and supply processes. En: *Comprehensive Physiology* (2010), p. 1075–1123

[18] BROCCA, Lorenza ; CANNAVINO, Jessica ; COLETTO, Luisa ; BIOLO, Gianni ; SANDRI, Marco ; BOTTINELLI, Roberto ; PELLEGRINO, Maria A.: The time course of the adaptations of human muscle proteome to bed rest and the underlying mechanisms. En: *The Journal of physiology* 590 (2012), Nr. 20, p. 5211–5230

[19] BROOKE, Michael H. ; KAISER, Kenneth K.: Muscle fiber types: how many and what kind? En: *Archives of neurology* 23 (1970), Nr. 4, p. 369–379

[20] BROOKE, MICHAEL H. ; KAISER, KENNETH K.: Three" myosin adenosine triphosphatase" systems: the nature of their pH lability and sulfhydryl dependence. En: *Journal of Histochemistry & Cytochemistry* 18 (1970), Nr. 9, p. 670–672

[21] BROWN, WE ; SALMONS, S ; WHALEN, RG: The sequential replacement of myosin subunit isoforms during muscle type transformation induced by long term electrical stimulation. En: *Journal of Biological Chemistry* 258 (1983), Nr. 23, p. 14686–14692

[22] BROWN, Wendy E. ; SALMONS, Stanley ; WHALEN, Robert G.: Mechanisms underlying the asynchronous replacement of myosin light chain isoforms during stimulation-induced fibre-type transformation of skeletal muscle. En: *FEBS letters* 192 (1985), Nr. 2, p. 235–238

[23] BURKE, RE ; TSAIRIS, P: Anatomy and innervation ratios in motor units of cat gastrocnemius. En: *The Journal of physiology* 234 (1973), Nr. 3, p. 749–765

[24] CALVO, B ; RAMÍREZ, A ; ALONSO, A ; GRASA, J ; SOTERAS, F ; OSTA, R ; MUÑOZ, M J.: Passive nonlinear elastic behaviour of skeletal muscle: Experimental results and model formulation. En: *Journal of Biomechanics* 43 (2010), Nr. 2, p. 318–325. – ISSN 0021–9290

[25] CAMERA, Donny M. ; EDGE, Johann ; SHORT, Michael J. ; HAWLEY, John A. ; COFFEY, Vernon G.: Early time course of Akt phosphorylation after endurance and resistance exercise. En: *Medicine and science in sports and exercise* 42 (2010), Nr. 10, p. 1843–1852

[26] CAMERA, Donny M. ; ONG, Jun N. ; COFFEY, Vernon G. ; HAWLEY, John A.: Selective modulation of microRNA expression with protein ingestion following concurrent resistance and endurance exercise in human skeletal muscle. En: *Frontiers in physiology* 7 (2016), p. 87

[27] CAMPOS, Gerson E. ; LUECKE, Thomas J. ; WENDELN, Heather K. ; TOMA, Kumika ; HAGERMAN, Fredrick C. ; MURRAY, Thomas F. ; RAGG, Kerry E. ; RATAMESS, Nicholas A. ; KRAEMER, William J. ; STARON, Robert S.: Muscular adaptations in response to three different resistance-training regimens: specificity of repetition maximum training zones. En: *European journal of applied physiology* 88 (2002), Nr. 1, p. 50–60

[28] CASTRO, MJ J. ; APPLE, D F. ; HILLEGASS, E A. ; DUDLEY, G A. ; JR, DF A.: Influence of complete spinal cord injury on skeletal muscle cross-sectional area within the first 6 months of injury. En: *European Journal Of Applied Physiology And Occupational Physiology* 80 (1999), p. 373–378

[29] CATALANOTTO, Caterina ; COGONI, Carlo ; ZARDO, Giuseppe: MicroRNA in control of gene expression: an overview of nuclear functions. En: *International journal of molecular sciences* 17 (2016), Nr. 10, p. 1712

[30] CHEN, JS ; SATYAMURTHY, K ; HIRSCHFELT, LR: Consistent finite element proce-
       dures for nonlinear rubber elasticity with a higher order strain energy function. En:
       Computers & structures 50 (1994), Nr. 6, p. 715–727

[31] CHIN, David ; MEANS, Anthony R.: Calmodulin: a prototypical calcium sensor. En:
       Trends in cell biology 10 (2000), Nr. 8, p. 322–328

[32] CHIN, Eva R.: Intracellular Ca2+ signaling in skeletal muscle: decoding a complex
       message. En: *Exercise and sport sciences reviews* 38 (2010), Nr. 2, p. 76–85

[33] CHIN, Eva R. ; OLSON, Eric N. ; RICHARDSON, James A. ; YANG, Quan ; HUMPHRIES,
       Caroline ; SHELTON, John M. ; WU, Hai ; ZHU, Weiguang ; BASSEL-DUBY, Rhonda
       ; WILLIAMS, R S.: A calcineurin-dependent transcriptional pathway controls skeletal
       muscle fiber type. En: *Genes & development* 12 (1998), Nr. 16, p. 2499–2509

[34] CIENIEWSKI-BERNARD, Caroline ; BASTIDE, Bruno ; MYSOET, Julien ; DUPONT,
       Erwan: Hypoactivity Affects IGF-1 Level and PI3K / AKT Signaling Pathway in
       Cerebral Structures Implied in Motor Control. En: *PLoS ONE* 9 (2014), Nr. 9

[35] CLOSE, R: Properties of motor units in fast and slow skeletal muscles of the rat. En:
       The Journal of physiology 193 (1967), Nr. 1, p. 45–55

[36] COFFEY, Vernon G. ; HAWLEY, John a.: The Molecular Basis of Training Adaptation.
       En: *Sports Medicine* 37 (2007), Nr. 9, p. 737–763

[37] COFFEY, Vernon G. ; HAWLEY, John a.: The Molecular Basis of Training Adaptation.
       En: *Sports Medicine* 37 (2007), Nr. 9, p. 737–763. – ISSN 0112–1642

[38] COFFEY, Vernon G. ; ZHONG, Zhihui ; SHIELD, Anthony ; CANNY, Benedict J. ;
       CHIBALIN, Alexander V. ; ZIERATH, Juleen R. ; HAWLEY, John a.: Early signaling
       responses to divergent exercise stimuli in skeletal muscle from well-trained humans.
       En: *FASEB journal : official publication of the Federation of American Societies for
       Experimental Biology* 20 (2006), Nr. 1, p. 190–192. – ISBN 1530–6860 (Electronic)

[39] COUNTS, Brittany R. ; BUCKNER, Samuel L. ; MOUSER, J G. ; DANKEL, Scott J. ;
       JESSEE, Matthew B. ; MATTOCKS, Kevin T. ; LOENNEKE, Jeremy P.: Muscle growth:
       To infinity and beyond? En: *Muscle & Nerve* 56 (2017), Nr. 6, p. 1022–1030

[40] CRAIG, R ; PADRÓN, Raúl: Molecular structure of the sarcomere. En: *Myology* 3
       (2004), p. 129–144

[41] CRAIG, Roger ; WOODHEAD, John L.: Structure and function of myosin filaments.
       En: *Current opinion in structural biology* 16 (2006), Nr. 2, p. 204–212

[42] CROMIE, Melinda J. ; SANCHEZ, Gabriel N. ; SCHNITZER, Mark J. ; DELP, Scott L.: Sarcomere lengths in human extensor carpi radialis brevis measured by microendoscopy. En: *Muscle & Nerve* 48 (2013), Nr. 2, p. 286–292

[43] DALLA LIBERA, Luciano ; SARTORE, Saverio ; PIEROBON-BORMIOLI, Sandra ; SCHIAFFINO, Stefano: Fast-white and fast-red isomyosins in guinea pig muscles. En: *Biochemical and biophysical research communications* 96 (1980), Nr. 4, p. 1662–1670

[44] DAMAS, Felipe ; PHILLIPS, Stuart M. ; LIXANDRÃO, Manoel E. ; VECHIN, Felipe C. ; LIBARDI, Cleiton A. ; ROSCHEL, Hamilton ; TRICOLI, Valmor ; UGRINOWITSCH, Carlos: Early resistance training-induced increases in muscle cross-sectional area are concomitant with edema-induced muscle swelling. En: *European journal of applied physiology* 116 (2016), Nr. 1, p. 49–56

[45] D'ANTONA, Giuseppe ; PELLEGRINO, Maria A. ; ADAMI, Raffaella ; ROSSI, Rosetta ; CARLIZZI, Carmine N. ; CANEPARI, Monica ; SALTIN, Bengt ; BOTTINELLI, Roberto: The effect of ageing and immobilization on structure and function of human skeletal muscle fibres. En: *The Journal of physiology* 552 (2003), Nr. 2, p. 499–511

[46] DASH, Ranjan K. ; DIBELLA, John A. ; CABRERA, Marco E.: A computational model of skeletal muscle metabolism linking cellular adaptations induced by altered loading states to metabolic responses during exercise. En: *Biomedical engineering online* 6 (2007), p. 14

[47] DAVIDSEN, Peter K. ; GALLAGHER, Iain J. ; HARTMAN, Joseph W. ; TARNOPOLSKY, Mark A. ; DELA, Flemming ; HELGE, Jørn W ; TIMMONS, James A. ; PHILLIPS, Stuart M.: High responders to resistance exercise training demonstrate differential regulation of skeletal muscle microRNA expression. En: *Journal of applied physiology* (2011)

[48] DE BOER, Maarten D. ; SELBY, Anna ; ATHERTON, Philip ; SMITH, Ken ; SEYNNES, Olivier R. ; MAGANARIS, Constantinos N. ; MAFFULLI, Nicola ; MOVIN, Tomas ; NARICI, Marco V. ; RENNIE, Michael J.: The temporal responses of protein synthesis, gene expression and cell signalling in human quadriceps muscle and patellar tendon to disuse. En: *The Journal of physiology* 585 (2007), Nr. 1, p. 241–251

[49] DE DEYNE, Patrick G.: Application of passive stretch and its implications for muscle fibers. En: *Physical therapy* 81 (2001), Nr. 2, p. 819–827

[50] DEFREITAS, Jason M. ; BECK, Travis W. ; STOCK, Matt S. ; DILLON, Michael A. ; KASISHKE, Paul R.: An examination of the time course of training-induced skeletal muscle hypertrophy. En: *European Journal of Applied Physiology* 111 (2011), Nr. 11, p. 2785–2790. – ISBN 1439–6319

[51] DREYER, H C. ; FUJITA, S ; CADENAS, J G. ; CHINKES, D L. ; VOLPI, E ; RAS-
      MUSSEN, B B.: Resistance exercise increases AMPK activity and reduces 4E-BP1
      phosphorylation and protein synthesis in human skeletal muscle. En: *J Physiol* 576
      (2006), Nr. Pt 2, p. 613–624

[52] EGERMAN, Marc a. ; GLASS, David J.: Signaling pathways controlling skeletal muscle
      mass. En: *Critical reviews in biochemistry and molecular biology* 49 (2014), Nr. 1, p.
      59–68

[53] EHLER, Elisabeth ; GAUTEL, Mathias: The sarcomere and sarcomerogenesis. En: *The
      Sarcomere and Skeletal Muscle Disease.* Springer, 2008, p. 1–14

[54] EISENBERG, Brenda R. ; SALMONS, Stanley: The reorganization of subcellular struc-
      ture in muscle undergoing fast-to-slow type transformation. En: *Cell and tissue re-
      search* 220 (1981), Nr. 3, p. 449–471

[55] ESKANDARI, Mona ; KUHL, Ellen: Systems biology and mechanics of growth. En:
      Wiley Interdisciplinary Reviews: Systems Biology and Medicine 7 (2015), Nr. 6, p.
      401–412

[56] FLITNEY, FW ; HIRST, DG: Cross-bridge detachment and sarcomere 'give' during
      stretch of active frog's muscle. En: *The Journal of Physiology* 276 (1978), Nr. 1, p.
      449–465

[57] GAUTEL, Mathias: The Sarcomere and Skeletal Muscle Disease. En: *The Sarcomere
      and the Nucleus: Functional Links to Hypertrophy, Atrophy and Sarcopenia.* New York
      : Springer New York, 2008, Kapitel 13, p. 176–191

[58] GAUTEL, Mathias: *Biomechanics and motor control of human movement.* 4. Springer
      Science and Business Media, 2009

[59] GERSHMAN, Lewis C. ; STRACHER, A ; DREIZEN, P: Subunit structure of myosin III.
      A proposed model for rabbit skeletal myosin. En: *Journal of Biological Chemistry* 244
      (1969), Nr. 10, p. 2726–2736

[60] GÖKTEPE, Serdar ; ABILEZ, Oscar J. ; KUHL, Ellen: A generic approach towards finite
      growth with examples of athlete's heart, cardiac dilation, and cardiac wall thickening.
      En: *Journal of the Mechanics and Physics of Solids* 58 (2010), Nr. 10, p. 1661–1680.
      – ISBN 0022–5096

[61] GÖKTEPE, Serdar ; ABILEZ, Oscar J. ; KUHL, Ellen: A generic approach towards finite
      growth with examples of athlete's heart, cardiac dilation, and cardiac wall thickening.
      En: *Journal of the Mechanics and Physics of Solids* 58 (2010), Nr. 10, p. 1661–1680

[62] GÖKTEPE, Serdar ; ABILEZ, Oscar J. ; PARKER, Kevin K. ; KUHL, Ellen: A multi-scale model for eccentric and concentric cardiac growth through sarcomerogenesis. En: *Journal of theoretical biology* 265 (2010), Nr. 3, p. 433–442

[63] GOLDSPINK, Geoffrey: Changes in muscle mass and phenotype and the expression of autocrine and systemic growth factors by muscle in response to stretch and overload. En: *The Journal of Anatomy* 194 (1999), Nr. 3, p. 323–334

[64] GORDON, AM ; HUXLEY, Andrew F. ; JULIAN, FJ: The variation in isometric tension with sarcomere length in vertebrate muscle fibres. En: *The Journal of physiology* 184 (1966), Nr. 1, p. 170–192

[65] GOROSTIAGA, EM ; NAVARRO-AMÉZQUETA, I ; CALBET, JAL ; SÁNCHEZ- MEDINA, L ; CUSSO, R ; GUERRERO, M ; GRANADOS, C ; GONZÁLEZ-IZAL, M ; IBÁÑEZ, J ; IZQUIERDO, M: Blood ammonia and lactate as markers of muscle metabolites during leg press exercise. En: *Journal of strength and conditioning research* 28 (2014), Nr. 10, p. 2775–2785

[66] GOSS, Richard J.: Muscle: Atrophy versus Hypertrophy. En: *The Physiology of Growth*. Academic Press, 1978. – ISBN 978–0–12–293055–3, p. 153 – 182

[67] GRASA, J ; HERNÁNDEZ-GASCÓN, B ; RAMÍREZ, A ; RODRÍGUEZ, J F. ; CALVO, B: Modelado numérico del comportamiento del tejido músculo-esquelético. En: *Revista Internacional de Métodos Numéricos para Cálculo y Diseño en Ingeniería* 28 (2012), Nr. 3, p. 177–186. – ISSN 0213–1315

[68] GREASER, MlARION L. ; MOSS, RICHARD L. ; REISER, PETER J.: Variations in contractile properties of rabbit single muscle fibres in relation to troponin T isoforms and myosin light chains. En: *The Journal of Physiology* 406 (1988), Nr. 1, p. 85–98

[69] HANSON, Jean ; HUXLEY, Hugh E.: Structural basis of the cross-striations in muscle. En: *Nature* 172 (1953), Nr. 4377, p. 530

[70] HAY, Nissim ; SONENBERG, Nahum: Upstream and downstream of mTOR. En: *Genes and Development* 18 (2004), Nr. 16, p. 1926–1945

[71] HEIDLAUF, Thomas ; KLOTZ, Thomas ; RODE, Christian ; SIEBERT, Tobias ; RÖHRLE, Oliver: A continuum-mechanical skeletal muscle model including actin-titin interaction predicts stable contractions on the descending limb of the force-length relation. En: *PLoS computational biology* 13 (2017), Nr. 10, p. e1005773

[72] HEMENWAY, Charles S. ; HEITMAN, Joseph: Calcineurin. En: *Cell biochemistry and biophysics* 30 (1999), Nr. 1, p. 115–151

[73] Hennebry, Alexander ; Oldham, Jenny ; Shavlakadze, Tea ; Grounds, Miranda D. ; Sheard, Philip ; Fiorotto, Marta L. ; Falconer, Shelley ; Smith, Heather K. ; Berry, Carole ; Jeanplong, Ferenc [u. a.]: IGF1 stimulates greater muscle hypertrophy in the absence of myostatin in male mice. En: *Journal of Endocrinology* 234 (2017), Nr. 2, p. 187–200

[74] Hernández-Gascón, B ; Grasa, J ; Calvo, B ; Rodríguez, JF: A 3D electro-mechanical continuum model for simulating skeletal muscle contraction. En: *Journal of theoretical biology* 335 (2013), p. 108–118

[75] Hikida, Robert S. ; Gollnick, Philip D. ; Dudley, Gary A. ; Convertino, Victor A. ; Buchanan, Paul: Structural and metabolic characteristics of human skeletal muscle following 30 days of simulated microgravity. En: *Aviation, Space, and Environmental Medicine* 60 (1989), Nr. 7, p. 664–670

[76] Holzapfel, Gerhard A.: *Nonlinear solid mechanics: a continuum approach for engineering.* Wiley, 2000

[77] Hoppeler, H: The range of mitochondrial adaptation in muscle fibers. En: *The dynamic state of muscle fibers* (1990), p. 567–586

[78] Hoppeler, H ; Hudlicka, O ; Uhlmann, E: Relationship between mitochondria and oxygen consumption in isolated cat muscles. En: *The Journal of Physiology* 385 (1987), Nr. 1, p. 661–675

[79] Hornberger, T. A.: Intracellular Signaling Specificity in Response to Uniaxial vs. Multiaxial Stretch: Implications for Mechanotransduction. En: *AJP: Cell Physiology* 0298 (2004), p. 185–194. – ISSN 0363–6143

[80] Huijing, Peter A.: Muscle as a collagen fiber reinforced composite: a review of force transmission in muscle and whole limb. En: *Journal of biomechanics* 32 (1999), Nr. 4, p. 329–345

[81] Huxley, AF: Cross-bridge action: present views, prospects, and unknowns. En: *Journal of biomechanics* 33 (2000), Nr. 10, p. 1189–1195

[82] Huxley, HE ; Hanson, Jean: The structural basis of the contraction mechanism in striated muscle. En: *Annals of the New York Academy of Sciences* 81 (1959), Nr. 2, p. 403–408

[83] Jones, Simon W. ; Hill, Roger J. ; Krasney, Philip A. ; O'Conner, Barbara ; Peirce, Nicholas ; Greenhaff, Paul L.: Disuse atrophy and exercise rehabilitation in humans profoundly affects the expression of genes associated with the regulation of skeletal muscle mass. En: *The FASEB journal* 18 (2004), Nr. 9, p. 1025–1027

[84]   KAWAKAMI, Yasuo ; ABE, Takashi ; KUNO, Shin-Ya ; FUKUNAGA, Tetsuo: Training-induced changes in muscle architecture and specific tension. En: *European journal of applied physiology and occupational physiology* 72 (1995), Nr. 1-2, p. 37–43

[85]   KENT-BRAUN, Jane A. ; NG, Alexander V.: Specific strength and voluntary muscle activation in young and elderly women and men. En: *Journal of applied physiology* 87 (1999), Nr. 1, p. 22–29

[86]   KJAER, Michael: Role of extracellular matrix in adaptation of tendon and skeletal muscle to mechanical loading. En: *Physiological reviews* 84 (2004), Nr. 2, p. 649–698

[87]   KLEE, CB ; CROUCH, TH ; RICHMAN, PG: Calmodulin. En: *Annual review of biochemistry* 49 (1980), Nr. 1, p. 489–515

[88]   KORTHUIS, Ronald J.: Skeletal muscle circulation. En: *Colloquium Series on Integrated Systems Physiology: From Molecule to Function* Vol. 3,4 Morgan & Claypool Life Sciences, 2011, p. 1–144

[89]   KRAUS, William E. ; TORGAN, Carol E. ; TAYLOR, Doris A.: Skeletal muscle adaptation to chronic low-frequency motor nerve stimulation. En: *Exercise and sport sciences reviews* 22 (1994), Nr. 1, p. 313–360

[90]   KUMAR, A.: Distinct Signaling Pathways Are Activated in Response to Mechanical Stress Applied Axially and Transversely to Skeletal Muscle Fibers. En: *Journal of Biological Chemistry* 277 (2002), Nr. 48, p. 46493–46503. – ISSN 00219258

[91]   LEE, E H.: Elastic-Plastic Deformation at Finite Strains. En: *Journal of Applied Mechanics* 36 (1969), Nr. 1, p. 1. – ISBN 0021–8936

[92]   LÉGER, Bertrand ; CARTONI, Romain ; PRAZ, Manu ; LAMON, Séverine ; DÉRIAZ, Olivier ; CRETTENAND, Antoinette ; GOBELET, Charles ; ROHMER, Paul ; KONZELMANN, Michel ; LUTHI, François ; RUSSELL, Aaron P.: Akt signalling through GSK-3beta, mTOR and Foxo1 is involved in human skeletal muscle hypertrophy and atrophy. En: *The Journal of physiology* 576 (2006), Nr. Pt 3, p. 923–33

[93]   LI, Yanjun ; LAI, Nicola ; KIRWAN, John P. ; SAIDEL, Gerald M.: Computational model of cellular metabolic dynamics in skeletal muscle fibers during moderate intensity exercise. En: *Cellular and molecular bioengineering* 5 (2012), Nr. 1, p. 92–112

[94]   LIEBER, Richard L.: *Skeletal muscle structure, function, and plasticity.* 2. Lippincott Williams & Wilkins, 2002

[95]   LIEBER, Richard L. ; FRIDÉN, Jan: Functional and clinical significance of skeletal muscle architecture. En: *Muscle & Nerve: Official Journal of the American Association of Electrodiagnostic Medicine* 23 (2000), Nr. 11, p. 1647–1666

[96] LIU, Y ; SCHLUMBERGER, A ; WIRTH, K ; SCHMIDTBLEICHER, D ; STEINACKER, Jürgen M: Different effects on human skeletal myosin heavy chain isoform expression: strength vs. combination training. En: *Journal of Applied Physiology* 94 (2003), Nr. 6, p. 2282–2288

[97] LIU, Yewei ; CSERESNYÉS, Zoltán ; RANDALL, William R. ; SCHNEIDER, Martin F.: Activity-dependent nuclear translocation and intranuclear distribution of NFATc in adult skeletal muscle fibers. En: *The Journal of cell biology* 155 (2001), Nr. 1, p. 27–40

[98] LOPEZ-GUAJARDO, Ana ; SUTHERLAND, Hazel ; JARVIS, Jonathan C. ; SALMONS, Stanley: Dynamics of stimulation-induced muscle adaptation: insights from varying the duty cycle. En: *Journal of Muscle Research & Cell Motility* 21 (2000), Nr. 8, p. 725–735

[99] LOPEZ-GUAJARDO, Ana ; SUTHERLAND, Hazel ; JARVIS, Jonathan C. ; SALMONS, Stanley: Induction of a fatigue-resistant phenotype in rabbit fast muscle by small daily amounts of stimulation. En: *Journal of Applied Physiology* 90 (2001), Nr. 5, p. 1909–1918

[100] LOUIS, Emily ; RAUE, Ulrika ; YANG, Yifan ; JEMIOLO, Bozena ; TRAPPE, Scott: Time course of proteolytic , cytokine , and myostatin gene expression after acute exercise in human skeletal muscle. En: *Journal of applied physiology (Bethesda, Md. : 1985)* 47306 (2007), p. 1744–1751

[101] LOWEY, Susan ; SLAYTER, Henry S. ; WEEDS, Alan G. ; BAKER, Harry: Substructure of the myosin molecule: I. Subfragments of myosin by enzymic degradation. En: *Journal of molecular biology* 42 (1969), Nr. 1, p. 1–29

[102] MAMMUCARI, Cristina ; MILAN, Giulia ; ROMANELLO, Vanina ; MASIERO, Eva ; RUDOLF, Ruediger ; DEL PICCOLO, Paola ; BURDEN, Steven J. ; DI LISI, Raffaella ; SANDRI, Claudia ; ZHAO, Jinghui [u. a.]: FoxO3 controls autophagy in skeletal muscle in vivo. En: *Cell metabolism* 6 (2007), Nr. 6, p. 458–471

[103] MARTINS, J. A. C. ; PIRES, E. B. ; SALVADO, R. ; DINIS, P. B.: A numerical model of passive and active behavior of skeletal muscles. En: *Computer Methods in Applied Mechanics and Engineering* 151 (1998), Nr. 97, p. 419–433. – ISBN 0045–7825

[104] MATTHEWS, Bryan H.: The response of a muscle spindle during active contraction of a muscle. En: *The Journal of physiology* 72 (1931), Nr. 2, p. 153–174

[105] MAUREL, Walter ; THALMANN, D ; WU, Yin ; THALMANN, NM ; MAGNEAT THALMAN, N. ; THALMAN, D.: *Biomechanical Models for Soft Tissue Simulation.* 1. 1998. – 174 p.. – ISBN 3540637427

[106] McCarthy, John J. ; Esser, Karyn A.: MicroRNA-1 and microRNA-133a expression are decreased during skeletal muscle hypertrophy. En: *Journal of applied physiology* 102 (2007), Nr. 1, p. 306–313

[107] McDonagh, Jennifer C. ; Binder, Marc D. ; Reinking, Robert M. ; Stuart, Douglas G.: A commentary on muscle unit properties in cat hindlimb muscles. En: *Journal of morphology* 166 (1980), Nr. 2, p. 217–230

[108] McMahon, Elaine M. ; Corcoran, Paul ; Regan, Grace O. ; Keeley, Helen ; Cannon, Mary ; Carli, Vladimir ; Wasserman, Camilla ; Hadlaczky, Gergö: Physical activity in European adolescents and associations with anxiety , depression and well - being. En: *European Child & Adolescent Psychiatry* 26 (2017). – ISSN 1435–165X

[109] Means, Anthony R. ; Dedman, John R.: Calmodulin—an intracellular calcium receptor. En: *Nature* 285 (1980), Nr. 5760, p. 73–77

[110] Melzer, W ; Rios, E ; Schneider, MF: Time course of calcium release and removal in skeletal muscle fibers. En: *Biophysical journal* 45 (1984), Nr. 3, p. 637–641

[111] Miller, Mark S. ; Bedrin, Nicholas G. ; Ades, Philip A. ; Palmer, Bradley M. ; Toth, Michael J.: Molecular determinants of force production in human skeletal muscle fibers: effects of myosin isoform expression and cross-sectional area. En: *American Journal of Physiology-Cell Physiology* 308 (2015), Nr. 6, p. C473–C484

[112] Miokovic, Tanja ; Armbrecht, Gabriele ; Felsenberg, Dieter ; Belavỳ, Daniel L.: Heterogeneous atrophy occurs within individual lower limb muscles during 60 days of bed rest. En: *Journal of applied physiology* 113 (2012), Nr. 10, p. 1545–1559

[113] Molkentin, Jeffery D. ; Lu, Jian-Rong ; Antos, Christopher L. ; Markham, Bruce ; Richardson, James ; Robbins, Jeffrey ; Grant, Stephen R. ; Olson, Eric N.: A calcineurin-dependent transcriptional pathway for cardiac hypertrophy. En: *Cell* 93 (1998), Nr. 2, p. 215–228

[114] Morrow, Duane A. ; Donahue, Tammy L H. ; Odegard, Gregory M. ; Kaufman, Kenton R.: Transversely isotropic tensile material properties of skeletal muscle tissue. En: *Journal of the mechanical behavior of biomedical materials* 3 (2010), Nr. 1, p. 124–129

[115] Mounier, Y ; Holy, X ; Stevens, L: Compared properties of the contractile system of skinned slow and fast rat muscle fibres. En: *Pflügers Archiv* 415 (1989), Nr. 2, p. 136–141

[116] NIELSEN, Søren ; SCHEELE, Camilla ; YFANTI, Christina ; ÅKERSTRÖM, Thorbjörn ; NIELSEN, Anders R. ; PEDERSEN, Bente K. ; LAYE, Matthew: Muscle specific microRNAs are regulated by endurance exercise in human skeletal muscle. En: *The Journal of physiology* 588 (2010), Nr. 20, p. 4029–4037

[117] NORTHROP, Jeffrey P. ; HO, Steffan N. ; CHEN, Lei ; THOMAS, Daryl J. ; TIMMER-MAN, Luika A. ; NOLAN, Garry P. ; ADMON, Arie ; CRABTREE, Gerald R.: NF-AT components define a family of transcription factors targeted in T-cell activation. En: *Nature* 369 (1994), Nr. 6480, p. 497–502

[118] OGASAWARA, Riki ; AKIMOTO, Takayuki ; UMENO, Tokushi ; SAWADA, Shuji ; HAMAOKA, Takafumi ; FUJITA, Satoshi: MicroRNA expression profiling in skeletal muscle reveals different regulatory patterns in high and low responders to resistance training. En: *Physiological genomics* 48 (2016), Nr. 4, p. 320–324

[119] PADDON-JONES, Douglas ; LEVERITT, Michael ; LONERGAN, Andrew ; ABERNETHY, Peter: Adaptation to chronic eccentric exercise in humans: the influence of contraction velocity. En: *European journal of applied physiology* 85 (2001), Nr. 5, p. 466–471

[120] PADYKULA, HELEN A. ; GAUTHIER, GF: Morphological and cytochemical characteristics of fiber types in normal mammalian skeletal muscle. En: *Exploratory Concepts in Muscular Dystrophy and Related Disorders* Vol. 147. Excerpta Medica Foundation Amsterdam, 1967, p. 117–128

[121] PANDIYAN, Balamurugan ; MERRILL, Stephen J. ; DI BARI, Flavia ; ANTONELLI, Alessandro ; BENVENGA, Salvatore: A patient-specific treatment model for Graves' hyperthyroidism. En: *Theoretical Biology and Medical Modelling* 15 (2018), Nr. 1, p. 1

[122] PERNELLE, Jean-Jacques ; CHAFEY, Philippe ; LOGNONNE, Jean-Luc ; RIGHETTI, Pier G. ; BOSISIO, Adriana B. ; WAHRMANN, Juan P.: High-resolution two-dimensional electrophoresis of myofibrillar proteins with immobilized pH gradients. En: *Electrophoresis* 7 (1986), Nr. 4, p. 159–165

[123] PETER, James B. ; BARNARD, R J. ; EDGERTON, V R. ; GILLESPIE, Cynthia A. ; STEMPEL, Kerstin E.: Metabolic profiles of three fiber types of skeletal muscle in guinea pigs and rabbits. En: *Biochemistry* 11 (1972), Nr. 14, p. 2627–2633

[124] PETTE, D ; STARON, RS: Molecular basis of the phenotypic characteristics of mammalian muscle fibres. En: *Ciba Foundation Symposium* Vol. 138, 1988, p. 22–34

[125] PETTE, Dirk ; SCHNEZ, Ursula: Myosin light chain patterns of individual fast and slow-twitch fibres of rabbit muscles. En: *Histochemistry* 54 (1977), Nr. 2, p. 97–107

[126] PETTE, Dirk ; STARON, Robert S.: Cellular and molecular diversities of mammalian skeletal muscle fibers. En: *Reviews of Physiology, Biochemistry and Pharmacology, Volume 116.* Springer, 1990, p. 1–76

[127] PETTE, Dirk ; STARON, Robert S.: Mammalian skeletal muscle fiber type transitions. En: *International review of cytology* 170 (1997), p. 143–223

[128] PETTE, Dirk ; STARON, Robert S.: Myosin isoforms, muscle fiber types, and transitions. En: *Microscopy research and technique* 50 (2000), Nr. 6, p. 500–509

[129] POLLACK, GERALD H.: The cross-bridge theory. En: *Physiological reviews* 63 (1983), Nr. 3, p. 1049–1113

[130] POWERS, Scott K. ; KAVAZIS, Andreas N. ; DERUISSEAU, Keith C.: Mechanisms of disuse muscle atrophy: role of oxidative stress. En: *American journal of physiology. Regulatory, integrative and comparative physiology* 288 (2005), Nr. 2, p. R337–R344. – ISBN 0363–6119

[131] PSATHA, Maria ; WU, Zhiqing ; GAMMIE, Fiona M. ; RATKEVICIUS, Aivaras ; WACKERHAGE, Henning ; LEE, Jennifer H. ; REDPATH, Thomas W. ; GILBERT, Fiona J. ; ASHCROFT, George P. ; MEAKIN, Judith R. [u. a.]: A longitudinal MRI study of muscle atrophy during lower leg immobilization following ankle fracture. En: *Journal of Magnetic Resonance Imaging* 35 (2012), Nr. 3, p. 686–695

[132] RAMÍREZ, A ; GRASA, J ; ALONSO, A ; SOTERAS, F ; OSTA, R ; MUÑOZ, MJ ; CALVO, B: Active response of skeletal muscle: in vivo experimental results and model formulation. En: *Journal of theoretical biology* 267 (2010), Nr. 4, p. 546–553

[133] RANDALL, David ; BURGGREN, Warren ; FRENCH, Kathleen ; ECKERT, Roger [u. a.]: *Eckert animal physiology.* Macmillan, 2002

[134] RAO, Anjana ; LUO, Chun ; HOGAN, Patrick G.: Transcription factors of the NFAT family: regulation and function. En: *Annual review of immunology* 15 (1997), Nr. 1, p. 707–747

[135] REED, Sarah A. ; SANDESARA, Pooja B. ; SENF, Sarah M. ; JUDGE, Andrew R.: Inhibition of FoxO transcriptional activity prevents muscle fiber atrophy during cachexia and induces hypertrophy. En: *The FASEB journal* 26 (2012), Nr. 3, p. 987–1000

[136] RODRIGUEZ, E K. ; HOGER, A ; MCCULLOCH, A D.: Stress-dependent finite growth in soft elastic tissues. En: *Journal of biomechanics* 27 (1994), Nr. 4, p. 455–67

[137] RODRIGUEZ, J. ; VERNUS, B. ; CHELH, I. ; CASSAR-MALEK, I. ; GABILLARD, J. C. ; HADJ SASSI, A. ; SEILIEZ, I. ; PICARD, B. ; BONNIEU, A.: Myostatin and the skeletal

muscle atrophy and hypertrophy signaling pathways. En: *Cellular and Molecular Life Sciences* 71 (2014), Nr. 22, p. 4361–4371

[138] RUI, Yanning ; BAI, Jianwu ; PERRIMON, Norbert: Sarcomere formation occurs by the assembly of multiple latent protein complexes. En: *PLoS Genetics* 6 (2010), Nr. 11

[139] RUSNAK, Frank ; MERTZ, Pamela: Calcineurin: form and function. En: *Physiological reviews* 80 (2000), Nr. 4, p. 1483–1521

[140] SAKUMA, Kunihiro ; YAMAGUCHI, Akihiko: Molecular mechanisms controlling skeletal muscle mass. En: *Muscle cell tissue* 484 (2015)

[141] SANDRI, Marco: Signaling in muscle atrophy and hypertrophy. En: *Physiology (Bethesda, Md.)* 23 (2008), Nr. 3, p. 160–70

[142] SANDRI, Marco ; SANDRI, Claudia ; GILBERT, Alex ; SKURK, Carsten ; CALABRIA, Elisa ; PICARD, Anne ; WALSH, Kenneth ; SCHIAFFINO, Stefano ; LECKER, Stewart H. ; GOLDBERG, Alfred L.: Foxo transcription factors induce the atrophy-related ubiquitin ligase atrogin-1 and cause skeletal muscle atrophy. En: *Cell* 117 (2004), Nr. 3, p. 399–412

[143] SCHIAFFINO, Stefano ; MAMMUCARI, Cristina: Regulation of skeletal muscle growth by the IGF1-Akt/PKB pathway: insights from genetic models. En: *Skeletal muscle* 1 (2011), Nr. 1, p. 4

[144] SCHIAFFINO, Stefano ; SANDRI, Marco ; MURGIA, Marta: Activity-dependent signaling pathways controlling muscle diversity and plasticity. En: *Physiology* 22 (2007), Nr. 4, p. 269–278

[145] SCHIAFFINO, Stefano ; SERRANO, AntonioL: Calcineurin signaling and neural control of skeletal muscle fiber type and size. En: *Trends in pharmacological sciences* 23 (2002), Nr. 12, p. 569–575

[146] SCHMID, H ; PAULI, L ; PAULUS, A ; KUHL, Ellen ; ITSKOV, M: Consistent formulation of the growth process at the kinematic and constitutive level for soft tissues composed of multiple constituents. En: *Computer methods in biomechanics and biomedical engineering* 15 (2012), Nr. 5, p. 547–561

[147] SCOTT, Wayne ; STEVENS, Jennifer ; BINDER-MACLEOD, Stuart A.: Human Skeletal Muscle Fiber Type Classifications. En: *Physical Therapy* 81 (2001), Nr. 11, p. 1810–1816

[148] Seynnes, O R. ; Boer, M D. ; Narici, M V.: Early skeletal muscle hypertrophy and architectural changes in response to high-intensity resistance training. En: *Journal of Applied Physiology* (2007), p. 368–373

[149] Sharma, Mridula ; Juvvuna, Prasanna K. ; Kukreti, Himani ; McFarlane, Craig: Mega roles of microRNAs in regulation of skeletal muscle health and disease. En: *Frontiers in physiology* 5 (2014), p. 239

[150] Shen, Wei H. ; Boyle, David W. ; Wisniowski, Paul ; Bade, Aashia ; Liechty, Edward A.: Insulin and IGF-I stimulate the formation of the eukaryotic initiation factor 4F complex and protein synthesis in C2C12 myotubes independent of availability of external amino acids. En: *Journal of Endocrinology* 185 (2005), Nr. 2, p. 275–289

[151] Solaini, Giancarlo ; Baracca, Alessandra ; Lenaz, Giorgio ; Sgarbi, Gianluca: Hypoxia and mitochondrial oxidative metabolism. En: *Biochimica et biophysica acta* 1797 (2010), Nr. 6-7, p. 1171–7. – ISBN 0005–2728

[152] Song, G ; Ouyang, G ; Bao, S: The activation of Akt/PKB signaling pathway and cell survival. En: *J Cell Mol Med* 9 (2005), Nr. 1, p. 59–71

[153] Sooknanan, J ; Comissiong, D M G.: A mathematical model for the treatment of delinquent behaviour. En: *Socio-Economic Planning Sciences* 63 (2018), p. 1–10. – ISSN 0038–0121

[154] Spamer, Cornelia ; Pette, Dirk: Activity patterns of phosphofructokinase, glyceraldehydephosphate dehydrogenase, lactate dehydrogenase and malate dehydrogenase in microdissected fast and slow fibres from rabbit psoas and soleus muscle. En: *Histochemistry* 52 (1977), Nr. 3, p. 201–206

[155] Staron, Robert S. ; Gohlsch, Bärbel ; Pette, Dirk: Myosin polymorphism in single fibers of chronically stimulated rabbit fast-twitch muscle. En: *Pflügers Archiv* 408 (1987), Nr. 5, p. 444–450

[156] Staron, RS ; Hikida, RS ; Hagerman, FC: Reevaluation of human muscle fasttwitch subtypes: evidence for a continuum. En: *Histochemistry* 78 (1983), Nr. 1, p. 33–39

[157] Staron, RS ; Karapondo, DL ; Kraemer, WJ ; Fry, AC ; Gordon, SE ; Falkel, J E. ; Hagerman, FC ; Hikida, RS: Skeletal muscle adaptations during early phase of heavy-resistance training in men and women. En: *Journal of applied physiology* 76 (1994), Nr. 3, p. 1247–1255

[158] Staron, RS ; Pette, D: Correlation between myofibrillar ATPase activity and myosin heavy chain composition in rabbit muscle fibers. En: *Histochemistry* 86 (1986), Nr. 1, p. 19–23

[159] STEIN, John M. ; PADYKULA, Helen A.: Histochemical classification of individual skeletal muscle fibers of the rat. En: *American Journal of Anatomy* 110 (1962), Nr. 2, p. 103–123

[160] STEMMER, Paul M. ; KLEE, Claude B.: Dual calcium ion regulation of calcineurin by calmodulin and calcineurin B. En: *Biochemistry* 33 (1994), Nr. 22, p. 6859–6866

[161] STEPHENSON, DG ; WILLIAMS, DA: Effects of sarcomere length on the force-pCa relation in fast-and slow-twitch skinned muscle fibres from the rat. En: *The Journal of Physiology* 333 (1982), Nr. 1, p. 637–653

[162] STOCK, Matt S. ; MOTA, Jacob A. ; DEFRANCO, Ryan N. ; GRUE, Katherine A. ; JACOBO, A U. ; CHUNG, Eunhee ; MOON, Jordan R. ; DEFREITAS, Jason M. ; BECK, Travis W.: The time course of short-term hypertrophy in the absence of eccentric muscle damage. En: *European journal of applied physiology* 117 (2017), Nr. 5, p. 989–1004

[163] STÅLHAND, J. ; KLARBRING, A. ; HOLZAPFEL, G A.: Smooth muscle contraction : Mechanochemical formulation for homogeneous finite strains. En: *Progress in Biophysics and Molecular Biology* 96 (2008), p. 465–481

[164] STUEMPFLE, Kristin J. ; DRURY, Daniel G.: The Physiological Consequences of Bed Rest. En: *Health Sciences Faculty Publications Health Sciences Journal of Exercise Physiology* 6 (2007), Nr. 103, p. 32–41. – ISSN 1073–4449

[165] SUETTA, Charlotte ; HVID, Lars G. ; JUSTESEN, Lene ; CHRISTENSEN, Ulrik ; NEERGAARD, Kirsten ; SIMONSEN, Lene ; ORTENBLAD, Niels ; MAGNUSSON, S P. ; KJAER, Michael ; AAGAARD, Per: Effects of aging on human skeletal muscle after immobilization and retraining. En: *Journal of Applied Physiology* 107 (2009), Nr. 4, p. 1172–1180

[166] SUTHERLAND, Hazel ; JARVIS, Jonathan C. ; KWENDE, Martin M. ; GILROY, Stephen J. ; SALMONS, Stanley: The dose-related response of rabbit fast muscle to long-term low-frequency stimulation. En: *Muscle & Nerve: Official Journal of the American Association of Electrodiagnostic Medicine* 21 (1998), Nr. 12, p. 1632–1646

[167] SWEENEY, H L. ; KUSHMERICK, MJ ; MABUCHI, K ; SRETER, FA ; GERGELY, J: Myosin alkali light chain and heavy chain variations correlate with altered shortening velocity of isolated skeletal muscle fibers. En: *Journal of Biological Chemistry* 263 (1988), Nr. 18, p. 9034–9039

[168] TAKAZA, Michael ; MOERMAN, Kevin M. ; GINDRE, Juliette ; LYONS, Garry ; SIMMS, Ciaran K.: The anisotropic mechanical behaviour of passive skeletal muscle tissue

subjected to large tensile strain. En: *Journal of the mechanical behavior of biomedical materials* 17 (2013), p. 209–220

[169] TAVI, Pasi ; WESTERBLAD, Håkan: The role of in vivo Ca2+ signals acting on Ca2+–calmodulin-dependent proteins for skeletal muscle plasticity. En: *The Journal of physiology* 589 (2011), Nr. 21, p. 5021–5031

[170] TRAPPE, Scott ; GALLAGHER, Philip ; HARBER, Matthew ; CARRITHERS, John ; FLUCKEY, James ; TRAPPE, Todd: Single muscle fibre contractile properties in young and old men and women. En: *The Journal of physiology* 552 (2003), Nr. 1, p. 47–58

[171] VAN LOOCKE, Mélanie ; LYONS, CG ; SIMMS, CK: Viscoelastic properties of passive skeletal muscle in compression: stress-relaxation behaviour and constitutive modelling. En: *Journal of biomechanics* 41 (2008), Nr. 7, p. 1555–1566

[172] VARY, Thomas C.: IGF-I stimulates protein synthesis in skeletal muscle through multiple signaling pathways during sepsis. En: *American journal of physiology. Regulatory, integrative and comparative physiology* 290 (2006), Nr. 2, p. R313–R321

[173] VILLOTA-NARVAEZ, Yesid ; GARZON-ALVARADO, Diego A. ; RAMIREZ-MARTINEZ, Angelica M.: A dynamical system for the IGF1-AKT signaling pathway in skeletal muscle adaptation. En: *Biosystems* (2021), p. 104355

[174] WANG, Yu ; ZHOU, Yanmin ; GRAVES, Dana T. ; WANG, Yu ; ZHOU, Yanmin ; GRAVES, Dana T.: FOXO transcription factors: their clinical significance and regulation. En: *BioMed research international* 2014 (2014), Nr. Figure 1, p. 925350. – ISBN 2314–6141 (Electronic)

[175] WEISS, Jeffrey A. ; MAKER, Bradley N. ; GOVINDJEE, Sanjay: Finite element implementation of incompressible, transversely isotropic hyperelasticity. En: *Computer Methods in Applied Mechanics and Engineering* 135 (1996), Nr. 1, p. 107 – 128. – ISSN 0045–7825

[176] WESTERBLAD, H ; ALLEN, DG: Changes of myoplasmic calcium concentration during fatigue in single mouse muscle fibers. En: *The Journal of general physiology* 98 (1991), Nr. 3, p. 615–635

[177] WESTWOOD, SA ; HUDLICKA, O ; PERRY, SV: Phosphorylation in vivo of the P light chain of myosin in rabbit fast and slow skeletal muscles. En: *Biochemical Journal* 218 (1984), Nr. 3, p. 841–847

[178] WIDRICK, Jeffrey J. ; TRAPPE, Scott W. ; COSTILL, David L. ; FITTS, Robert H.: Force-velocity and force-power properties of single muscle fibers from elite master runners and sedentary men. En: *American Journal of Physiology-Cell Physiology* 271 (1996), Nr. 2, p. C676–C683

[179] WINTER, David A.: *Biomechanics and Motor Control of Human Movement*. Vol. 2nd. 4. 2009. – 277 p.. – ISBN 9780470549148

[180] WORLD HEALTH ORGANIZATION: Global recommendations on physical activity for health. En: *WHO*, 2010, p. –

[181] ZÖLLNER, Alexander M. ; ABILEZ, Oscar J. ; BÖL, Markus ; KUHL, Ellen: Stretching Skeletal Muscle: Chronic Muscle Lengthening through Sarcomerogenesis. En: *PLoS ONE* 7 (2012), Nr. 10